

6-DoF Modelling and Control of a Remotely Operated Vehicle

by

Chu-Jou Wu, *B.Eng. (Electrical)*

Academic Supervisor: Assoc Prof. Karl Sammut

Engineering Discipline

College of Science and Engineering

Flinders University

July, 2018

A thesis submitted to the Flinders University in partial fulfilment of the requirements for the degree of Master of Engineering (Electronics)

Abstract

Remotely Operated Vehicles (ROVs) are today commonly deployed in a range of underwater applications, including offshore oil and gas, defence, aquaculture and scientific research, mostly for inspection and intervention roles. In order to meet the requirements for these roles and operate underwater effectively, the vehicles need accurate navigation and control systems to allow the vehicle to manoeuvre and maintain station with little effort from the operator.

This master's thesis is concerned with two major phases: the first is modelling and system identification of an observation class mini ROV, named BlueROV2 Heavy; and the second is the design and development of a 6-DoF robust control system for this vehicle. Modelling and system identification comprises mathematical modelling and the subsequent estimation of the relevant parameters. The modelling of the BlueROV2 Heavy was carried out in 6-DoF and consists of developing the thruster model and the dynamic model of motion of the vehicle. A system identification approach of immersion tank testing with the use of on-board sensors is proposed for parameter estimation where the unknown parameters are estimated from the experimental data utilising the least squares algorithm. Due to unforeseen delays in receiving the BlueROV2 Heavy in time, these experiments could not be performed. Instead, the unknown parameters are currently determined by utilising the BlueROV2 Heavy's technical specifications in combination with published data of the BlueROV.

The determined model from the system identification process was utilised to design the 6-DoF control system for BlueROV2 Heavy in which a conventional PID controller and a nonlinear model-based PID controller were applied, respectively. The thesis examines and compares the performance of both controllers from results of simulations where the nonlinear model-based control system achieves significant improvement in accuracy especially when external disturbance is applied or when multiple movements or rotations are required. Monte Carlo method was applied to analyse the robustness of both control systems in consideration of random disturbances and uncertainties in the process model. The simulation results demonstrate that the designed 6-DoF nonlinear model-based control system is feasible to be implemented on the BlueROV2 Heavy.

Declaration

I certify that this thesis does not incorporate without acknowledgment any material previously submitted for a degree or diploma in any university; and that to the best of my knowledge and belief it does not contain any material previously published or written by another person except where due reference is made in the text.



July, 2018

Acknowledgements

I would like to acknowledge my supervisor Assoc. Prof. Karl Sammut with my sincerest gratitude for giving me this opportunity and for his invaluable guidance throughout this research. There are no words that can sufficiently express my gratitude for his continuous support and belief towards me. This is a treasured experience that I will carry on to my next challenge.

I would like to thank Dr. Andrew Lammas with much appreciation for his valuable advice, comprehensive knowledge, time and patience. His guidance and technical support provides me direction and motivation to make this possible.

I would also like to thank Jonathan Where for his support in academic and technical and for being willing to help in any possible way.

Finally, I would like to thank my entire family and my close friends for their support and encouragement even without having them around during my studies.

Chu-Jou Wu

July, 2018

Adelaide

Table of Contents

Abstract.....	i
Declaration.....	ii
Acknowledgements.....	iii
Table of Contents.....	iv
List of Figures.....	vi
List of Tables.....	vii
Chapter 1 Introduction.....	1
1.1 Background & Motivation.....	1
1.2 Problem Statement.....	1
1.3 Objective.....	2
1.4 Approach.....	3
1.5 Contributions and Thesis Organisation.....	3
1.5.1 Outline of the Thesis.....	3
1.5.2 Contributions.....	4
Chapter 2 Literature Review.....	6
2.1 ROV Classification and Related Works.....	6
2.2 Review of Existing Control Solutions for Underwater Vehicles.....	11
2.2.1 Proportional Integral Derivative (PID) Control and PID Variations.....	12
2.2.2 Linear Quadratic Regulator/Gaussian (LQR/LQG).....	14
2.2.3 Sliding Mode Control (SMC).....	14
2.2.4 Intelligent Control.....	15
2.3 Review of Mathematical Modelling for Underwater Vehicles.....	16
2.3.1 Dynamic Model.....	17
2.3.2 Thruster Model.....	19
2.4 Review of Parameter Estimation Methods for Underwater Vehicles.....	20
2.4.1 Experimental Approaches.....	20
2.4.2 Numerical Approaches.....	22
2.5 Summary.....	22
Chapter 3 Experimental Platform: BlueROV2 Heavy.....	24
3.1 BlueROV2 Heavy Overview.....	24
3.2 BlueROV2 Heavy Type T200 Thrusters.....	25
3.3 Assumptions of BlueROV2 Heavy on Dynamics.....	27
3.4 Summary.....	27
Chapter 4 Modelling of the ROV.....	28
4.1 Notations.....	28
4.2 Kinematic Model.....	30
4.2.1 Reference Frames.....	30

4.2.2 Transformations Between BODY and NED	31
4.3 Kinetic Model.....	34
4.3.1 Rigid Body Dynamics	35
4.3.2 Vehicle Hydrodynamics.....	36
4.3.3 Hydrostatics	38
4.4 Thruster Model and Control Allocation.....	39
4.5 Summary	42
Chapter 5 System Identification	43
5.1 System Identification Approach	43
5.1.1 The Least Squares (LS) Technique.....	44
5.1.2 Static Experiments	45
5.1.3 Dynamic Experiments	46
5.2 Parameter Determination.....	47
5.3 Thrust Identification	49
5.4 Summary	49
Chapter 6 Control of the ROV	51
6.1 Control System Design.....	52
6.1.1 Linear Conventional PID Control.....	53
6.1.2 Nonlinear Model-based PID Control.....	54
6.2 Control System Simulations & Result Analysis	56
6.2.1 Linear Conventional PID Control.....	56
6.2.2 Nonlinear Model-based PID Control.....	60
6.2.3 Performance Comparison of Linear Model-less and Nonlinear Model-based PID Control Systems.....	63
6.3 Robustness Analysis of Control Systems	64
6.3.1 Effect of Model Uncertainty	64
6.3.2 Effect of Current Disturbance	66
6.3.3 Effect of Model Uncertainty and Current Disturbance.....	68
6.3.4 Robustness Analysis of Model-less and Model-based Control Systems.....	72
6.4 Summary	75
Chapter 7 Conclusion	76
7.1 Summary	76
7.2 Conclusions.....	77
7.3 Recommendations for Future Work	79
7.3.1 Improvement of System Identification	79
7.3.2 Improvement of Controller.....	80
7.4 Epilogue	81
Bibliography	82

List of Figures

Figure 2.1 Block diagram of a feedback control system (Fossen and Johansen 2006)	12
Figure 2.2 Motion in 6 DoFs (Fossen 2011)	18
Figure 3.1 The BlueROV2 Heavy Configuration Retrofit Kit (BlueRobotics 2018a).....	25
Figure 3.2 Diagram of hardware components on the BlueROV2 Heavy and the topside and their connections. Communication between BlueROV2 Heavy and the topside computer is made via Ethernet signals whereas connection between the on-board operating processing unit Raspberry Pi 3 and the autopilot Pixhawk is made through USB.....	25
Figure 3.3 The T200 Thruster of the BlueROV2 Heavy (BlueRobotics 2018c)	26
Figure 3.4 BlueROV2 Heavy thruster configuration from top-down view. Green and blue thrusters indicate counter-clockwise and clockwise propellers, respectively. (BlueRobotics 2018b).	26
Figure 4.1 ROV Body Frame Coordinate System Backing Image from BlueROV2 Heavy (BlueRobotics 2018a)	31
Figure 4.2 Top view and front view of BlueROV2 Heavy thruster configuration. Backing Image from BlueROV2 Heavy Retrofit Documentation (BlueRobotics 2018b).....	40
Figure 5.1 T200 thruster: thrust vs control input signal mapping (BlueRobotics 2018c).....	50
Figure 6.1 Open-loop control system block diagram (currently supported for BlueROV2 Heavy) ..	52
Figure 6.2 Feedback control system block diagram	52
Figure 6.3 Linear conventional PID control system block diagram	54
Figure 6.4 Nonlinear model-based PID control system block diagram.....	56
Figure 6.5 Step responses for the position in 6 DoFs using conventional PID	58
Figure 6.6 Path following simulation results with linear PID without external disturbance.....	59
Figure 6.7 Path following simulation results with linear PID applying current speed of 0.1 m/s on the x and y directions	59
Figure 6.8 Step responses for the position in 6 DoFs using model-based PID	61
Figure 6.9 Path following simulation results with model-based PID without external disturbance ..	62
Figure 6.10 Path following simulation results with model-based PID applying current speed of 0.1 m/s on the x and y directions	62
Figure 6.11 Comparison of step responses for 6 DoFs based on model-less and model-based control systems using Monte Carlo simulations with model uncertainties	65
Figure 6.12 Comparison of step responses for 6 DoFs based on model-less and model-based control systems using Monte Carlo simulations applying water current at 0.25 m/s (within $\pm 10\%$ variation) in the x, y and z directions	67
Figure 6.13 Settling time comparison of step responses for 6 DoFs based on model-less and model-based control systems using Monte Carlo simulations with increasing current speeds (within $\pm 10\%$ variation) in the x, y and z directions	69
Figure 6.14 Steady-state error comparison of step responses for 6 DoFs based on model-less and model-based control systems using Monte Carlo simulations with increasing current speeds (within $\pm 10\%$ variation) in the x, y and z directions	70
Figure 6.15 Comparison of step responses for 6 DoFs based on model-less and model-based control systems using Monte Carlo simulations in the presence of model uncertainties and current speed of 0.25 m/s with random noise in the x, y and z directions	71
Figure 6.16 Robustness analysis comparison of two control schemes regarding model uncertainties	73
Figure 6.17 Robustness analysis comparison of two control schemes regarding current disturbance	74
Figure 6.18 Robustness analysis comparison of two control schemes concerning both model uncertainties and current disturbance	75

List of Tables

Table 2.1 List of ROV Usage Research – 1	9
Table 2.2 List of ROV Usage Research – 2	10
Table 2.3 List of ROV Usage Research – 3	11
Table 4.1 The SNAME notation for marine vessels (SNAME 1950)	29
Table 4.2 Moment arms of 8 thrusters of BlueROV2 Heavy	40
Table 5.1 A Priori information for parameters in rigid body dynamics and restoring forces	48
Table 5.2 Determined added mass parameters	48
Table 5.3 Determined linear and quadratic damping parameters	48
Table 6.1 The gains used in the 6-DoF PID controller	56
Table 6.2 The gains used in the 6-DoF model-based PID controller	60
Table 6.3 Performance comparison of model-less and model-based control systems.....	63

CHAPTER 1

INTRODUCTION

1.1 Background & Motivation

Since there has been an increasing interest in studying, exploring and exploiting the oceans' underwater environments in recent years, Unmanned Underwater Vehicles (UUVs) are becoming more and more prevalent and extensively utilised in surveying, scientific, industrial and military applications. Based on operations and shapes of the underwater vehicles, UUVs are generally classified into two categories: Autonomous Underwater Vehicles (AUVs) and Remotely Operated Vehicles (ROVs). An AUV can travel underwater independently for long distances without connected cables and command inputs from operators and often has a cylindrical shape, whereas an ROV is controlled by an operator via a tether and generally operates at low speeds in a certain range with the design of a box shape. Due to the features of ROVs, they have become widely used in the offshore industry for marine inspection.

Fish farming is one of the most common types of aquaculture where floating cages with flexible nets are employed. In order to reduce the risk of fish escapes with limited operators and costs, the development of ROV technology is invaluable for underwater operations such as mooring and nets inspection. With the increase of the use and accessibility of ROVs to the public for effective and safe independent operations, the demand for applying autonomy onto ROVs has become significant for a large number of circumstances. In consideration of autonomous operations of an ROV, the development of a control system is then crucial for controlling the behaviour of the ROV.

1.2 Problem Statement

BlueROV2 Heavy from Blue Robotics (BlueRobotics 2018a) has been newly released in 2018 providing configuration of eight thrusters and provides the capability of full six degrees of freedom (DoFs) control. Although BlueROV2 Heavy has a control system implemented in its platform, it uses an open-loop controller, which can provide control abilities for manual operation where a high level of precision is not required. Nevertheless, for autonomous

operations of an ROV, a robust control system is needed due to accuracy requirements and safety of the vehicle.

The system properties for describing the behaviour of an ROV operating underwater can be investigated using models. The development of these models is challenging and time-consuming in both theoretical development and experimental testing. The complexity involves highly nonlinear properties of an ROV, substantial unknown parameters in the models, incomplete state information provided by sensors containing noisy measurements, and system influenced by unpredictable disturbance such as currents in a coupled manner. However, knowing system properties allows us to optimise the control design and improve the accuracy and performance of the vehicle. Hence, this thesis will cover the modelling and identifying BlueROV2 Heavy's system properties as well as developing a nonlinear model-based control algorithm based on these properties.

1.3 Objective

The level of motion control of an ROV is based on the number of DoFs that could be controlled, which is depending on the thruster configuration of the vehicle. BlueROV2 Heavy was chosen for this project because its thruster configuration can provide the 6-DoF control ability. The full 6 DoFs gives ROV capability for movements and rotations in every possible direction. Accordingly, a 6-DoF control system allows the ROV to manoeuvre complex structures. Hence, the objective of this research is to develop a 6-DoF model of BlueROV2 Heavy and to utilise this model to design a robust 6-DoF control system for BlueROV2 Heavy. The objective can be subdivided into the following parts:

1. Develop a 6-DoF mathematical dynamic model of BlueROV2 Heavy's motion.
2. Develop BlueROV2 Heavy's mathematical thruster model by analysing thrust configuration.
3. Identify unknown parameters of 6-DoF dynamic model of BlueROV2 Heavy.
4. Identify thruster characteristics of BlueROV2 Heavy.
5. Design a robust 6-DoF control system for BlueROV2 Heavy platform where a linear model-less controller and a nonlinear model-based controller will be developed

individually and perform simulations to evaluate the performance of both control systems.

1.4 Approach

First of all, an analytical study of theoretical models in 6 DoFs for underwater vehicles was undertaken while a literature review was carried out to examine current knowledge and existing solutions from previous UUV research. With the analysis of BlueROV2 Heavy's physical characteristics and operating speeds, several assumptions were made for the dynamics of the vehicle in order to simplify the 6-DoF mathematical models and reduce the number of unknown parameters in the models.

Next, a scheme of estimating parameters in the model was formulated based on the review of system identification. This proposed approach is comprised of performing a series of designed immersion tank experiments and then applying a suitable estimation technique to determine unknown parameters from experimental data. However, since the BlueROV2 Heavy is currently not available for experiments, analysis of the ROV's technical specifications and application of parameters derived from previous BlueROV research were applied.

Finally, since the system properties of ROVs are nonlinear, with the use of attained system models, a nonlinear model-based controller was utilised to design a robust 6-DoF control system for BlueROV2 Heavy while a linear controller was also designed separately. Various predetermined experiments were operated to evaluate and compare the effectiveness and performance of linear model-less and nonlinear model-based controllers.

1.5 Contributions and Thesis Organisation

1.5.1 Outline of the Thesis

Chapter 2 examines classification of ROVs and related research that have been done previously; and reviews a number of control solutions that have been applied for underwater

vehicles as well as mathematical modelling methods and system identification approaches for underwater vehicles.

Chapter 3 describes the BlueROV2 Heavy package and its components. The capabilities of the vehicle and its operating system are concisely explained. The assembled BlueROV2 Heavy is shown and the assertions on dynamics about BlueROV2 Heavy that were made are presented in this chapter

Chapter 4 presents fundamental theories and procedures of 6-DoF mathematical models for underwater vehicles, organised by kinematic, kinetic and thruster models. The applied assumptions based on BlueROV2 Heavy characteristics for model simplification are also discussed.

Chapter 5 presents a system identification approach of experiment design and estimation algorithm for determining the parameters in 6-DoF models derived in chapter 4. While the experimental platform is not available for performing experiments, parameters determined by analysing published technical specifications for the BlueROV2 Heavy and other available published literature relating to the BlueROV are used instead in this chapter.

Chapter 6 concisely describes the control problem and proposes the 6-DoF nonlinear model-based controller for the control system of BlueROV2 Heavy. The designed control system simulations are presented and the simulation results are discussed and compared with control system using linear model-less controller.

Chapter 7 concludes the overall results and presents suggestions for further work.

1.5.2 Contributions

To the author's knowledge, the modelling of the BlueROV2 Heavy and the development and analysis of the control algorithms are presented in this thesis are novel contributions. More specifically, the following highlights the contributions made to the thesis.

1. Development of 6-DoF mathematical modelling of the BlueROV2 Heavy
2. Proposal of system identification experiments for the BlueROV2 Heavy

3. Determination of parameters in the 6-DoF model of the BlueROV2 Heavy by utilising published technical specifications for the BlueROV2 Heavy and published literature relating to the BlueROV
4. Development of a 6-DoF linear conventional PID control system and a 6-DoF nonlinear model-based PID control system for the BlueROV2 Heavy, and performance comparison of both algorithms by simulations
5. Robustness analysis of both control systems by applying Monte Carlo simulations and statistical analysis

CHAPTER 2

LITERATURE REVIEW

This chapter presents a comprehensive literature review on existing control algorithms, mathematical modelling methods and system identification approaches that have been applied for underwater vehicles while ROV classification and previously developed platforms with associated research are also examined. Accordingly, a feasible approach for developing a robust 6-DoF control system for BlueROV2 Heavy is proposed.

2.1 ROV Classification and Related Works

ROVs can be categorised into two major classes based on the purpose of use and their functions: observation class ROVs and work class ROVs (Capocci, Dooly et al. 2017). Observation class ROVs are utilised for visual inspection and light intervention tasks, whereas work class ROVs perform more serious subsea work and deep-water installations with manipulative capability and wide power variations.

Capocci et al. presents a review of classification of ROVs in regard to size and capability, and discusses common subsystems of the ROV. Observation class ROVs, also called inspection ROVs, are generally small vehicles deployed in waters no deeper than a few hundred metres and their propulsion power is limited to several kilowatts. This class of ROVs can be subdivided into micro, mini and medium ROVs according to the size of the vehicle. They are often fitted with thrusters, imaging devices and various types of sensors. Work class ROVs can be divided into light and heavy work class models based on the level of heavy duty work they are able to carry out. However, work class ROVs employ considerable volume of equipment that leads to high overall system complexity and significant costs for operation. Hence, when the functionalities of these large ROVs are not required, observation class ROVs are preferred for a wide variety of applications (Capocci, Dooly et al. 2017).

Christ and Wernli provide a manual on how to use small-scale observation class ROVs for inspection, survey and research purposes that can be applied in both scientific and industrial

studies (Christ and Wernli 2007). The history of ROV development and the technology improvement of observation class ROVs were addressed in this book. It then details necessary knowledge for the design and operations of underwater robotics and navigation tools to attain their mission results in an efficient way. Huang discusses the degree of autonomy for unmanned systems regarding operator controlled or program controlled by which they might be functioned under operation modes of fully autonomous, semi-autonomous, tele-operation and remote control depending on the levels of human intervention (Huang 2004).

A tethered ROV can be operated with autonomy and artificial intelligence. There are three main systems within the autonomy architecture of unmanned underwater vehicles, which are guidance system, navigation system and control system (Fossen 2002, Fossen 2011). The guidance system produces the desired path for the vehicle; the navigation system determines the current state of the vehicle, such as its position, velocity and acceleration; the control system provides command signals in controlling the vehicle in a multi-axis motion to follow its desired trajectory. The techniques of the design of these systems are discussed in detail in (Fossen 2002, Fossen 2011), and examples on different areas of research by the usage of ROVs will be examined in the following.

Fernandes developed a model-based multiple input multiple output (MIMO) output feedback motion control system along with an open-loop guidance system for an observation-class ROV named Minerva using existing modelled parameters (Fernandes, Sørensen et al. 2015). In the guidance system, a path generation scheme was used to produce efficient references of position, velocity and acceleration in order to guide the ROV's motion, and a reference model was proposed to synthesise continuous references with respect to a single DoF motion. The applied motion control system contains dynamic positioning and trajectory tracking capabilities such that the ROV is capable of keeping position and heading angle at a depth of 70 m by controlling 4 DoFs of surge, sway heave and yaw of the ROV under the assumption that the remaining DoFs of roll and pitch are self-stable (i.e. metacentric stability) due to the design of the ROV. The author concluded that the use of the dynamic model achieves a steadier motion such that steadier hydrodynamic effects and less plant parameter variation would be induced as well as the higher overall motion accuracy could be obtained.

Sandøy designed uDrone, a model-based advanced control system containing both an observer and a controller for a mini ROV called BlueROV from Blue Robotics (Blue Robotics 2016). The controller uses the estimated states produced by the observer and evaluates optimised corrective signals to control the vehicle. Although the BlueROV includes 6 thrusters, the system was simplified to the 4-DoF control of surge, sway, heave and yaw motions. The author validated the design of the system by the implementation in Simulink and interfaced with Robot Operating System (ROS) (Sandøy 2016). Aili and Ekelund also modelled and developed a control system for BlueROV (Blue Robotics 2016) in which the model parameters were estimated using EKF-based sensor fusion method in order to design attitude, angular velocity and depth controllers. However, the attitude controller was not able to achieve a stable system while using the feedback linearisation (Aili and Ekelund 2016). Gonzalez designed and constructed an AUV named Mako, including mechanical and electrical systems (Gonzalez 2004). The system identification of Mako and the simulation of a control system were carried out for 4 DoFs of surge, heave, pitch and yaw motion control. Lapierre et al. proposed a nonlinear path following control system using Lyapunov theory and backstepping techniques and the simulation was performed for an underactuated AUV with the simplified dynamic model along a desired path (Lapierre, Soetanto et al. 2003).

Image capturing is another main capability for ROVs. Jakobsen developed a software system for a micro ROV to inspect fish cage net integrity by analysing the video feed from the ROV. The algorithm processes and analyses camera sensor data in real-time, with the objective of generating control signals for the ROV to move in a pattern for the investigation of the whole cage net. Although this was not achieved as a result of the lack of sway motion ability of the ROV, it has proven the use of an autonomous ROV for aquaculture monitoring applications (Jakobsen 2011). In oceanography research, there are application examples in detecting and tracking underwater objects (Walther, Edgington et al. 2004), underwater environment mapping and reconstruction (Singh, Roman et al. 2007, Sedlazeck, Koser et al. 2009, Marsh, Copley et al. 2013). Table 2.1 to Table 2.3 lists a number of previously developed platforms and associated research.

Table 2.1 List of ROV Usage Research – 1

Name	Producer	Area of Research	Figure
VORTEX	VORTEX Degree	Control Systems (Perrier and Canudas-De-Wit 1996)	 <p>(Perrier and Canudas-De-Wit 1996)</p>
Hercules	Institute For Exploration (Ocean Exploration Trust)	Image Mapping (Singh, Roman et al. 2007, Roman, Inglis et al. 2010)	 <p>(OceanExplorationTrust 2003)</p>
Seaeye Falcon	SAAB	Guidance and Control Systems (Soylu, Buckham et al. 2008)	 <p>(SAAB 2002)</p>
Sub-Fighter 7500 (Minerva)	SPERRE	Control Systems (Svendby 2007, Dukan, Ludvigsen et al. 2011, Fernandes, Sorensen et al. 2013, Dukan 2014, Fernandes, Sørensen et al. 2015)	 <p>(NTNU 2018)</p>

Table 2.2 List of ROV Usage Research – 2

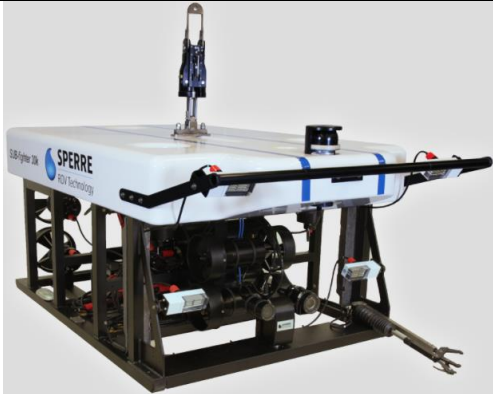
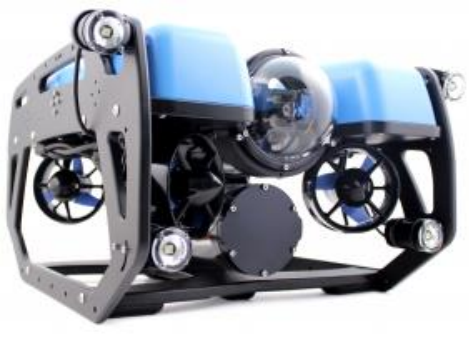
Name	Producer	Area of Research	Figure
Sub-Fighter 30 K	SPERRE	Control Systems for ROV Manipulator (Haugen 2012) for ROV (Dukan 2014, Rist-Christensen 2016)	 <p>(SPERRE 2012)</p>
VideoRay PRO 3S	VideoRay	Computer Vision Systems (Jakobsen 2011)	 <p>(VideoRay 2018a)</p>
VideoRay Explorer	VideoRay	Image Analysis (Amado-Filho, Pereira-Filho et al. 2012)	 <p>(VideoRay 2018b)</p>
VideoRay PRO 4	VideoRay	Control Systems (Arnesen 2016, Mai, Pedersen et al. 2017)	 <p>(VideoRay 2018c)</p>

Table 2.3 List of ROV Usage Research – 3

Name	Producer	Area of Research	Figure
BlueROV	BlueRobotics	Control Systems (Aili and Ekelund 2016, Sandøy 2016, Yahya and Arshad 2016)	 <p>(Sandøy 2016)</p>
BlueROV2	BlueRobotics	Computer Vision Systems (Chalkiadakis, Papandroulakis et al. 2017)	 <p>(BlueRobotics 2017)</p>
Isis	National Oceanography Centre	Image Analysis (Marsh, Copley et al. 2013) Computer Vision Systems (Erikson, Gansel et al. 2016)	 <p>(NationalOceanographyCentre 2018)</p>

2.2 Review of Existing Control Solutions for Underwater Vehicles

The fundamental principle of a feedback control system of an ROV is illustrated in Figure 2.1 where the controller produces generalised control forces and the control allocation distributes these generalised control forces to the actuators (Fossen and Johansen 2006). Since control systems are based on the design of controllers, this section will review a variety of control algorithms that have been applied to underwater vehicles.

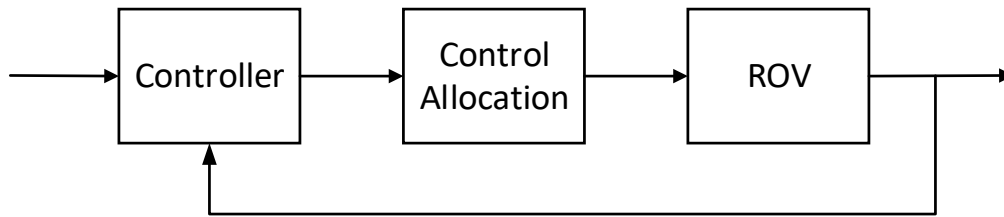


Figure 2.1 Block diagram of a feedback control system (Fossen and Johansen 2006)

2.2.1 Proportional Integral Derivative (PID) Control and PID Variations

In control systems, the classical proportional-integral-derivative (PID) control is usually favoured for unmanned underwater vehicles and marine vessels in general (Fossen 1994, Strand 1999, Smallwood and Whitcomb 2004, Sørensen 2012) as well as for industrial control applications (Åström and Hägglund 2006, Raptis 2010). PID control was firstly introduced by Minorsky with a theoretical analysis of automatic steering systems for ships where he formulated the three control terms of proportional, integral and derivative, and used their impact on the controller output to employ optimal control (Minorsky 1922). His system was a single-input single-output (SISO) linear control system in which the applied PD and subsequently PID controllers were tuned empirically to control the heading of the ship automatically. Upon which, a conventional PID control system can be generalised to a nonlinear multiple input multiple output (MIMO) system (Fossen 1991). The PID controller is capable of removing steady state bias and predicting the future by integral and derivative operations, respectively as its integral, proportional and derivative feedback is on the basis of the past, the present and the future control error, respectively. As a result, it is a highly sufficient control method particularly when coupled nonlinear time varying plant dynamics of the process are low (Åström and Hägglund 1995). Since underwater vehicles are low speed travelling and generally identified as uncoupled dynamic models, PID controllers are commonly used due to its synthesis and the relative simplicity of implementation and a number of successful applications with experimental results shown can be found in literature (Perrier and Canudas-De-Wit 1996, Caccia and Veruggio 2000, Antonelli, Chiaverini et al. 2001, Smallwood and Whitcomb 2004, Hoang and Kreuzer 2007, Dukan, Ludvigsen et al. 2011, Fernandes, Sørensen et al. 2015).

The first dynamic positioning system was implemented by the use of traditional PID controllers in cascade for surge, sway and yaw motions in combination with notch filters to restrain the effects of wave forces under the assumption that the interactions are negligible (Sargent and Cowgill 1976). However, the integral action of the controller could not be sufficient due to couplings between motions of surge, sway and yaw. Furthermore, the introduction of motion measurements notch filtering results in the phase lag in the control loops.

In several applications, the conventional PID controller has its performance limitations. When PID controllers are used alone, the exact trajectory tracking of nonlinear time varying dynamics cannot be achieved. Moreover, PID controllers are unable to dynamically compensate for unmodelled hydrodynamic forces of the vehicle. Yet by incorporating other techniques into the PID design it is possible to circumvent these limitations. The nonlinear model-based exact linearisation can be obtained either applying state feedback of the robotics computed torque control technique (Franklin, Powell et al. 1994, Silpa-Anan, Abdallah et al. 2000, Gonzalez 2004) or using reference feedforward terms (Smallwood and Whitcomb 2004, Fernandes, Sørensen et al. 2015) to exactly linearise the plant dynamics.

Alternatively, since the process dynamics varies, two approaches have been suggested to automatically alter the gains of the PID controller with regard to adapting the corresponding variations in the dynamic properties to the process. The first method called gain scheduling updates the controller gains discretely based on measurable disturbance inputs (Caccia and Veruggio 2000, Sørensen 2012). The other approach of continuous adaptation (or self-adaptation) tunes the system continuously on the basis of a measurement of its closed-loop performance. While Hsu implemented the dynamic positioning system using PI and model-based adaptive controller on an ROV (Hsu, Costa et al. 2000), employing an nonlinear adaptive PD controller in the dynamic positioning for AUVs (Sun and Cheah 2003) and ROVs (Hoang and Kreuzer 2007) has been proposed. Antonelli developed a 6-DoF adaptive control algorithm for AUVs in the unknown dynamic parameters and time varying underwater environments validated by sufficient experimental results (Antonelli, Chiaverini et al. 2001). Perrier and Canudas-De-Wit designed a nonlinear robust control system using a PID controller with an additional nonlinear loop, and performed experiments on the VORTEX ROV (Perrier and Canudas-De-Wit 1996) while Alvarez et al presented the control of an AUV using a robust PID controller to undertake oceanographic sampling tasks (Alvarez,

Caffaz et al. 2009). More applications of the nonlinear robust adaptive control strategy for UUVs can be found in literature (Yuh 1990, Do, Pan et al. 2004, Li, Yang et al. 2012).

2.2.2 Linear Quadratic Regulator/Gaussian (LQR/LQG)

Another optimal control technique of model linearisation called linear quadratic regulator (LQR) operates a dynamic system and provides an automated design procedure to find a suitable state feedback controller by minimising the quadratic continuous time cost function so as to give the best possible performance. Wahl and Gilles presented an automatic track-keeping control system using an LQR combined with a feedforward cancellation scheme (Wahl and Gilles 1999). Goheen and Jefferys presented a linear quadratic self-tuning controller of linearised plant models and the performance of controlling an ROV was examined by a nonlinear simulation (Goheen and Jefferys 1990). Arnesen developed motion control systems to allow the Videoray Pro 4 ROV to achieve path-following in which the heading and depth of the ROV were controlled by using a PID controller and an LQR, respectively (Arnesen 2016). As far as the uncertainty of the system and incomplete state information are concerned, the combination of a linear quadratic estimator (LQE) of a Kalman filter with a LQR forms the linear quadratic Gaussian (LQG) in order for systems to include Gaussian noise and for circumstances of that when the full state of the system might not be directly observed. Simple LQG controllers have been applied in Juul and others (Juul, McDermott et al. 1994, Naeem, Sutton et al. 2003, Sandøy 2016).

2.2.3 Sliding Mode Control (SMC)

Sliding mode control is a nonlinear control technique in which the dynamics of the nonlinear system are altered by employing a discontinuous control signal to cause the system slide along a prescribed path. Its methodology is described and derived in detail in literature (Utkin 1977, Slotine and Sastry 1983). The primary benefit of sliding mode control is that the closed-loop response are insensitive to parameter variations and external disturbances so as to obtain good quality of trajectory tracking and achieve robust control. Yoerger and Slotine applied SMC in control of underwater vehicles concerning their highly nonlinear and time varying dynamics parameters as well as model uncertainties and disturbances,

whereupon they presented how this method deals with nonlinearities directly to produce robust controllers that perform predictably using a nonlinear vehicle simulations with modest amounts of computation required (Yoerger and Slotine 1985). Haugen proposed a suitable controller using SMC principle with the intention of forcing the manipulator of the SubFighter 30K ROV to track a desired path in the joint space, though an alternative commercial control system was achieved by simulations that the robot was capable of following the generated joint trajectories (Haugen 2012). More examples of control systems for underwater vehicles based on the sliding mode approach to attain robust controllers with good simulation results of adapting the changing dynamics and operating conditions can be found in literature (Cristi, Papoulias et al. 1990, Healey and Lienard 1993, Gomes, Sousa et al. 2003, Soylyu, Buckham et al. 2008).

2.2.4 Intelligent Control

Intelligent control algorithm is a class of control techniques that applies a number of artificial intelligence computing approaches to a control system that include fuzzy logic, neural networks, Bayesian probability, machine learning, genetic algorithm and evolutionary computation. Fuzzy logic and neural networks are the two most broadly used intelligent control algorithms. The fuzzy logic scheme performs many-valued logic in which the analogue input values are analysed as logical variables, and the truth values of variables are continuous values between 0 and 1, instead of discrete levels of truth (either 1 or 0). Raimondi and Melluso presented a closed-loop fuzzy motion control system on the basis of Lyapunov's stability for an under-actuated ROV where the controller ensures robustness in relation to uncertainties caused by deep sea environment and saturation of the control signals and an Kalman filter was implemented to compensate measurement noises (Raimondi and Melluso 2010). Neural network controllers involve two stages of system identification and control where a neural network model of the plant is trained in the system identification stage for the control design. An adaptive neural network approach was applied in (Chu, Zhu et al. 2017) for an ROV trajectory tracking control system. Furthermore, several studies have proposed the combined use of fuzzy logic and neural network control techniques for underwater vehicles with numerical simulations (Mills and Harris 1995, Wang and Lee 2003). Although intelligent control algorithms contain considerable uncertainty and

can provide a control solution when the vehicle's dynamics are not well known, the implementation of the controllers consist of their own mathematical complexity and require extensive computational resources as well as lengthy tuning processes.

Recently, combinations of the various control solutions discussed above have been commonly used in the control of underwater vehicles such as sliding mode fuzzy controllers for an AUV (Song and Smith 2000), adaptive fuzzy sliding mode controller for ROVs (Sebastián and Sotelo 2007, Bessa, Dutra et al. 2010), and an adaptive neuro-fuzzy sliding mode based on genetic algorithm control system for an ROV (Javadi-Moghaddam and Bagheri 2010). The integration of different control schemes offers the benefits of combining each controller's useful properties in order to increase robustness and fault tolerance of the overall control system.

2.3 Review of Mathematical Modelling for Underwater Vehicles

It is vital to investigate the physical properties of the model of the underwater vehicle for control system design for a number of purposes. Since underwater vehicles might operate under various operating conditions and they are highly complex mechatronic devices, nonlinearities due to hydrodynamic forces and kinematics of the vehicle are considerable. Hence, investigating and modelling these nonlinear influences is significant to the performance and robustness of the ROV control system. Besides, the technique of nonlinear control design offers the opportunity to directly compensate the model's nonlinear dynamics. Furthermore, analysing the a priori information about the dynamic equations and kinematics of the underwater vehicle provides the ability to recognise the terms in the model that can be eliminated so as to simplify the model and allow a simpler nonlinear control design. Lastly, structural and parametric uncertainties will be introduced when a linear approximation of a nonlinearity is used. By identifying the nonlinearity, the structural uncertainty can be included in the model and the parametric uncertainty can be compensated by the use of adaptive or robust control algorithms (Fossen 1991).

In spite of some proposed neural network modelling methods (Kodogiannis, Lisboa et al. 1996, Sayyaadi and Ura 1999), most published work on system identification for underwater vehicles is based upon the dynamic equations of motion. Kalske presented a survey of

dynamic equations of motion for ROVs and submarine simulation (Kalske 1989). Modelling and simulation of ROVs have been analysed in the literature (Lewis, Lipscombe et al. 1984). Humphrey and Watkinson addressed the nonlinear and linear equations of motion of the AUV UNH-EAVE (Humphreys and Watkinson 1982) while Fossen and Sagatun described the nonlinear motion dynamics of the ROV in detail (Fossen 1991).

The motions of a marine craft take effects in 6 DoFs, which are the set of independent movements along three directions defined as surge, sway and heave; and rotations about three axes defined as roll, pitch and yaw as illustrated in Figure 2.2. In many cases marine crafts are under-actuated, thus reduced-order models are commonly used in motion control systems. However, a 6-DoF model can be used when designing state-of-the-art control systems for a fully-actuated ROV so as to achieve controllability in all DoFs.

2.3.1 Dynamic Model

Dynamic modelling can be classified into two categories: kinematics and kinetics. Kinematics considers geometrical aspects of motion whereas kinetics investigates the forces that cause changes of motion. A vectorial representation can be exploited to model physical system properties of the vehicle in 6 DoFs. The use of physical system properties is beneficial as it allows the number of coefficients required for control system design to be reduced. It is expressed utilising reference frames of body-fixed frame and navigation frame, hence appropriate kinematic transformations between body frame and navigation frame needs to be obtained (Fossen 1994). The kinematic equations have been derived by the Euler angle representation based on ship steering framework (Abkowitz 1964). Alternatively, kinematics has also been derived and demonstrated using spacecraft systems (Kane, Likins et al. 1983, Hughes 1986). The analysis and derivation of quaternion kinematic was discussed in detail in Chou (Chou 1992). The more recent and detailed examination on kinematics can be found in literature (Goldstein 1980, Egeland and Gravdahl 2002).

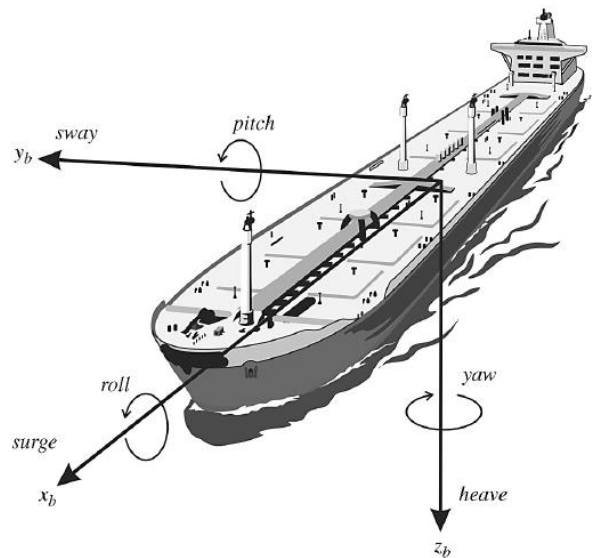


Figure 2.2 Motion in 6 DoFs (Fossen 2011)

In kinetics, the motion equations can be derived by using the Newton-Euler formulation on the basis of Newton's Second Law or using Euler-Lagrange equation in mechanics (Fossen 1991). Newtonian and Lagrangian mechanics have been discussed in detail in literature extensively (Goldstein 1980, Kane, Likins et al. 1983, Hughes 1986, Meirovitch 1990, Egeland and Gravdahl 2002). The physical properties of the system contain rigid-body and hydrodynamic models (Berge and Fossen 2000). By using the robot model, the rigid-body kinetics in complete 6 DoFs can be derived and represented in a vectorial form (Fossen 1994, Fossen 2011).

Two main theories of manoeuvring and seakeeping are often used to model the effect of external forces and moments on a marine craft. In manoeuvring theory, the vessel is moving in calm water without wave excitation and the hydrodynamic coefficients are assumed to be frequency independent such that the nonlinear mass damper spring system contains constant hydrodynamic coefficients whereas wave excitation is acknowledged in seakeeping theory. Since underwater vehicles are considered to operate below the wave affected zone, they can be modelled with constant added mass and damping coefficients (Fossen 2011). The hydrodynamic model of the manoeuvring theory is suitable for designing a control system based on system identification. This model can be used to compute mass, inertia, damping, and restoring forces, and the detailed discussion on this is found in literature (Newman, Sarpkaya and Isaacson 1981, Faltinsen 1990, Triantafyllou and Hover 2003).

2.3.2 Thruster Model

In order to compute optimal control inputs of the actuators of an underwater vehicle, thruster modelling should be applied as the thruster is the lowest layer in the control loop of the system. The desired thrust of each thruster can be determined by control allocation, which distributes the induced control forces to the thrusters in an optimum aspect. That is, the control allocation is the inverse of thruster model; therefore, the thruster control input signal can be computed with the use of the thruster model and the Moore-Penrose pseudo-inverse. The thrust configuration and thrust coefficient matrices for underwater vehicles are examined in detail in (Fossen 2011). However, accurately modelling thrusters is challenging in practice as thrust forces are influenced by motor model, hydrodynamic effects and propeller mapping. Several thruster modelling schemes for mapping relationship between the thrust and the control signal have been proposed to resolve these difficulties. While Yoerger et al. proposed a one-state model including motor dynamics (Yoerger, Cooke et al. 1990), Healey et al. presented a two-state model containing dynamic flow effects to represent the four quadrant behaviour of thrusters using aerofoil propeller blades lift and drag force data to formulate thrust and torque equations (Healey, Rock et al. 1994). In Healey's experimental results and comparison of two models, it was concluded that the two-state model is capable of demonstrating the thrust overshoot in transient response whereas the one-state model is not. However, the two-state model of Healey's is only valid when the forward speed of the underwater vehicle is around zero. Whitcomb and Yoerger compared both previous models by performing experimental verifications (Whitcomb and Yoerger 1999) and additionally suggested two new model-based thrust control algorithms, yet high-bandwidth fluid flow velocity sensors and highly accurate plant model parameters are required. In order for the model to match with experimental results better, instead of previous offline paradigm of thruster modelling, Bachmayer et al. proposed an online adaptive thruster identification algorithm to determine lift and drag coefficients using look-up tables (Bachmayer and Whitcomb 2003). Meanwhile, a three-state model with the transient effect in the flow included was presented (Blanke, Lindegaard et al. 2000) where non-dimensional propeller characteristics data from open water tests, thrust coefficient and advance ratio were utilised; still the model did not show a sufficient match with experimental results for the whole range of the advance ratio. As far as the effects of ambient flow velocity and angle are concerned, Kim and Chung proposed a more accurate three-state thrust modelling using

measurable states of ambient flow velocity and propeller shaft velocity to represent the thruster axial flow velocity (Kim and Chung 2006).

2.4 Review of Parameter Estimation Methods for Underwater Vehicles

2.4.1 Experimental Approaches

There have been a wide range of methodologies proposed to estimate the hydrodynamic coefficients of dynamic equations of motion for unmanned underwater vehicles. Conventional methods include tow tank experiments by using the underwater vehicle itself (Goheen 1986) or a scale model of it (Nomoto and Hattori 1986) while measuring the forces and moments applied to the vehicle under various operating circumstances. A routine dynamic testing of utilising a Planar Motion Mechanism (PMM) above the towing tank was introduced (Goodman 1960) to shift the ROV in a planar motion. Since a PMM mounted in a towing tank can move the ROV in multiple directions by rotating the ROV, it allows a complete model identification of hydrodynamic coefficients in all 6 DoFs to be attained. However, PMMs are fairly costly and the test procedures consume significant amount of time.

Another approach of on-board sensor based identification uses the measured data from on-board sensors along with information of thrust control signals to determine the most important dynamic parameters by a set of designed simple water tests (Indiveri 1998, Caccia, Indiveri et al. 2000, Smallwood and Whitcomb 2003). The main advantage of using on-board sensors is that there is no external equipment required and it can be carried out every time the vehicle setup is altered. In other words, this approach is cost effective and highly repeatable that suits variable configuration ROVs. Nevertheless, during these experiments, the motion of the vehicle needs to be restrained at a single DoF to identify the simplified uncoupled model. Thus, the effectiveness of the results considerably relies on the accuracy of the sensors and test procedures performed. Moreover, using only on-board sensor data to identify the forces applied to the ROV by the thrusters can be challenging as a result of the effects of thruster-hull and thruster-thruster interactions (Goheen and Jefferys 1990).

As a consequence, a number of on-board sensor based identification methods have been proposed in the interest of accurate hydrodynamic parameter estimation. Since the underwater vehicle dynamic equations of motion can be described as a set of equations that are linear with respect to the parameters, the least squares (LS) technique is one of the most common methods for estimation (Goheen and Jefferys 1990, Caccia, Indiveri et al. 2000, Smallwood and Whitcomb 2003, Gonzalez 2004, Ridao, Tiano et al. 2004). Caccia et al. presented an offline identification estimating hydrodynamic coefficients by LS on the basis of position measurements from both a compass and a digital altimeter (Caccia, Indiveri et al. 2000) whereas Smallwood and Whitcomb proposed an online adaptive parameter identification using LS with the data of position provided by a Sonic High Accuracy Ranging and Positioning System (SHARPS) time-of-flight hard-wired acoustic navigation (Smallwood and Whitcomb 2003), though a SHARPS is relatively expensive. More recently, the employment of computer vision-based navigation systems has become a popular option for estimating the position of the vehicle in identification (Ridao, Tiano et al. 2004, Chen, Chang et al. 2007) as they are low-cost and able to provide accurate location data although developing vision-based navigation algorithms can be time-consuming.

In addition, Abkowitz firstly proposed and implemented another estimation technique of utilising Extended Kalman Filter (EKF) in finding hydrodynamic coefficients for surface vessels (Abkowitz 1980) and an EKF-based identification application for ships was presented by (Liu 1993) while Goheen and Jefferys suggested to optimally integrate measurements from different sensors using EKF for underwater vehicle identification (Goheen and Jefferys 1990) and an application for the NPS Phoenix AUV on surge motion parameter identification based on EKF was described by (Marco and Healey 1998). Additionally, an application of combining both LS and EKF techniques for an ROV identification was proposed by (Alessandri, Caccia et al. 1998).

The classical free decay test applied in determining hydrodynamic coefficients has been introduced by Morrison and Yoerger in which the ROV oscillated in the water using three springs and the parameters in a single DoF of heave motion were identified while the position data was measured by SHARPS (Morrison and Yoerger 1993). Ross et al. proceeded to apply this method to a multiple DoFs of surge and sway motions of an UUV, which is connected to four springs and the method was validated by computer simulations (Ross, Fossen et al. 2004). However, the precise states of the vehicle are required for this method

and a sufficient localisation system such as SHARPS is costly. The use of pendulum is another type of free decay experiments in which the scaled ROV model is attached to a pendulum instead of springs and the displacement of the pendulum is measured over time (Eng, Lau et al. 2008, Yi and Al-Qrimli 2017). The motion of the pendulum can be interpreted by the dynamics equations to obtain the hydrodynamic parameters of the scaled model and the corresponding values for the full scale ROV can be predicted by scale-up. Yet, the results attained can differ widely with various initial conditions.

2.4.2 Numerical Approaches

A Numerical approach of Computational Fluid Dynamic (CFD), which solves the Navier-Stokes equations in fluid dynamics has been used for hydrodynamic computations of underwater vehicles in recent years (de Barros, Dantas et al. 2008). The hydrodynamic tests such as PMM towing tank experiments can be simulated by using CFD software so as to obtain hydrodynamic coefficients. CFD programs that have been used to determine the hydrodynamic model of the ROV include ANSYS Fluent (Zhang, Xu et al. 2010), Wave Analysis MIT (WAMIT) combined with the use of Computer-aided design (CAD) software (Eng, Chin et al. 2014, Chin, Lin et al. 2017), Phoenisc (Sarkar, Sayer et al. 1997), and Wave Analysis by Diffraction and Morison Theory (WADAM) (Eidsvik 2015). The numerical method provides a feasible alternative when hydrodynamic test facilities and instrumentation are not available. However, since the numerical approach of CFD is not able to capture the highly turbulence effect, the accuracy of its analysis is limited.

2.5 Summary

The literature review has comprehensively examined the methods of system identification and control solutions for underwater vehicles as well as related previous works on ROVs. This shows that there are a number of options available and each algorithm has its advantages and limitations. Therefore, these properties of these methods have been analysed with respect to the use of BlueROV2 Heavy for inspection and intervention. In order to attain maximum controllability for the BlueROV2 Heavy, a full 6-DoF control system will be developed applying the following approaches:

- Dynamic equations of motion modelling using vectorial representation
- Static and dynamic experiments of immersion tank testing using on-board sensors for hydrodynamic parameter estimations
- Bollard pull tests in immersion tank for thruster characteristics identification
- The least squares algorithm for determining unknown parameters from experimental data
- 6-DoF nonlinear model-based PID controller for controlling BlueROV2 Heavy in 6 DoFs

The next chapter describes the ROV BlueROV2 Heavy applied in this project as well as introduces its hardware, thrusters, capabilities and assumptions that can be made for the vehicle.

CHAPTER 3

EXPERIMENTAL PLATFORM: BLUEROV2 HEAVY

This chapter introduces the system of the ROV used in this thesis, named BlueROV2 Heavy (BlueRobotics 2018a). A brief introduction of the vehicle's hardware components, thrusters and capabilities is presented. Additionally, a list of assumptions made on the basis of BlueROV2 Heavy's features is presented.

3.1 BlueROV2 Heavy Overview

The Blue Robotics BlueROV2 Heavy, as shown in Figure 3.1, is an observation class mini ROV that is capable of depths of 100 metres. It is an upgraded configuration of BlueROV2 and includes four horizontal and four vertical thrusters of type T200 thrusters in order to produce 6-DoF control capacity. On the BlueROV2 Heavy, a companion computer uses a Raspberry Pi 3 as the processing unit, which is running Ubuntu 14.04 Robot Operating System (ROS), an open-source meta-operating system for software development of robot applications (Quigley, Conley et al. 2009). The Raspberry Pi 3 is connected to a 3DR Pixhawk autopilot and a live streaming HD video camera. The Pixhawk autopilot has multiple on-board sensors including a compass, gyroscopes and accelerometers that can determine the attitude of the vehicle. Moreover, an external water pressure sensor is also connected to the autopilot by I2C bus for depth measurement. The autopilot collects sensor data and sends control input signals to electronics speed controllers (ESC) for controlling thrusters whereas the companion computer streams HD video to the surface workstation. The ROV is self-powered by the use of an on-board battery that supports the vehicle up to 4 hours of continuous operation.

On the surface, a topside computer is likewise running Ubuntu 14.04 ROS and a gamepad controller is supported for manual operation. Communication between the ROV and the topside is made via a 300 metres long neutrally buoyant CAT5 tether cable connected at either end to a Fathom-X Tether interface board. Figure 3.2 depicts the hardware of ROV components and topside components as well as their communication.



Figure 3.1 The BlueROV2 Heavy Configuration Retrofit Kit (BlueRobotics 2018a)

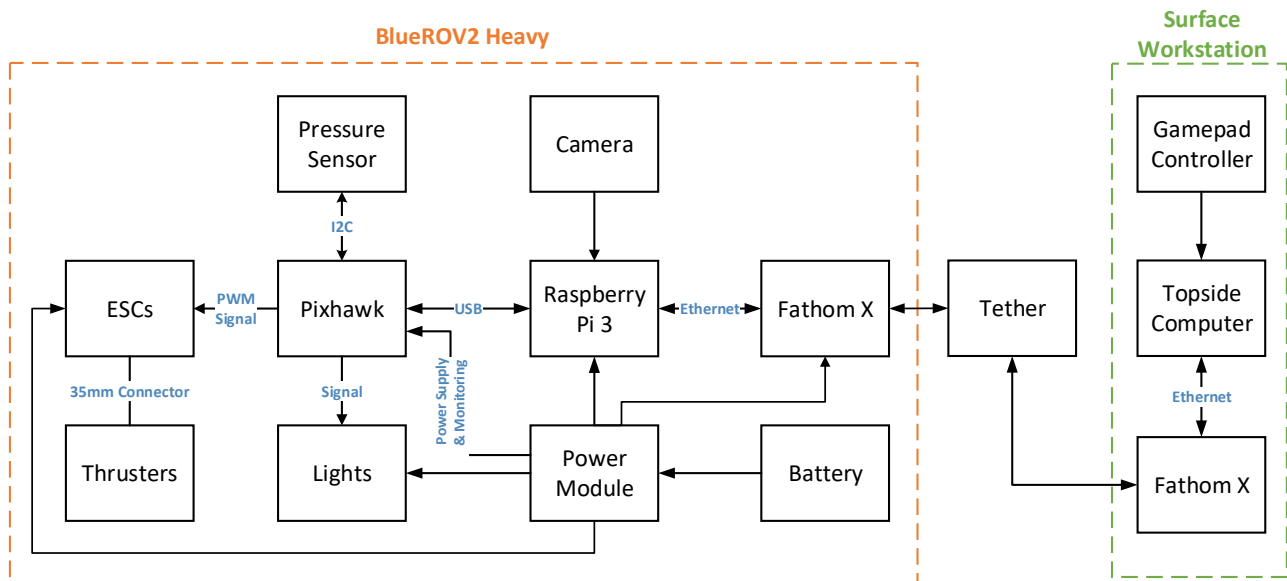


Figure 3.2 Diagram of hardware components on the BlueROV2 Heavy and the topside and their connections. Communication between BlueROV2 Heavy and the topside computer is made via Ethernet signals whereas connection between the on-board operating processing unit Raspberry Pi 3 and the autopilot Pixhawk is made through USB.

3.2 BlueROV2 Heavy Type T200 Thrusters

BlueROV2 Heavy has eight thrusters of type T200 thrusters (BlueRobotics 2018c) depicted in Figure 3.3 with four horizontal and four vertical thrusters as the configuration illustrated in Figure 3.4. BlueRobotics provides thrusters in clockwise and counter-clockwise propeller orientation to minimise torque reactions. In Figure 3.4, green thrusters and blue thrusters illustrate counter-clockwise propellers and clockwise propellers, respectively. These thrusters are controlled by pulse width modulation (PWM) signals sent from the Pixhawk autopilot to motor controllers.



Figure 3.3 The T200 Thruster of the BlueROV2 Heavy (BlueRobotics 2018c)

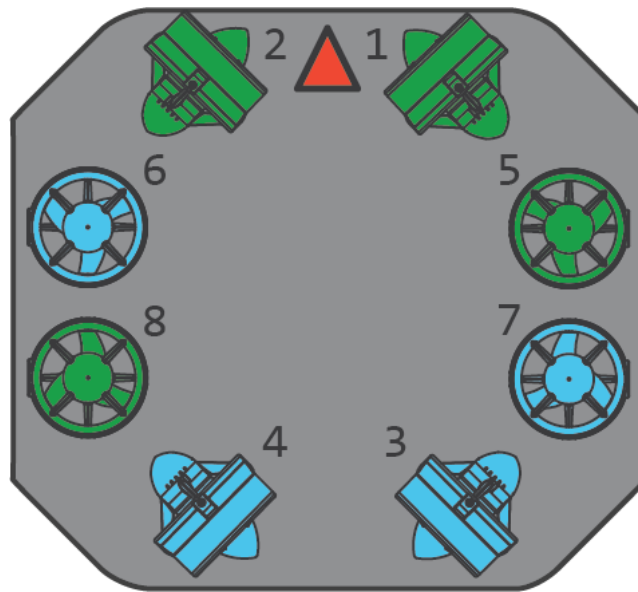


Figure 3.4 BlueROV2 Heavy thruster configuration from top-down view. Green and blue thrusters indicate counter-clockwise and clockwise propellers, respectively. (BlueRobotics 2018b).

The PWM signal ranges from 1100 to 1900. The maximum forward thrust (about 50 Newton at operating voltage of 16 V) is produced with PWM signal of 1900 and the maximum reverse thrust (about 40 Newton at operating voltage of 16 V) is produced with PWM signal of 1100. With the PWM signal of 1500, zero thrust occurs with a dead zone of ± 25 , meaning that zero thrust is produced within the PWM signal range between 1475 and 1525.

3.3 Assumptions of BlueROV2 Heavy on Dynamics

In Fossen (Fossen 2011), a complete 6-DoF dynamic model of kinetics for underwater vehicles written in vectorial representation is given by:

$$M\dot{v} + C(v)v + D(v)v + g(\eta) = \tau \quad (3.1)$$

These various matrices M , $C(v)$ and $D(v)$, and vector $g(\eta)$ (will be described in the following chapter) contain more than 300 unknown parameters in total. As a result, estimation of all parameters is infeasible. Yet, based on the features and operating speeds of the vehicle, several assumptions can be made to simplify the dynamic model and reduce the number of unknown parameters in the model. The assumptions that have been made for the dynamics of the BlueROV2 Heavy are listed in the following:

1. Since BlueROV2 Heavy operates at relative low speeds (i.e. less than 2 m/s), lift forces can be neglected.
2. BlueROV2 Heavy is assumed to have port-starboard symmetry and fore-aft symmetry; and the centre of gravity (CG) is assumed to be located in the symmetry planes.
3. BlueROV2 Heavy is assumed to be hydrodynamically symmetrical about 6-DoF. Accordingly, the motions between DoFs of the vehicle in hydrodynamic can be decoupled.
4. BlueROV2 Heavy is assumed to operate below the wave-affected zone. As a result, disturbances of waves on the vehicle are negligible.

3.4 Summary

An overview of the system of BlueROV2 Heavy was presented in this chapter. A number of assumptions made for the vehicle were also demonstrated. The following chapter discusses the mathematical modelling of BlueROV2 Heavy in 6-DoF along with applying these assumptions to simplify the dynamic model of the vehicle.

CHAPTER 4

MODELLING OF THE ROV

Mathematical models of an ROV will be developed in this chapter. Fundamental theories applied in this thesis for modelling an ROV are described in Fossen (Fossen 2011), which demonstrates the mathematical models for all types of marine vessels with full 6 DoFs. The dynamic equations of motion of an ROV adopted from Fossen's vectorial robot model (Fossen 2011) contain the kinematic equation (4.1) and the kinetic equation (4.2) as below:

$$\dot{\eta} = J(\eta)v \quad (4.1)$$

$$M\dot{v} + C(v)v + D(v)v + g(\eta) = \tau \quad (4.2)$$

The kinematics in (4.1) describes geometrical aspects of the ROV's motion in terms of motion representation in different coordinate systems whereas the kinetics in (4.2) analyses the forces and moments inducing the ROV's motion. These various matrices, vectors and their features in (4.1) and that in (4.2) will be described in Section 4.2 and Section 4.3, respectively while the notation used in generalised vectors of η, v and τ will be firstly introduced in Section 4.1. Section 4.3 will derive the 6-DoF forces and moments produced by thrusters for BlueROV2 Heavy and the distribution of generalised control forces to thrusters, which are thruster model and control allocation, respectively.

4.1 Notations

The motion of an ROV in 6 DoFs can be represented in a vectorial form using the SNAME notation (SNAME 1950) in Table 4.1 where six individual coordinates are generalised to describe the position and orientation; and their time derivatives describe the linear and angular velocities of the vehicle.

Table 4.1 The SNAME notation for marine vessels (SNAME 1950)

No.	DoF	Forces and moments	Linear and angular velocities	Positions and Euler angles
1	Surge	X	u	x
2	Sway	Y	v	y
3	Heave	Z	w	z
4	Roll	K	p	ϕ
5	Pitch	M	q	θ
6	Yaw	N	r	ψ

According to the SNAME notation (SNAME 1950), the generalised pose and velocity coordinates can be addressed by (4.3) and (4.4) vectors, respectively.

$$\eta = [x \ y \ z \ \phi \ \theta \ \psi]^T \quad (4.3)$$

$$v = [u \ v \ w \ p \ q \ r]^T \quad (4.4)$$

In addition, their sub-vectors are given by using the following vector notations:

Position $p = \begin{bmatrix} x \\ y \\ z \end{bmatrix} \in \mathbb{R}^3 \quad (4.5)$

Euler angles $\theta = \begin{bmatrix} \phi \\ \theta \\ \psi \end{bmatrix} \in SO(3) \quad (4.6)$

Linear velocity $v = \begin{bmatrix} u \\ v \\ w \end{bmatrix} \in \mathbb{R}^3 \quad (4.7)$

Angular velocity $\omega = \begin{bmatrix} p \\ q \\ r \end{bmatrix} \in \mathbb{R}^3 \quad (4.8)$

where \mathbb{R}^3 denotes the three dimensional of Euclidean space and $SO(3)$ indicates the three dimensional sphere in which three angles are defined on the interval of $[-\pi, \pi)$ for ϕ and ψ , and the interval of $(-\pi/2, \pi/2)$ for θ . Moreover, the force vector with components associating the 6 DoFs is given by (4.9), which describe the forces and moments acting on the ROV with its sub-vectors given by (4.10) and (4.11).

$$\tau = [X \ Y \ Z \ K \ M \ N]^T \quad (4.9)$$

$$\text{Force on ROV} \quad f = \begin{bmatrix} X \\ Y \\ Z \end{bmatrix} \in \mathbb{R}^3 \quad (4.10)$$

$$\text{Moment on ROV} \quad m = \begin{bmatrix} K \\ M \\ N \end{bmatrix} \in \mathbb{R}^3 \quad (4.11)$$

Therefore, the general motion of an ROV in 6 DoFs can be described by the following vectors:

$$\text{Position and orientation vector} \quad \eta = \begin{bmatrix} p \\ \theta \end{bmatrix} \in \mathbb{R}^3 \times SO(3) \quad (4.12)$$

$$\text{Linear and angular velocity vector} \quad v = \begin{bmatrix} v \\ \omega \end{bmatrix} \in \mathbb{R}^6 \quad (4.13)$$

$$\text{Force and moment vector} \quad \tau = \begin{bmatrix} f \\ m \end{bmatrix} \in \mathbb{R}^6 \quad (4.14)$$

4.2 Kinematic Model

4.2.1 Reference Frames

When modelling an ROV, the following two reference frames need to be defined to describe the motion:

- NED: The North East Down world frame with axes $\{n\} = (x_n, y_n, z_n)$ and origin o_n
- BODY: The body reference frame with axes $\{b\} = (x_b, y_b, z_b)$ and origin o_b

The NED world frame refers to the real world in which the x_n , y_n , and z_n axes point towards north, east and downwards normal to the Earth's surface, respectively. The origin o_n is defined at an arbitrary longitude and latitude position. The body frame of an ROV is a moving coordinate frame that is fixed to the vehicle. The origin o_b is generally defined at the geometric centre of the vehicle in order to exploit physical symmetries. As depicted in Figure 4.1, the x_b , y_b , and z_b axes point towards the ROV's forward direction, the right-hand side of the ROV and vertically downwards from the ROV, respectively. Both geographic reference frames use the right-handed Cartesian coordinate system.

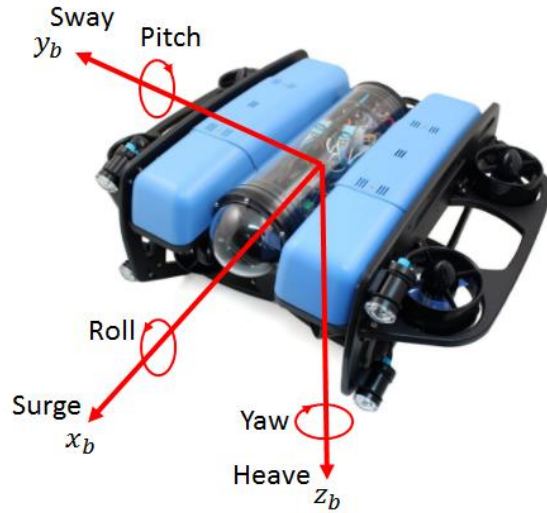


Figure 4.1 ROV Body Frame Coordinate System
Backing Image from BlueROV2 Heavy (BlueRobotics 2018a)

A vector that is decomposed in one coordinate frame can be transformed to another using a rotation matrix. For instance, $V^x \in \mathbb{R}^3$ is a vector V in reference frame x , and by applying the rotation matrix R_x^y , this vector can be transformed to the reference frame y , which is denoted $V^y \in \mathbb{R}^3$. This transformation operation of a vector V between two reference frames from x to y is then given by (4.15).

$$V^y = R_x^y V^x \quad (4.15)$$

Since the Newtonian mechanics are represented in the body frame by (4.2), (4.1) is used to convert it from the body frame $\{b\}$ to the NED world frame $\{n\}$ where the body-fixed velocity v is expressed in $\{b\}$ and the vehicle position η is expressed in $\{n\}$. In the next section, the kinematic relation between $\{b\}$ and $\{n\}$ in (4.1) will be presented.

4.2.2 Transformations Between BODY and NED

Euler Angle Transformation

The Euler angles Θ in (4.6), defining the rotation angles about the x , y , and z axes as roll ϕ , pitch θ , and yaw ψ , can be used in the velocity transformation between BODY and NED. The transformation for linear velocities from $\{b\}$ to $\{n\}$ is given by:

$$v^n = R_b^n(\Theta)v^b \quad (4.16)$$

where v^b and v^n are the linear velocity vectors in {b} and {n}, respectively; and $R_b^n(\Theta)$ is the rotation matrix from {b} to {n} and computed as:

$$R_b^n(\Theta) = R_z(\psi)R_y(\theta)R_x(\phi) \quad (4.17)$$

where

$$R_z(\psi) = \begin{bmatrix} \cos \psi & -\sin \psi & 0 \\ \sin \psi & \cos \psi & 0 \\ 0 & 0 & 1 \end{bmatrix} \quad (4.18)$$

$$R_y(\theta) = \begin{bmatrix} \cos \theta & 0 & \sin \theta \\ 0 & 1 & 0 \\ -\sin \theta & 0 & \cos \theta \end{bmatrix} \quad (4.19)$$

$$R_x(\phi) = \begin{bmatrix} 1 & 0 & 0 \\ 0 & \cos \phi & -\sin \phi \\ 0 & \sin \phi & \cos \phi \end{bmatrix} \quad (4.20)$$

Hence, the rotation matrix can be represented by:

$$R_b^n(\Theta) = \begin{bmatrix} \cos \psi \cos \theta & -\sin \psi \cos \phi + \cos \psi \sin \theta \sin \phi & \sin \psi \sin \phi + \cos \psi \cos \phi \sin \theta \\ \sin \psi \cos \theta & \cos \psi \cos \phi + \sin \phi \sin \theta \sin \psi & -\cos \psi \sin \phi + \sin \theta \sin \psi \cos \phi \\ -\sin \theta & \cos \theta \sin \phi & \cos \theta \cos \phi \end{bmatrix} \quad (4.21)$$

Similarly, the transformation of angular velocities is given by:

$$\dot{\Theta} = T_\Theta(\Theta)\omega^b \quad (4.22)$$

where ω^b and $\dot{\Theta}$ are the angular velocity vectors in {b} and {n}, respectively; and $T_\Theta(\Theta)$ is the angular transformation matrix from {b} to {n} and derived as:

$$T_\Theta(\Theta) = \begin{bmatrix} 1 & \sin \phi \tan \theta & \cos \phi \tan \theta \\ 0 & \cos \phi & -\sin \phi \\ 0 & \sin \phi / \cos \theta & \cos \phi / \cos \theta \end{bmatrix} \quad (4.23)$$

As a consequence, the 6-DoF kinematic equation can be represented in vector setting by:

$$\dot{\eta} = J(\eta)v \Leftrightarrow \begin{bmatrix} \dot{p} \\ \dot{\Theta} \end{bmatrix} = \begin{bmatrix} R_b^n(\Theta) & 0_{3 \times 3} \\ 0_{3 \times 3} & T_\Theta(\Theta) \end{bmatrix} \begin{bmatrix} v^b \\ \omega^b \end{bmatrix} \quad (4.24)$$

Hence, the transformation matrix from the vehicle body frame to the NED world reference frame using Euler angle transformation is given by:

$$J_\Theta(\eta) = \begin{bmatrix} R_b^n(\Theta) & 0_{3 \times 3} \\ 0_{3 \times 3} & T_\Theta(\Theta) \end{bmatrix} \quad (4.25)$$

Quaternions Transformation

In order to avoid the singularity and discontinuity of the Euler angles, the use of unit quaternions containing four parameters is an alternative method. According to the study of quaternion kinematics (Chou 1992), a quaternion q is defined as a complex number formed by four units:

$$q = [q_0 \ q_1 \ q_2 \ q_3]^T \quad (4.26)$$

where q_0 is a real parameter and the other three units are imaginary parameters. They can be determined by using one rotation θ around a unit vector $u = [u_1 \ u_2 \ u_3]^T$ (i.e. $|u| = 1$) as (Chou 1992):

The real part
$$q_0 = \cos \frac{\theta}{2} \quad (4.27)$$

The imaginary part
$$\begin{bmatrix} \varepsilon_1 \\ \varepsilon_2 \\ \varepsilon_3 \end{bmatrix} = \begin{bmatrix} u_1 \sin \frac{\theta}{2} \\ u_2 \sin \frac{\theta}{2} \\ u_3 \sin \frac{\theta}{2} \end{bmatrix} \quad (4.28)$$

As a consequence, the quaternion can be represented by:

$$q = \begin{bmatrix} q_0 \\ \varepsilon_1 \\ \varepsilon_2 \\ \varepsilon_3 \end{bmatrix} = \begin{bmatrix} \cos \frac{\theta}{2} \\ u_1 \sin \frac{\theta}{2} \\ u_2 \sin \frac{\theta}{2} \\ u_3 \sin \frac{\theta}{2} \end{bmatrix} = \begin{bmatrix} \cos \frac{\theta}{2} \\ u \sin \frac{\theta}{2} \end{bmatrix} \quad (4.29)$$

Since the unit quaternion satisfies $q^T q = 1$, the transformation matrix for linear velocity transformation in (4.30) is obtained given by (4.31).

$$\dot{p} = R_b^n(q)v^b \quad (4.30)$$

where

$$R_b^n(q) = \begin{bmatrix} 1 - 2(\varepsilon_2^2 + \varepsilon_3^2) & 2(\varepsilon_1\varepsilon_2 - \varepsilon_3\eta) & 2(\varepsilon_1\varepsilon_3 - \varepsilon_2\eta) \\ 2(\varepsilon_1\varepsilon_2 - \varepsilon_3\eta) & 1 - 2(\varepsilon_1^2 + \varepsilon_3^2) & 2(\varepsilon_2\varepsilon_3 - \varepsilon_1\eta) \\ 2(\varepsilon_1\varepsilon_3 - \varepsilon_2\eta) & 2(\varepsilon_2\varepsilon_3 - \varepsilon_1\eta) & 1 - 2(\varepsilon_1^2 + \varepsilon_2^2) \end{bmatrix} \quad (4.31)$$

In addition, the transformation matrix for angular velocity transformation in (4.32) is obtained given by (4.33).

$$\dot{q} = T_q(q)\omega^b \quad (4.32)$$

where

$$T_q(q) = \frac{1}{2} \begin{bmatrix} -\varepsilon_1 & -\varepsilon_2 & -\varepsilon_3 \\ \eta & -\varepsilon_3 & \varepsilon_2 \\ \varepsilon_2 & \eta & -\varepsilon_1 \\ -\varepsilon_2 & \varepsilon_1 & \eta \end{bmatrix} \quad (4.33)$$

As a result, the 6-DoF kinematic equation can be represented using the unit quaternions by seven equations for $\eta = [N \ E \ D \ \eta \ \varepsilon_1 \ \varepsilon_2 \ \varepsilon_3]^T$:

$$\dot{\eta} = J(\eta)v \Leftrightarrow \begin{bmatrix} \dot{p} \\ \dot{q} \end{bmatrix} = \begin{bmatrix} R_b^n(q) & 0_{3 \times 3} \\ 0_{4 \times 3} & T_q(q) \end{bmatrix} \begin{bmatrix} v^b \\ \omega^b \end{bmatrix} \quad (4.34)$$

Hence, the transformation matrix from the vehicle body frame to the NED world reference frame using quaternion representation is given by:

$$J_q(\eta) = \begin{bmatrix} R_b^n(q) & 0_{3 \times 3} \\ 0_{4 \times 3} & T_q(q) \end{bmatrix} \quad (4.35)$$

4.3 Kinetic Model

The kinetic dynamic equation of an ROV's motion in (4.2) is derived from the Newton-Euler formulation. In Equation (4.2), M is the system inertia matrix, $C(v)$ is the Coriolis and centripetal matrix, $D(v)$ is the hydrodynamic damping matrix, $g(\eta)$ is the vector of the gravitational and buoyancy forces, τ is the external force and moment vector acting on the ROV and v is the generalised velocity vector represented in $\{b\}$. If the water current is considered, since M and $C(v)$ contain rigid-body dynamics and hydrodynamic parts, the model can be expressed by:

$$M_{RB}\dot{v} + C_{RB}(v)v + M_A\dot{v}_w + C_A(v_w)v_w + D(v_w)v_w + g(\eta) = \tau \quad (4.36)$$

where $M_{RB} \in \mathbb{R}^{6 \times 6}$ and $M_A \in \mathbb{R}^{6 \times 6}$ are the rigid-body and added mass matrices, respectively; $C_{RB}(v) \in \mathbb{R}^{6 \times 6}$ is the rigid-body Coriolis and centripetal matrix induced by M_{RB} due to the rotation of the body frame about the NED world frame while $C_A(v) \in \mathbb{R}^{6 \times 6}$ is the added mass Coriolis and centripetal matrix induced by M_A due to the rotation of the body frame about the NED world frame, and v_w is the relative velocity vector determined by:

$$v_w = v - v_c \quad (4.37)$$

4.3.1 Rigid Body Dynamics

In accordance with the derivation of rigid body equations of motion by applying Newtonian formulation (Fossen 2011), the rigid-body mass matrix is computed as:

$$M_{RB} = \begin{bmatrix} m & 0 & 0 & 0 & mz_g & -my_g \\ 0 & m & 0 & -mz_g & 0 & mx_g \\ 0 & 0 & m & my_g & -mx_g & 0 \\ 0 & -mz_g & my_g & I_x & -I_{xy} & -I_{xz} \\ mz_g & 0 & -mx_g & -I_{yx} & I_y & -I_{yz} \\ -my_g & mx_g & 0 & -I_{zx} & -I_{zy} & I_z \end{bmatrix} \quad (4.38)$$

where m is the mass of the vehicle, I_x , I_y and I_z are the inertia moments about the x_b , y_b , and z_b axes in $\{b\}$, and $I_{xy} = I_{yx}$, $I_{xz} = I_{zx}$ and $I_{yz} = I_{zy}$ are the inertia products (Fossen 2011); $r_g = [x_g \ y_g \ z_g]^T$ is the position of the centre of gravity (CG) in relation to the centre of the vehicle. Since the origin of the body-frame o_b is placed at the geometric centre of the ROV, the vehicle has symmetry in the xz -plane (port-starboard) and xy -plane (fore-aft). Accordingly, the rigid-body mass matrix can be simplified as (4.39) in which $x_g = y_g = 0$ and $I_{xy} = I_{xz} = I_{yz} = 0$ are assumed whereas $z_g \neq 0$ under the consideration that CG might not be the origin of o_b on the z axis.

$$M_{RB} = \begin{bmatrix} m & 0 & 0 & 0 & mz_g & 0 \\ 0 & m & 0 & -mz_g & 0 & 0 \\ 0 & 0 & m & 0 & 0 & 0 \\ 0 & -mz_g & 0 & I_x & 0 & 0 \\ mz_g & 0 & 0 & 0 & I_y & 0 \\ 0 & 0 & 0 & 0 & 0 & I_z \end{bmatrix} \quad (4.39)$$

Subsequently, using the skew-symmetric cross-product operation on M_{RB} yields the result of the rigid-body Coriolis and centripetal matrix $C_{RB}(v)$ given by:

$$C_{RB}(v) = \begin{bmatrix} 0 & 0 & 0 & 0 & mw & 0 \\ 0 & 0 & 0 & -mw & 0 & 0 \\ 0 & 0 & 0 & mv & -mu & 0 \\ 0 & mw & -mv & 0 & I_z r & -I_y q \\ -mw & 0 & -mu & -I_z r & 0 & I_x p \\ mv & -mu & 0 & I_y q & -I_x p & 0 \end{bmatrix} \quad (4.40)$$

4.3.2 Vehicle Hydrodynamics

Added Mass and Coriolis

In hydrodynamic terms, the added mass matrix M_A and the added mass Coriolis and centripetal matrix $C_A(v)$ can be derived by applying an energy approach based upon Kirchhoff's equation (Fossen 2011). The added mass of an ROV in a fluid is determined by the added mass matrix M_A defined as:

$$M_A = - \begin{bmatrix} X_{\dot{u}} & X_{\dot{v}} & X_{\dot{w}} & X_{\dot{p}} & X_{\dot{q}} & X_{\dot{r}} \\ Y_{\dot{u}} & Y_{\dot{v}} & Y_{\dot{w}} & Y_{\dot{p}} & Y_{\dot{q}} & Y_{\dot{r}} \\ Z_{\dot{u}} & Z_{\dot{v}} & Z_{\dot{w}} & Z_{\dot{p}} & Z_{\dot{q}} & Z_{\dot{r}} \\ K_{\dot{u}} & K_{\dot{v}} & K_{\dot{w}} & K_{\dot{p}} & K_{\dot{q}} & K_{\dot{r}} \\ M_{\dot{u}} & M_{\dot{v}} & M_{\dot{w}} & M_{\dot{p}} & M_{\dot{q}} & M_{\dot{r}} \\ N_{\dot{u}} & N_{\dot{v}} & N_{\dot{w}} & N_{\dot{p}} & N_{\dot{q}} & N_{\dot{r}} \end{bmatrix} \quad (4.41)$$

where M_A is assumed to be a symmetrical matrix: $M_A = M_A^T$. The hydrodynamic derivatives are represented using the SNAME notation (SNAME 1950). For example, the hydrodynamic derivative $Z_{\dot{u}}$ is the hydrodynamic added mass force Z in the z direction (in heave) due to an acceleration \dot{u} along the x axis (in surge), expressed by:

$$Z_{\dot{u}} = \frac{\partial Z}{\partial \dot{u}} \quad (4.42)$$

Note that for most practical applications, the off diagonal terms of M_A are small compared with the diagonal ones. In particular, since motions between DoFs of BlueROV2 Heavy in hydrodynamic are assumed to be decoupled, the off diagonal terms of M_A can be neglected. Subsequently, the added mass matrix M_A can be simplified as:

$$M_A = - \begin{bmatrix} X_{\dot{u}} & 0 & 0 & 0 & 0 & 0 \\ 0 & Y_{\dot{v}} & 0 & 0 & 0 & 0 \\ 0 & 0 & Z_{\dot{w}} & 0 & 0 & 0 \\ 0 & 0 & 0 & K_{\dot{p}} & 0 & 0 \\ 0 & 0 & 0 & 0 & M_{\dot{q}} & 0 \\ 0 & 0 & 0 & 0 & 0 & N_{\dot{r}} \end{bmatrix} \quad (4.43)$$

Accordingly, the nonlinear hydrodynamic Coriolis and centripetal matrix $C_A(v)$, a function of added mass matrix, can be calculated as:

$$C_A(v) = \begin{bmatrix} 0 & 0 & 0 & 0 & z_{\dot{w}}w & 0 \\ 0 & 0 & 0 & -z_{\dot{w}}w & 0 & -X_{\dot{u}}u \\ 0 & 0 & 0 & -Y_{\dot{v}}v & X_{\dot{u}}u & 0 \\ 0 & -z_{\dot{w}}w & Y_{\dot{v}}v & 0 & -N_{\dot{r}}r & M_{\dot{q}}q \\ z_{\dot{w}}w & 0 & -X_{\dot{u}}u & N_{\dot{r}}r & 0 & -K_{\dot{p}}p \\ -Y_{\dot{v}}v & X_{\dot{u}}u & 0 & -M_{\dot{q}}q & K_{\dot{p}}p & 0 \end{bmatrix} \quad (4.44)$$

Hydrodynamic Damping

There are four major sources causing hydrodynamic damping for a marine craft, including potential damping, wave drift damping, skin friction and damping due to vortex shedding (Fossen 2011). Yet, the effects of potential damping and wave drift damping are neglected for underwater vehicles. Subsequently, the ROV damping $D(v)$ can be approximated with a linear damping term D_L caused by skin friction and a quadratic damping term $D_{NL}(v)$ mainly due to vortex shedding expressed by:

$$D(v) = D_L + D_{NL}(v) \quad (4.45)$$

Similarly, the damping matrix is derived to be diagonal due to decoupling such that the linear and quadratic damping matrices are given by (4.46) and (4.47), respectively.

$$D_L = -diag[X_u, Y_v, Z_w, K_p, M_q, N_r] \quad (4.46)$$

$$D_{NL}(v) = -diag[X_{u|u}|u|, Y_{v|v}|v|, Z_{w|w}|w|, K_{p|p}|p|, M_{q|q}|q|, N_{r|r}|r|] \quad (4.47)$$

where D_L and $D_{NL}(v)$ are determined from experiments. Hence, the overall hydrodynamic damping matrix $D(v)$ is obtained as:

$$D(v) = - \begin{bmatrix} X_u + X_{u|u}|u| & 0 & 0 & 0 & 0 & 0 \\ 0 & Y_v + Y_{v|v}|v| & 0 & 0 & 0 & 0 \\ 0 & 0 & Z_w + Z_{w|w}|w| & 0 & 0 & 0 \\ 0 & 0 & 0 & K_p + K_{p|p}|p| & 0 & 0 \\ 0 & 0 & 0 & 0 & M_q + M_{q|q}|q| & 0 \\ 0 & 0 & 0 & 0 & 0 & N_r + N_{r|r}|r| \end{bmatrix} \quad (4.48)$$

4.3.3 Hydrostatics

In hydrostatics, the forces and moments acting on the ROV due to the gravitational and buoyancy forces are called restoring forces. Given that m is the mass of the vehicle, g is the acceleration of gravity, ρ is the water density and ∇ is the volume of fluid displaced by the ROV, the weight of the body W and buoyancy force B are determined by:

$$W = mg \quad (4.49)$$

$$B = \rho g \nabla \quad (4.50)$$

The centre of buoyancy (CB) of the vehicle is defined as $r_b = [x_b, y_b, z_b]^T$. If the centre of the vehicle's body frame is placed at the centre of buoyancy, r_b becomes:

$$r_b = [0, 0, 0]^T \quad (4.51)$$

Since the vehicle has symmetry in the xz-plane and xy-plane, the position of the centre of gravity (CG) of the vehicle r_g becomes:

$$r_g = [x_g \ y_g \ z_g]^T = [0, 0, z_g]^T \quad (4.52)$$

Then the overall restoring force vector $g(\eta)$ can be calculated using Euler angle transformation written as:

$$g(\eta) = \begin{bmatrix} (W - B) \sin \theta \\ -(W - B) \cos \theta \sin \phi \\ -(W - B) \cos \theta \cos \phi \\ z_g W \cos \theta \sin \phi \\ z_g W \sin \theta \\ 0 \end{bmatrix} \quad (4.53)$$

Alternatively, the gravitational and buoyancy force vector $g(\eta)$ can be computed using quaternions expressed as:

$$g(\eta) = \begin{bmatrix} (B - W)(2\varepsilon_1\varepsilon_3 - 2\varepsilon_2\eta) \\ (B - W)(2\varepsilon_2\varepsilon_3 - 2\varepsilon_1\eta) \\ (W - B)(2\varepsilon_1^2 + 2\varepsilon_2^2 - 1) \\ z_g W(2\varepsilon_2\varepsilon_3 + 2\varepsilon_1\eta) \\ z_g W(2\varepsilon_1\varepsilon_3 - 2\varepsilon_2\eta) \\ 0 \end{bmatrix} \quad (4.54)$$

4.4 Thruster Model and Control Allocation

Thruster Model

The control force due to a thruster can be represented by (assuming linearity):

$$F = Ku \quad (4.55)$$

where u is the control input and K is the thrust coefficient, which is a scaling factor mapping from the control input to the thrust force. Since BlueROV2 Heavy contains 8 thrusters, the thruster forces can be represented using a vector $F = [F_1, F_2, F_3, F_4, F_5, F_6, F_7, F_8]^T$, the control inputs can be represented using a vector $u = [u_1, u_2, u_3, u_4, u_5, u_6, u_7, u_8]^T$, and the thrust coefficient K is a diagonal matrix expressed as:

$$K = \text{diag}[K_1, K_2, K_3, K_4, K_5, K_6, K_7, K_8] \quad (4.56)$$

Given the force vector $f = [F_x, F_y, F_z]^T$ and the moment arms $r = [l_x, l_y, l_z]^T$, the forces and moments in 6 DoFs can be determined by:

$$\tau = \begin{bmatrix} f \\ r \times f \end{bmatrix} = \begin{bmatrix} F_x \\ F_y \\ F_z \\ F_z l_y - F_y l_z \\ F_x l_z - F_z l_x \\ F_y l_x - F_x l_y \end{bmatrix} \quad (4.57)$$

Hence, considering BlueROV2 Heavy with 8 thrusters, the generalised forces and moments in 6 DoFs $\tau \in R^6$ due to 8 thrusters in terms of control inputs $u \in R^8$ can be then modelled as:

$$\tau = T(\alpha)F = T(\alpha)Ku \quad (4.58)$$

where $T = [t_1, t_2, t_3, t_4, t_5, t_6, t_7, t_8] \in \mathbb{R}^{6 \times 8}$ is the thrust configuration matrix and $\alpha \in R^8$ is the thrust rotation angle vector. As a consequence, the thrust configuration matrix T can be then computed by using Equation (4.57). Figure 4.2 depicts the top view, front view and section view of BlueROV2 Heavy thruster configuration. Accordingly, the moment arms of 8 thrusters relative to centre of gravity (CG) are computed and listed in Table 4.2.

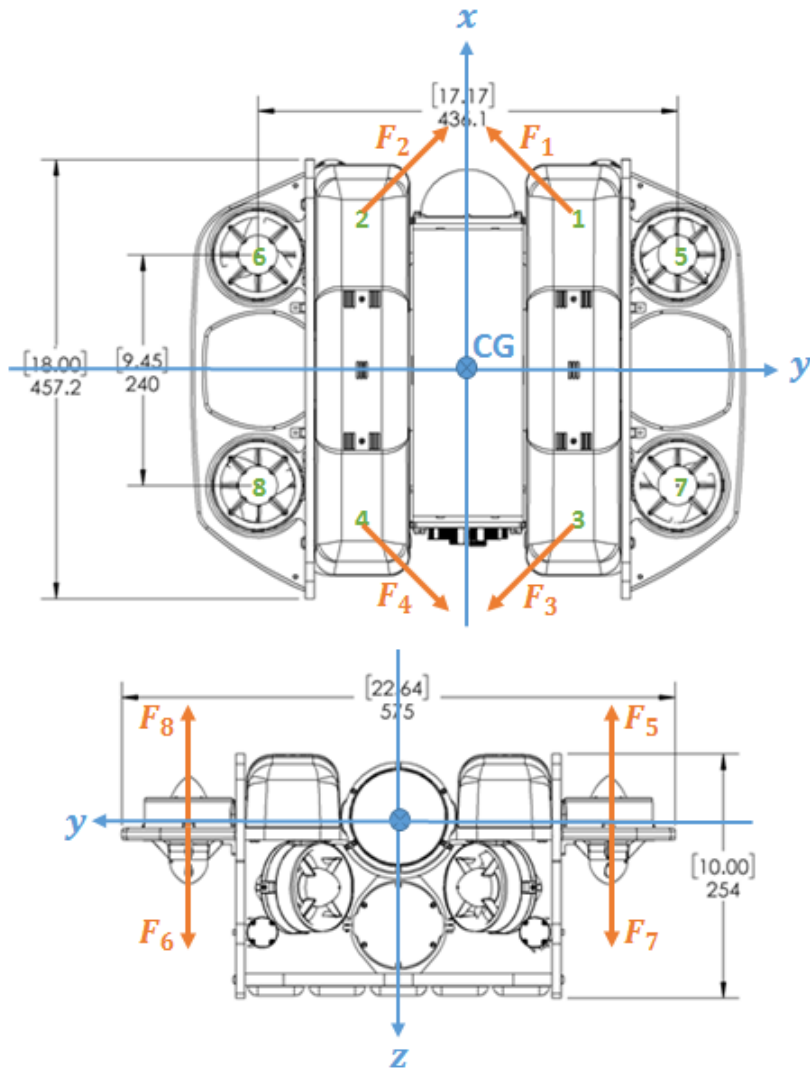


Figure 4.2 Top view and front view of BlueROV2 Heavy thruster configuration. Backing Image from BlueROV2 Heavy Retrofit Documentation (BlueRobotics 2018b).

Table 4.2 Moment arms of 8 thrusters of BlueROV2 Heavy

T_i	l_{xi} (mm)	l_{yi} (mm)	l_{zi} (mm)
T_1	156	111	85
T_2	156	-111	85
T_3	-156	111	85
T_4	-156	-111	85
T_5	120	218	0
T_6	120	-218	0
T_7	-120	218	0
T_8	-120	-218	0

The rotation angles for horizontal thrusters of T_1 to T_4 are $\pi/4$, $-\pi/4$, $-3\pi/4$ and $3\pi/4$, respectively and thruster T_5 to T_8 are vertical thrusters without horizontal rotations. Subsequently, the forces and moments produced by thruster T_1 can be computed by:

$$\tau_1 = \begin{bmatrix} F_{x1} \\ F_{y1} \\ F_{z1} \\ F_{z1}l_{y1} - F_{y1}l_{z1} \\ F_{x1}l_{z1} - F_{z1}l_{x1} \\ F_{y1}l_{x1} - F_{x1}l_{y1} \end{bmatrix} = \begin{bmatrix} F_1 \cos(\pi/4) \\ -F_1 \sin(\pi/4) \\ 0 \\ F_1 \sin(\pi/4) \times 0.085 \\ F_1 \cos(\pi/4) \times 0.085 \\ -F_1 \sin(\pi/4) \times 0.156 - F_1 \cos(\pi/4) \times 0.111 \end{bmatrix} = \begin{bmatrix} 0.707 \\ -0.707 \\ 0 \\ 0.06 \\ 0.06 \\ -0.1888 \end{bmatrix} F_1 \quad (4.59)$$

Hence,

$$t_1 = \begin{bmatrix} 0.707 \\ -0.707 \\ 0 \\ 0.06 \\ 0.06 \\ -0.1888 \end{bmatrix} \quad (4.60)$$

By following the same procedure, the forces and moments produced by total 8 thrusters are found to be:

$$\tau = T(\alpha)F = \begin{bmatrix} 0.707 & 0.707 & -0.707 & -0.707 & 0 & 0 & 0 & 0 \\ -0.707 & 0.707 & -0.707 & 0.707 & 0 & 0 & 0 & 0 \\ 0 & 0 & 0 & 0 & -1 & 1 & 1 & -1 \\ 0.06 & -0.06 & 0.06 & -0.06 & -0.218 & -0.218 & 0.218 & 0.218 \\ 0.06 & 0.06 & -0.06 & -0.06 & 0.120 & -0.120 & 0.120 & -0.120 \\ -0.1888 & 0.1888 & 0.1888 & -0.1888 & 0 & 0 & 0 & 0 \end{bmatrix} \begin{bmatrix} F_1 \\ F_2 \\ F_3 \\ F_4 \\ F_5 \\ F_6 \\ F_7 \\ F_8 \end{bmatrix} \quad (4.61)$$

Therefore, the thrust configuration matrix T for BlueROV2 Heavy is given by:

$$T = \begin{bmatrix} 0.707 & 0.707 & -0.707 & -0.707 & 0 & 0 & 0 & 0 \\ -0.707 & 0.707 & -0.707 & 0.707 & 0 & 0 & 0 & 0 \\ 0 & 0 & 0 & 0 & -1 & 1 & 1 & -1 \\ 0.06 & -0.06 & 0.06 & -0.06 & -0.218 & -0.218 & 0.218 & 0.218 \\ 0.06 & 0.06 & -0.06 & -0.06 & 0.120 & -0.120 & 0.120 & -0.120 \\ -0.1888 & 0.1888 & 0.1888 & -0.1888 & 0 & 0 & 0 & 0 \end{bmatrix} \quad (4.62)$$

Control Allocation

Control allocation computes the control input signal u to apply to the thrusters such that the overall desired control forces τ can be generalised. Since the control forces and moments due to thrusters with regard to control inputs are expressed by (4.58), the control input vector can be derived as:

$$u = K^{-1}T^{-1}\tau \quad (4.63)$$

However, since the thrust configuration matrix T for BlueROV2 Heavy is non-square, the Moore-Penrose pseudo-inverse T^+ is applied given by:

$$T^+ = T^T(TT^T)^{-1} \quad (4.64)$$

Hence, the control input vector u can be calculated as:

$$u = K^{-1}T^+\tau \quad (4.65)$$

4.5 Summary

The vectorial representation of dynamic model and the thruster model of BlueROV2 Heavy has been presented in this chapter while assumptions were applied to simplify the complex dynamic model. The derived models will be utilised extensively for the vehicle's system identification and control system design in the following chapters. The next chapter will demonstrate the estimation of unknown parameters in the derived models.

CHAPTER 5

SYSTEM IDENTIFICATION

In order to identify the system property of the BlueROV2 Heavy, the parameters in the dynamic and the thruster models derived in the last chapter need to be estimated. This chapter firstly presents a system identification approach that could be performed in the immersion tank with the use of on-board sensors. While the experimental platform is currently not available for estimating parameters experimentally, necessary parameters are determined by analysing the BlueROV2 Heavy's technical specifications (BlueRobotics 2018b) and published literature relating to BlueROV (Sandøy 2016).

5.1 System Identification Approach

The experimental system identification of a complete ROV model requires a complete state information that is complex, lengthy and expensive (Caccia, Indiveri et al. 2000). Several schemes for estimating parameters in the ROV model have been reviewed in Section 2.4. With the application of a system identification approach demonstrated in Indiveri (Indiveri 1998) and Caccia (Caccia, Indiveri et al. 2000), a methodology of immersion tank testing system identification using on-board sensors is proposed to identify the parameters in the dynamic model. This approach exploits the characteristics of the vehicle and assumes decoupling between DoFs in hydrodynamics. As a consequence, each DoF can be conducted independently and the experiments become highly repeatable. This approach involves a combination of static and dynamic experiments for each DoF and then utilises the least squares algorithm to estimate parameters from the experimental data.

Since each DoF can be treated individually, the dynamic model in Equation (4.2) can be adapted to be written into a single DoF as the following:

$$m_{\xi}\dot{\xi} + d_{\xi}\xi + d_{\xi|\xi}|\xi|\xi + g_{\xi} = \tau_{\xi} \quad (5.1)$$

where ξ is the velocity for a particular DoF, m_{ξ} represents the system inertial parameter containing rigid-body mass $m_{RB,\xi}$ and added mass $m_{A,\xi}$ components, d_{ξ} and $d_{\xi|\xi}$ are the

linear and quadratic damping parameters, g_ξ is the gravitational and buoyancy force and τ_ξ is the force applied to the vehicle; all the above parameters are for the considered DoF.

5.1.1 The Least Squares (LS) Technique

The least squares method is a commonly used regression analysis approach for approximating unknown parameters from overdetermined systems of equations by minimising the sum of residuals. Since the dynamic model in single DoF described in Equation (5.1) is a linear expression with respect to the parameters, the LS technique is used to estimate parameters for each DoF from a set of experimental data due to its ease of implementation. Equation (5.1) can be expressed in a regression form given by:

$$y = H\theta \quad (5.2)$$

where y is a vector of known values, H is a deterministic model matrix containing measured data from experiments, and θ represents the parameter vector that needs to be estimated. From the experimental data, the number of equations are larger than the number of unknown parameters, which is an overdetermined system. The LS technique is used to estimate the parameter θ by minimising the sum of squares of the residuals to fit the equations best. The parameter can be then estimated by using the following equation (Indiveri 1998):

$$\hat{\theta} = (H^T H)^{-1} H^T y \quad (5.3)$$

Additionally, the standard deviation of the estimated parameter is calculated given by:

$$\hat{\sigma}_\theta = \sqrt{\text{diag}(H^T H)^{-1} \hat{\sigma}^2} \quad (5.4)$$

where $\hat{\sigma}^2$ is the estimated Gaussian zero mean measurement noise variance given by:

$$\hat{\sigma}^2 = \frac{(y - H\hat{\theta})^T (y - H\hat{\theta})}{\text{dim}(y) - \text{dim}(\theta)} \quad (5.5)$$

The error of the estimated parameter is defined by:

$$\varsigma = \frac{\hat{\sigma}_\theta}{|\hat{\theta}|} \quad (5.6)$$

5.1.2 Static Experiments

Static experiments are utilised to identify damping parameters that concern measuring the velocity of the vehicle using on-board sensors when the steady-state speed condition holds. In static experiments, a particular force for a specific DoF is applied to the vehicle, and when the vehicle achieves the steady state speed, the velocity is constant whereas the acceleration is zero. Under this condition, this constant velocity and this particular force are recorded. For a single DoF, the dynamic model in (5.1) turns into:

$$d_{\xi}\dot{\xi} + d_{\xi|\xi}|\dot{\xi}| + g_{\xi} = \tau_{\xi} \quad (5.7)$$

where $\ddot{\xi} = 0$ and the system inertia term of m_{ξ} is eliminated from the model. Since the force τ_{ξ} and the gravitational and buoyance g_{ξ} are known, the linear damping term d_{ξ} and the quadratic damping term $d_{\xi|\xi}$ are the only unknown parameters that can be estimated by using the least squares technique for quadratic curve fitting of velocities ξ and drag forces (i.e. $\tau_{\xi} - g_{\xi}$). In the expression of Equation (5.2), for n inputs, the vector of known values y are drag forces for the considered DoF turning into:

$$y = \begin{bmatrix} \tau_{\xi,1} - g_{\xi} \\ \tau_{\xi,2} - g_{\xi} \\ \vdots \\ \tau_{\xi,n} - g_{\xi} \end{bmatrix} \quad (5.8)$$

The matrix H consists of the experimental data of constant velocities turning into:

$$H = \begin{bmatrix} \xi_1 & \xi_1|\xi_1| \\ \xi_2 & \xi_2|\xi_2| \\ \vdots & \vdots \\ \xi_n & \xi_n|\xi_n| \end{bmatrix} \quad (5.9)$$

The unknown parameter vector θ of damping turns into:

$$\theta = \begin{bmatrix} d_{\xi} \\ d_{\xi|\xi} \end{bmatrix} \quad (5.10)$$

Hence, the damping parameters can be estimated using Equation (5.3). By applying the same procedure for each 6 DoFs individually, damping parameters in 6 DoFs can be then attained.

5.1.3 Dynamic Experiments

Dynamic experiments are employed to identify inertia parameters that involve measuring the acceleration and velocity of the vehicle when the vehicle is accelerating. In dynamic experiments, a sinusoidal force for a specific DoF is provided to the vehicle while measuring the acceleration and the velocity of the vehicle using on-board sensors. Since the parameters of damping terms have been identified in the static experiments, the remaining parameters of the inertial term can now be determined. For a single DoF, the dynamic model in (5.1) can be rearranged to the following:

$$m_{\xi}\ddot{\xi} = \tau_{\xi} - g_{\xi} - d_{\xi}\dot{\xi} - d_{\xi|\xi}|\dot{\xi}|\xi| \quad (5.11)$$

where terms of τ_{ξ} , g_{ξ} , d_{ξ} and $d_{\xi|\xi}$ are known; therefore, the only unknown term of inertia parameter m_{ξ} can be estimated utilising the least squares technique where y , H and θ are now turning into:

$$y = \begin{bmatrix} \tau_{\xi,1} - g_{\xi} - d_{\xi}\dot{\xi}_1 - d_{\xi|\xi}|\dot{\xi}_1|\xi_1 \\ \tau_{\xi,2} - g_{\xi} - d_{\xi}\dot{\xi}_2 - d_{\xi|\xi}|\dot{\xi}_2|\xi_2 \\ \vdots \\ \tau_{\xi,n} - g_{\xi} - d_{\xi}\dot{\xi}_n - d_{\xi|\xi}|\dot{\xi}_n|\xi_n \end{bmatrix} \quad (5.12)$$

$$H = \begin{bmatrix} \dot{\xi}_1 \\ \dot{\xi}_2 \\ \vdots \\ \dot{\xi}_n \end{bmatrix} \quad (5.13)$$

$$\theta = m_{\xi} \quad (5.14)$$

Similarly, the system inertia parameter can be estimated using Equation (5.3). Note that the system inertia parameter m_{ξ} includes containing rigid-body mass $m_{RB,\xi}$ and added mass $m_{A,\xi}$ where the rigid-body mass is known from an a priori information of measured data of the vehicle. Hence, the added mass can be attained by:

$$m_{A,\xi} = \hat{m}_{\xi} - m_{RB,\xi} \quad (5.15)$$

Likewise, by applying the same procedure for each 6 DoFs individually, system inertia parameters in 6 DoFs can be obtained.

5.2 Parameter Determination

Due to the lack of the access to BlueROV2 Heavy, the system identification experiments have not been able to be carried out. As a consequence, the parameters in the dynamic models were determined by analysing the BlueROV2 Heavy's technical specifications (BlueRobotics 2018b) and available published literature relating to the BlueROV (Sandøy 2016). Technical specifications of the BlueROV2 Heavy from BlueRobotics (BlueRobotics 2018b) provide the vehicle's physical information such as mass of 11.5 kg and net buoyancy of 0.2 kg. Accordingly, the weight of the body and the buoyancy force are computed in Equation (5.16) and Equation (5.17), respectively.

$$W = mg = 11.5 \times 9.81 = 112.8 (N) \quad (5.16)$$

$$B = \text{Net Buoyancy} + W = 0.2 \times 9.81 + 112.8 = 114.8(N) \quad (5.17)$$

In previous BlueROV research by Sandøy, the distance between the centre of gravity (CG) and the centre of buoyance (CB) was found to be 0.00019 metres. In the case of BlueROV, the thruster configuration can only produce 4-DoF control of surge, sway, heave and yaw. Accordingly, roll and pitch motions are passively stable such that a reasonable distance between CG and CB is required to produce adequate restoring forces to keep the vehicle stable; however, the value of 0.00019 metres is not conceivable for this circumstance. As a result, a representative value of 0.02 metres was chosen. By placing the centre of the vehicle's body frame at the centre of buoyancy, $r_b = [0, 0, 0]^T$. Under the assumption of the centre of gravity with respect to the centre of buoyancy is 0.02 metres, $r_g = [0, 0, 0.02]^T$. Since there is no available parameter information in roll and pitch motions (considered negligible) from previous BlueROV research, the inertia moments about x_b , y_b , and z_b axes for BlueROV2 Heavy are assumed to be identical and determined using the yaw moment of inertia data from Sandøy. Ergo the a priori information is produced as shown in Table 5.1 that can be used to form the restoring force and moment vector and the rigid-body mass matrix.

The unknown hydrodynamic parameters of the added mass and damping were also determined by analysing published literature from Sandøy as illustrated in Table 5.2 and Table 5.3, respectively. Likewise, due to the limited information for roll and pitch motions, the added mass about x_b , y_b , and z_b axes are assumed to be identical and determined by

the data of yaw motion as well as for the damping parameter determination. The determined and computed parameters from Table 5.1 to Table 5.3 will be used to perform control system design simulations for the vehicle.

Table 5.1 A Priori information for parameters in rigid body dynamics and restoring forces

Parameter	Value
m	11.5 (kg)
W	112.8 (N)
B	114.8 (N)
r_b	$[0, 0, 0]^T$ (m)
r_g	$[0, 0, 0.02]^T$ (m)
I_x	0.16 (kg m ²)
I_y	0.16 (kg m ²)
I_z	0.16 (kg m ²)

Table 5.2 Determined added mass parameters

DoF	Added Mass	Value
Surge	$X_{\dot{u}}$	-5.5 (kg)
Sway	$Y_{\dot{v}}$	-12.7 (kg)
Heave	$Z_{\dot{w}}$	-14.57 (kg)
Roll	$K_{\dot{p}}$	-0.12 (kg m ² /rad)
Pitch	$M_{\dot{q}}$	-0.12 (kg m ² /rad)
Yaw	$N_{\dot{r}}$	-0.12 (kg m ² /rad)

Table 5.3 Determined linear and quadratic damping parameters

DoF	Linear Damping	Value	Quadratic Damping	Value
Surge	X_u	-4.03 (Ns/m)	$X_{u u }$	-18.18 (Ns ² /m ²)
Sway	Y_v	-6.22 (Ns/m)	$Y_{v v }$	-21.66 (Ns ² /m ²)
Heave	Z_w	-5.18 (Ns/m)	$Z_{w w }$	-36.99 (Ns ² /m ²)
Roll	K_p	-0.07 (Ns/rad)	$K_{p p }$	-1.55 (Ns ² /rad ²)
Pitch	M_q	-0.07 (Ns/rad)	$M_{q q }$	-1.55 (Ns ² /rad ²)
Yaw	N_r	-0.07 (Ns/rad)	$N_{r r }$	-1.55 (Ns ² /rad ²)

5.3 Thrust Identification

Since the thrust force applied to the ROV in the dynamic model is based on the control input from the motors, it is necessary to identify the thrust coefficient that represents the mapping from the control input signal to the thrust force. The thrust force can have considerable loss due to the effect of thruster-thruster and thruster-hull interactions. Hence, the bollard pull test in immersion tank is proposed to identify thrust characteristics experimentally. In this test, BlueROV2 Heavy is attached to a bracket that is connected to a 6-axis load cell. Thereupon, the thrust forces in 6-DoF are measured from the load cell while applying control input signals to thruster motors. Thruster coefficients can then be estimated with the use of the least squares technique explained in Section 5.1.

However, as BlueROV2 Heavy is not yet available for performing the immersion tank bollard pull tests, the thrust coefficient is alternatively identified making use of thrust mappings data of T200 thruster illustrated in Figure 5.1 provided by BlueRobotics (BlueRobotics 2018c) at this stage. Within the PWM operating range, the map depicts linear relationships with input signal and a zero thrust dead zone. The linear relationships are used to approximate the thrust coefficient of Equation (4.56) in the thrust model of Equation (4.58) discussed in Section 4.4. Since the eight thrusters of BlueROV2 Heavy are identical using T200 and the maximum thrust produced is about 40 Newton at least (including forward and reverse directions) at operating voltage of 16 V, the thrust coefficients of K_1 to K_8 in Equation (4.56) are approximated to 40. Therefore, the thrust coefficient matrix K is determined as below:

$$K = \text{diag}[40, 40, 40, 40, 40, 40, 40, 40] \quad (5.20)$$

5.4 Summary

In this chapter, a system identification approach of immersion tank testing has been demonstrated for identifying parameters in the vehicle's mathematical models derived in Chapter 4. Although these tests could not be executed due to the unavailability of the experimental platform, the unknown parameters were currently determined by making use of the BlueROV2 Heavy's technical specifications and published literature relating to the BlueROV. The next chapter will then use these determined parameters to perform simulations of control system design for BlueROV2 Heavy.

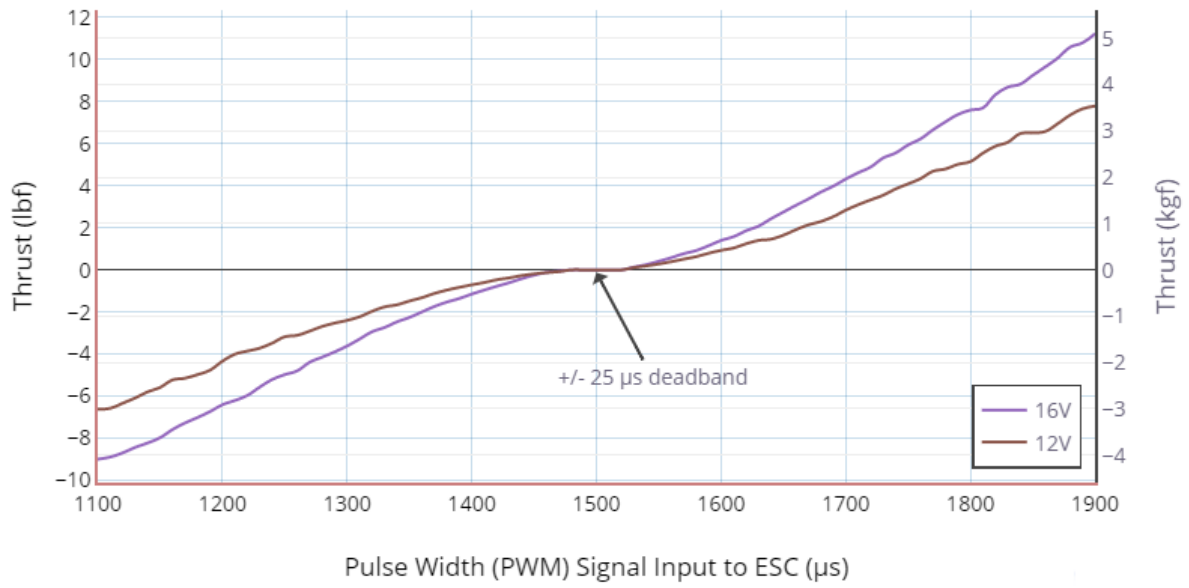


Figure 5.1 T200 thruster: thrust vs control input signal mapping (BlueRobotics 2018c)

CHAPTER 6

CONTROL OF THE ROV

The control of an ROV involves a number of challenges due to complex nonlinear forces acting on the vehicle, uncertainties in the dynamic model as well as unpredictable disturbances from the environment. Currently, the BlueROV2 Heavy can be controlled by an operator through a gamepad controller that sends command signals to the vehicle. Figure 6.1 depicts the currently supported open-loop control system block diagram for BlueROV2 Heavy. While this type of control systems has a simple layout, they have low accuracy due to the lack of a feedback mechanism. Therefore, they are only suitable for manual operations.

Automated control is a behaviour of regulating a process without requiring human operations where a feedback mechanism is essential to produce a reliable result. Figure 6.2 depicts the feedback (or closed-loop) control system block diagram for an ROV in which the observer provides the feedback of output (i.e. an estimate of the ROV's current state), a reference model provides the desired state for the vehicle, and the feedback controller uses the difference between the desired output and the measured value of output to produce control forces. Note that both Figure 6.1 and Figure 6.2 are ideal circumstances without disturbances effecting the ROV.

This chapter presents two controller techniques individually applied in the design of control systems. The simulation study of each control algorithm is demonstrated and robustness analysis of these control systems is examined by using Monte Carlo method.

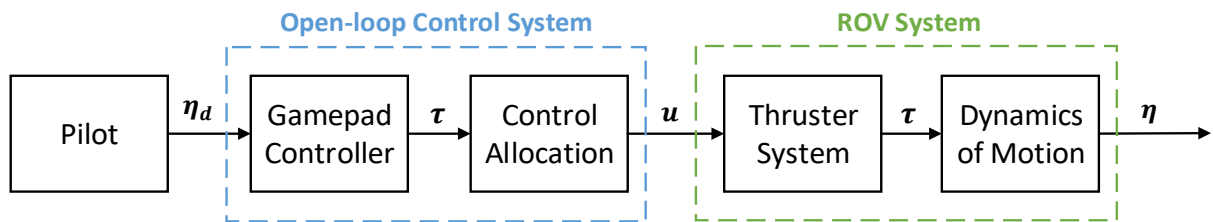


Figure 6.1 Open-loop control system block diagram (currently supported for BlueROV2 Heavy)

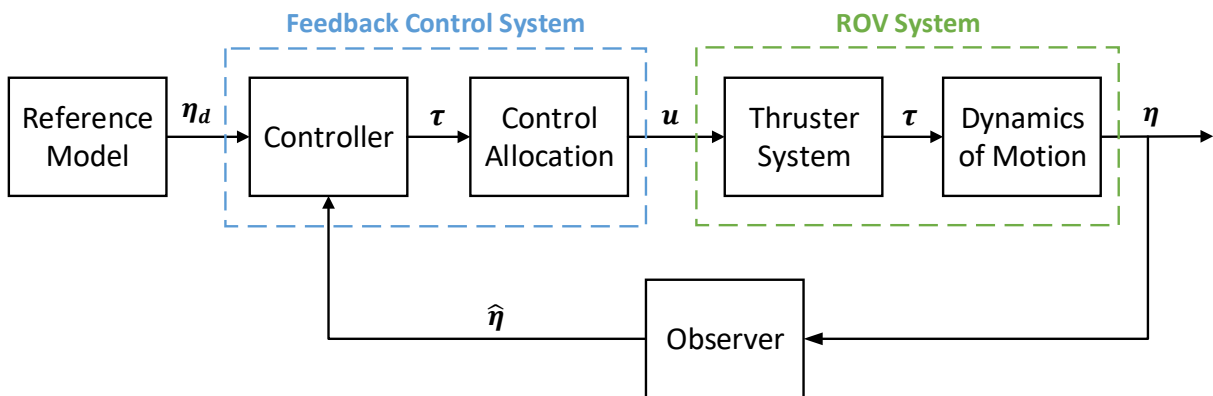


Figure 6.2 Feedback control system block diagram

6.1 Control System Design

The control system of underwater vehicles contains a controller (or control law) component and a control allocation component. The controller generates control forces that need to be provided for the vehicle whereas the control allocation distributes these control forces to the thrusters of the vehicle. Control allocation can be implemented by using Equation (4.65) in Section 4.4 while a range of controller design strategies that have been implemented on underwater vehicles are discussed in Section 2.2. Due to the simplicity and flexibility of the PID control algorithm, a linear conventional PID controller and a nonlinear model-based PID controller are chosen and individually applied for designing a 6-DoF control system to control the position of the BlueROV2 Heavy. This section presents how these algorithms are designed for controlling an ROV.

6.1.1 Linear Conventional PID Control

The fundamentals of the PID controller is to utilise an error signal that is generated from the difference between the desired state and the current state of the plant. For controlling the position of the ROV in order for the vehicle to follow a certain trajectory, this can be expressed by:

$$e = \eta_d - \eta \quad (6.1)$$

where e is called the tracking error, η_d is the desired position of the ROV and η is the current position of the ROV. This error signal in the body frame e^b is then employed to produce a corrective action by applying forces to the vehicle. The generated force by PID is given by:

$$\tau_{PID} = K_P e^b(t) + K_I \int_0^t e^b(t') dt' + K_D \frac{de^b(t)}{dt} \quad (6.2)$$

where K_P is the proportional gain, K_I is the integral gain, K_D is the derivative gain, and e^b is the error signal in the body frame determined by:

$$e^b = J^T(\eta)e \quad (6.3)$$

In the design of 6-DoF control for BlueROV2 Heavy, a simple multi-DoF PID controller is comprised of six uncoupled single DoF controllers such that each controller is designed for each DoF. In this design, a heuristic method of the Ziegler-Nichols tuning method (Ziegler and Nichols 1942) was utilised to tune the gains of the PID controller due to its feasibility and simplicity. A relative high proportional and derivative gains were produced to rapidly response to desired positions and provide damping to the motion of the vehicle, respectively whereas a small integral gain was utilised for adjusting the steady-state error.

A block diagram of the linear conventional PID control system for the ROV is illustrated in Figure 6.3 where Equation (6.2) is employed for the 6-DoF PID controller that takes the position tracking error in the body frame e^b to generate forces and moments in 6 DoFs while Equation (4.65) is utilised for the control allocation.

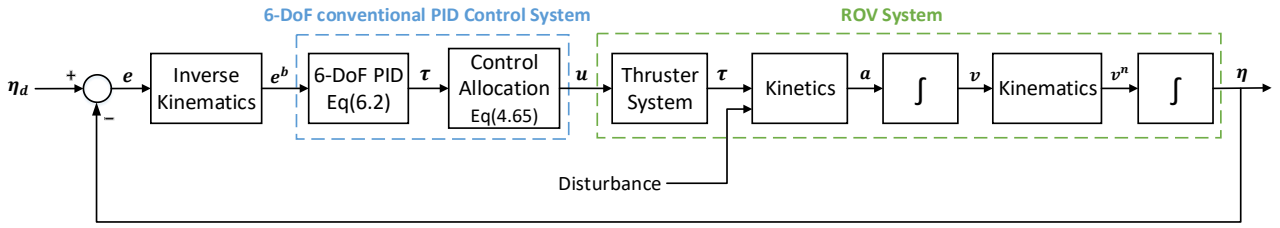


Figure 6.3 Linear conventional PID control system block diagram

In the ROV system, firstly, thruster system generates control forces in 6 DoFs. Then kinetics determines the acceleration in the body frame for the given forces, and kinematics defines the vehicle's velocity in the world frame v^n due to the velocity in the body frame. Note that disturbances from the environment influences the dynamics of motion of the ROV. Lastly, the position of the vehicle is determined in the next integrator and then fed back into the controller after being transformed to the body frame using inverse kinematics.

6.1.2 Nonlinear Model-based PID Control

The concept of the model-based control is to integrate a plant model of dynamics into the control system. Since the dynamic properties of the ROV is highly nonlinear, exploiting the understanding of the vehicle's dynamics is beneficial to providing an efficient control in comparison to the traditional approach. In the nonlinear model-based PID control system design, the dynamic model of the ROV is utilised to produce a 6-DoF predictive force and the model-based PID is used to provide a corrective force in 6 DoFs to adjust the error in the model. This is advantageous in that the model error and nonlinearities tend to be smaller than the dynamics themselves.

In the predictive force generation, a virtual reference trajectory strategy is introduced for the design of trajectory tracking. With the use of a scalar measure of tracking in Fossen (Fossen 1994), a virtual reference x_r can be defined that satisfies:

$$\dot{x}_r = \dot{x}_d + \lambda e^b \quad (6.4)$$

where $\lambda > 0$ is the control bandwidth that describes the amount of tracking error to the overall tracking performance, and e^b is the tracking error in the body frame given by (6.3). Since the velocity v is the time derivative of the position (i.e. $v = \dot{\eta}$), for a defined virtual reference position η_r , the following is satisfied:

$$v_r = v_d + \lambda e^b \quad (6.5)$$

where v_r is called virtual reference velocity and v_d represents the desired velocity. Furthermore, the virtual reference acceleration \dot{v}_r is given by:

$$\dot{v}_r = \dot{v}_d + \lambda(v_d - v) \quad (6.6)$$

where \dot{v}_d represents the desired acceleration and v represents the current velocity. Accordingly, a predictive force produced by the dynamic model of kinetic equation takes the form:

$$\tau_M = M\dot{v}_r + C_{RB}(v)v + C_A(v_w)v_w + D(v_w)v_{wr} + g(\eta) \quad (6.7)$$

where $v_w = v - v_c$ is relative velocity defined in Section 4.3 and v_{wr} is relative virtual reference velocity determined by:

$$v_{wr} = v_r - v_c = v_d + \lambda e^b - v_c \quad (6.8)$$

Hence, the resulting predictive force by the model is given by:

$$\tau_M = M(\dot{v}_d + \lambda(v_d - v)) + C_{RB}(v)v + C_A(v_w)v_w + D(v_w)(v_d + \lambda e^b - v_c) + g(\eta) \quad (6.9)$$

In addition to the predictive force, the PID controller based on the dynamic model is utilised to adjust the error in the model applying Equation (6.2) with relatively small gains of the PID. Thereupon, the nonlinear model-based PID controller takes the sum of the predictive force by the dynamic model and the corrective force by the PID given by:

$$\tau = \tau_M + \tau_{PID} \quad (6.10)$$

Finally, the control law for the nonlinear model-based PID controller is computed given by:

$$\begin{aligned} \tau = & M(\dot{v}_d + \lambda(v_d - v)) + C_{RB}(v)v + C_A(v_w)v_w + D(v_w)(v_d + \lambda e^b - v_c) + g(\eta) \\ & + K_P e^b(t) + K_I \int_0^t e^b(t') dt' + K_D \frac{de^b(t)}{dt} \end{aligned} \quad (6.11)$$

Figure 6.4 represents a block diagram of the nonlinear model-based PID control system for the ROV in which the 6-DoF predictive force is produced by applying Equation (6.9) and a 6-DoF corrective force is generated by using Equation (6.2) resulting the overall form of Equation (6.11). The state information of position and velocity of the ROV is fed back into the model-based controller for keeping up the respective tracking errors. External disturbance such as water current is also fed into the controller such that the model-based control system takes account of the current effect on the vehicle.

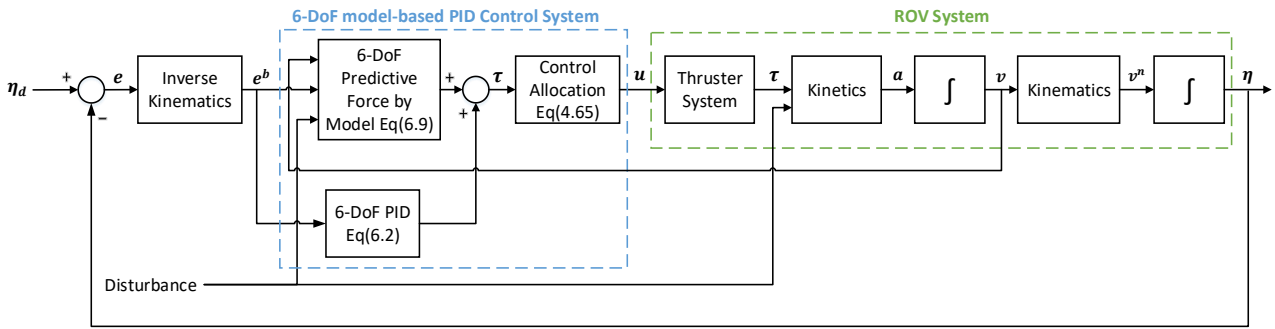


Figure 6.4 Nonlinear model-based PID control system block diagram

6.2 Control System Simulations & Result Analysis

In order to verify the designed control systems in Section 6.1, a simulation study is undertaken. The position tracking controller in Figure 6.3 and Figure 6.4 are implemented using Equation (6.2) and (6.11) respectively, whereas the ROV plant is implemented using the BlueROV2 Heavy model derived in Chapter 4 along with the determined parameters in Section 5.2 and 5.3. The ROV's current state information is assumed to be obtained from the on-board sensors of the vehicle and the theoretical values are simulated using the output of the ROV model. In order to simulate 6-DoF control of ROV's position, simulations of step responses are firstly performed for each DoF individually. Following this, a reference trajectory is generated for the ROV to follow. Simulations will be carried out in Matlab Simulink and simulation results will be presented in this section.

6.2.1 Linear Conventional PID Control

By using the Ziegler-Nichols tuning method (Ziegler and Nichols 1942), the gains of the 6-DoF PID controller are tuned as listed in Table 6.1 in the simulation.

Table 6.1 The gains used in the 6-DoF PID controller

6-DoF PID	Surge	Sway	Heave	Roll	Pitch	Yaw
K_P	3	3	3	4	4	2
K_I	0.2	0.2	0.2	0.3	0.3	0.1
K_D	2.5	2.5	0.5	0.5	1	0.5

For all simulations, the initial position of the ROV was set to a depth of 10 m as below:

$$\eta = [0 \ 0 \ 10 \ 0 \ 0 \ 0]^T \quad (6.12)$$

Note that the vehicle's position η is expressed in the NED world frame $\{n\}$. The simulation results of step responses for 6 DoFs by the 6-DoF conventional PID controller are shown in Figure 6.5. It can be seen that although there are some significant overshoot in surge and sway motions, overall motion in each DoF was controlled such that all motions have converged to their goal positions. However, for certain DoFs, it requires a fair amount of time to converge especially in roll, pitch and heave motions.

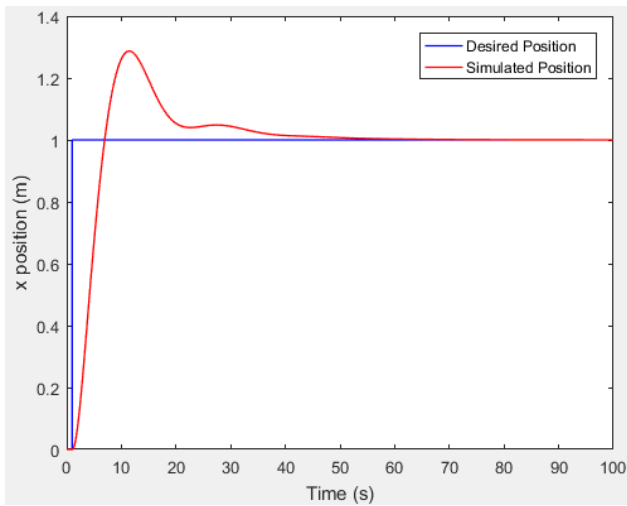
The second simulation sector of path following involves a generated path for the desired position that is set to be:

$$\eta_d = [0 \ 0 \ 10 \ 0 \ 0 \ 0]^T \rightarrow [5 \ 0 \ 10 \ 0 \ 0 \ 0]^T \rightarrow [5 \ 5 \ 10 \ 0 \ 0 \ 0]^T \rightarrow [0 \ 5 \ 10 \ 0 \ 0 \ 0]^T \quad (6.13)$$

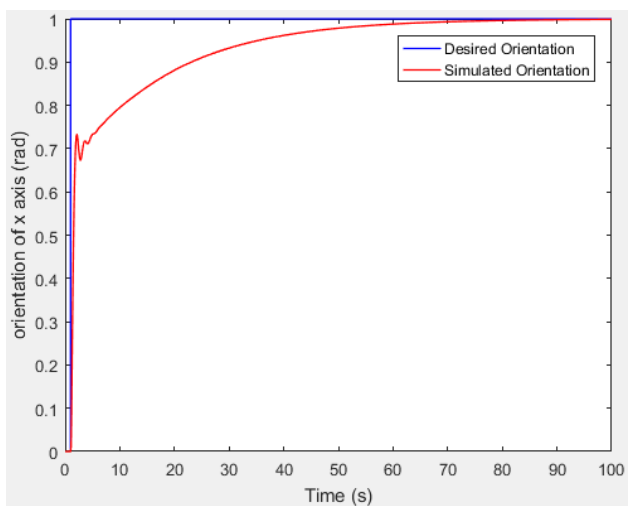
Figure 6.6 presents the path following simulation results in 3D and 2D of xy plane perspectives while no external disturbance is applied whereas Figure 6.7 shows that while the disturbance of water current is applied on the x and y position with current speed of 0.1 m/s, meaning that the velocity of water current in 6-DoF is given by:

$$v_c = [0.1 \ 0.1 \ 0 \ 0 \ 0 \ 0]^T \quad (6.14)$$

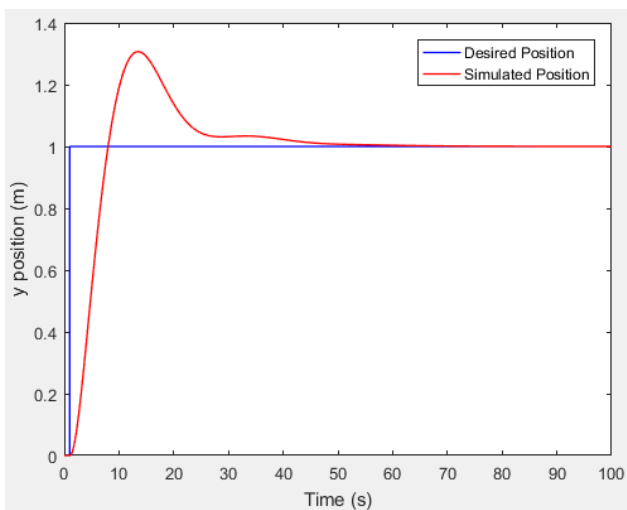
Note that the green arrow describes the direction of the generated path; and the orange arrow represents the direction of the water current. As can be seen in Fig. 6.6, the system follows the path well and achieves the goal positions even though with overshoots in x and y directions when there is no disturbance affecting the system. However, Fig. 6.7 reveals that after adding current disturbance, the system does not follow the path sufficiently. This is because the dynamic property of the ROV is highly nonlinear, the linear PID control system cannot cope with the dynamic effects of external forces on the vehicle efficiently.



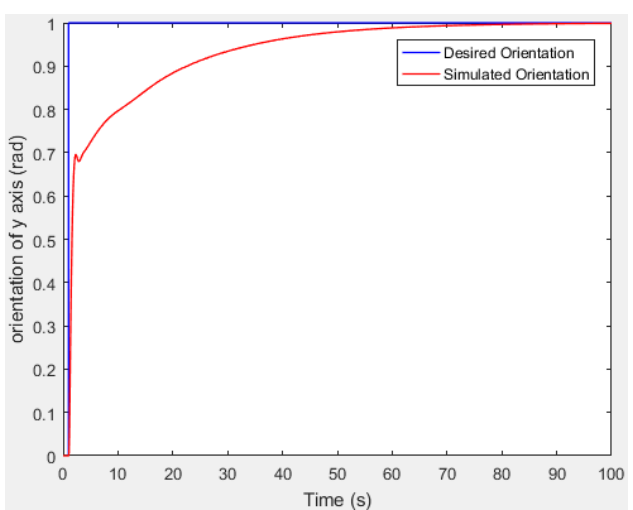
(a) Surge motion



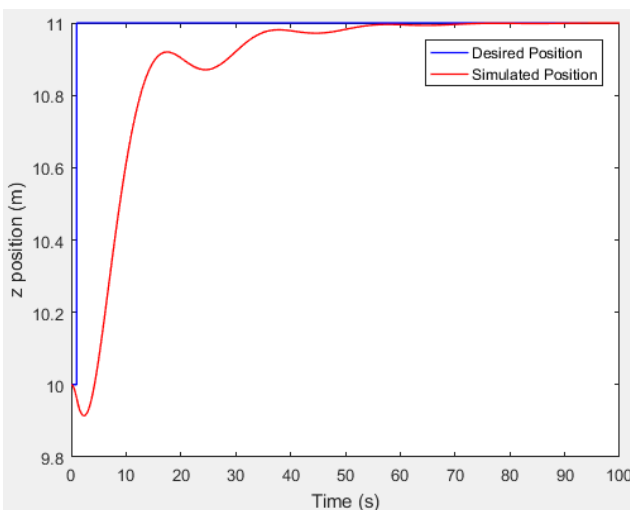
(b) Roll motion



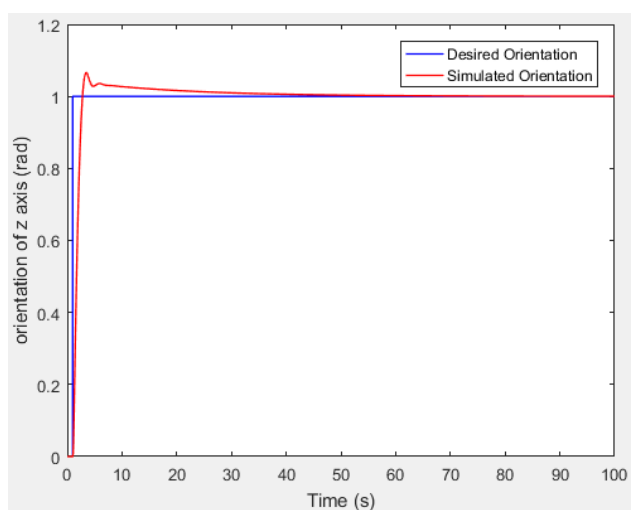
(c) Sway motion



(d) Pitch motion

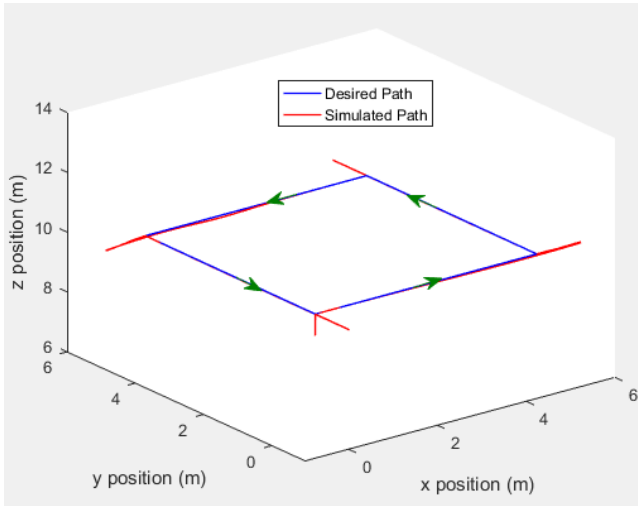


(e) Heave motion

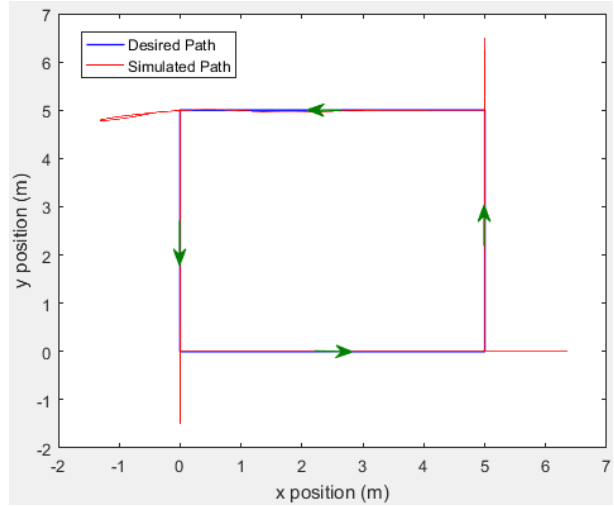


(f) Yaw motion

Figure 6.5 Step responses for the position in 6 DoFs using conventional PID

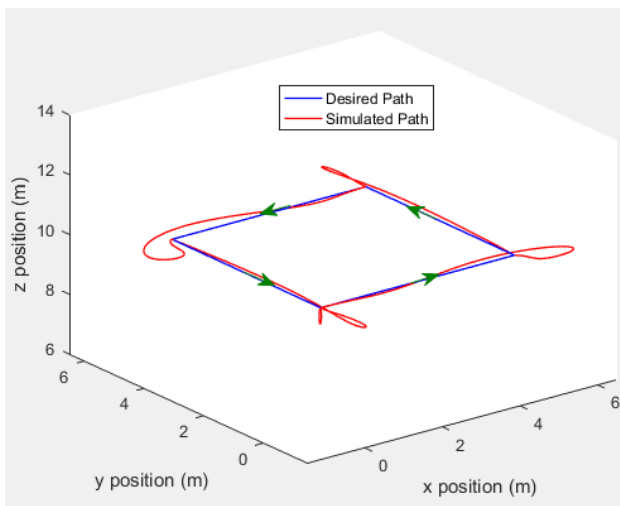


(a) 3D view

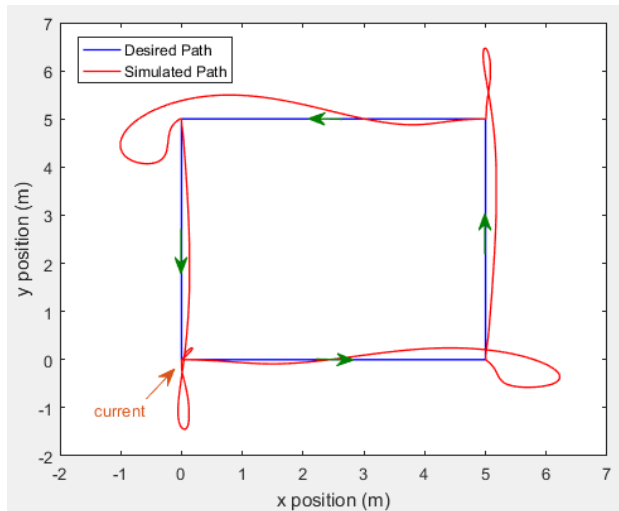


(b) 2D view

Figure 6.6 Path following simulation results with linear PID without external disturbance



(a) 3D view



(b) 2D view

Figure 6.7 Path following simulation results with linear PID applying current speed of 0.1 m/s on the x and y directions

6.2.2 Nonlinear Model-based PID Control

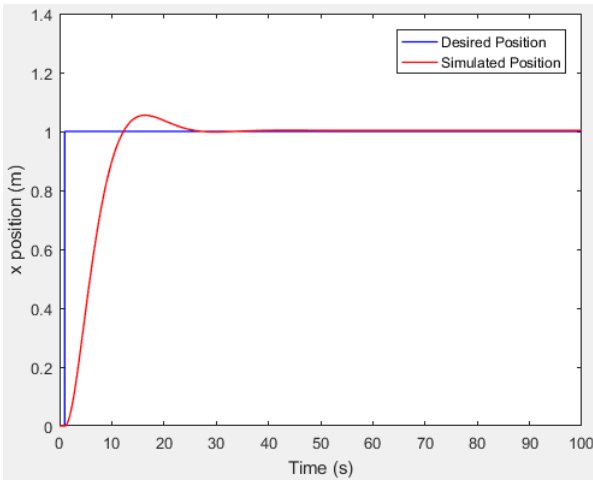
Likewise, with the use of the Ziegler-Nichols tuning method (Ziegler and Nichols 1942), the gains of the 6-DoF model-based PID controller are tuned as listed in Table 6.2. It can be seen that the used gains of the model-based PID are relatively small compared with the gains in Table 6.1. This is because in the model-based control system, the majority of control forces is contributed from the predictive force by the ROV's dynamic model and the residual error is corrected by the PID controller.

Similarly, step response simulations for 6 DoFs were performed firstly as the results shown in Figure 6.8. It is noticeable that the model-based PID control system produces slight overshoot and achieves the goal positions quickly. These features are highly desirable since the vehicle does not require significant direction reverse to accomplish the desired position and demands relatively small energy which results in efficient performance.

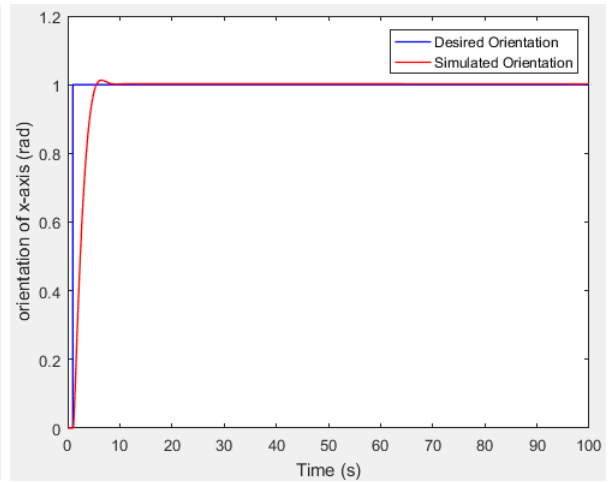
Next, the path following simulation results by the nonlinear model-based PID control system without external disturbance applied are shown in Figure 6.9 whereas Figure 6.10 presents the path following simulation results when a water current disturbance is applied on the x and y position with current speed of 0.1 m/s described by Equation (6.14). It can be seen that simulations results in Fig. 6.9 and Fig. 6.10 are almost identical, with sufficient performance, meaning that the system has high level of resistance to current disturbance at speed of 0.1 m/s. This is because the model-based control system exploits the dynamic model of the ROV so that considers the nonlinearity of the dynamic effects by the disturbance.

Table 6.2 The gains used in the 6-DoF model-based PID controller

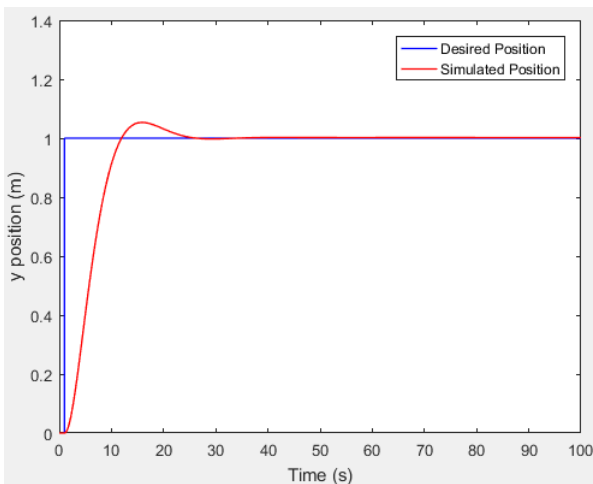
6-DoF PID	Surge	Sway	Heave	Roll	Pitch	Yaw
K_P	1	1	1.2	0.3	0.3	0.3
K_I	0.001	0.001	0.001	0.001	0.001	0.001
K_D	0	0	0	0.3	0.3	0.3



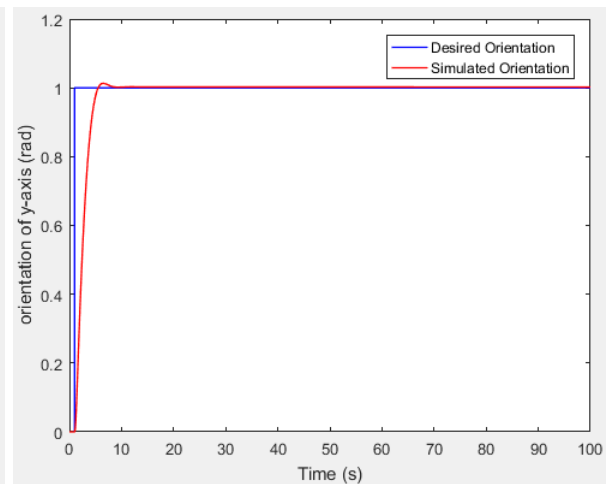
(a) Surge motion



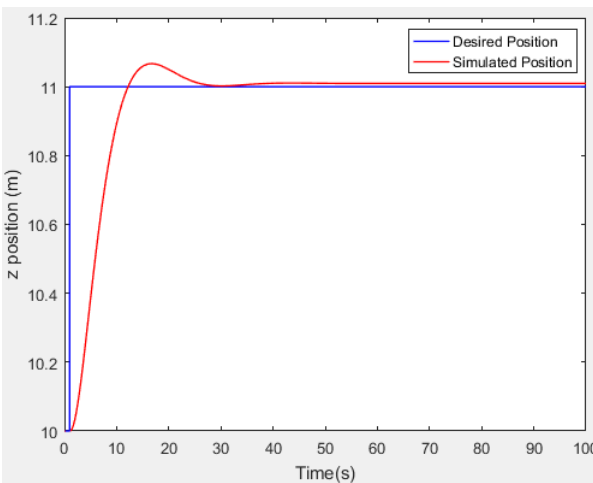
(b) Roll motion



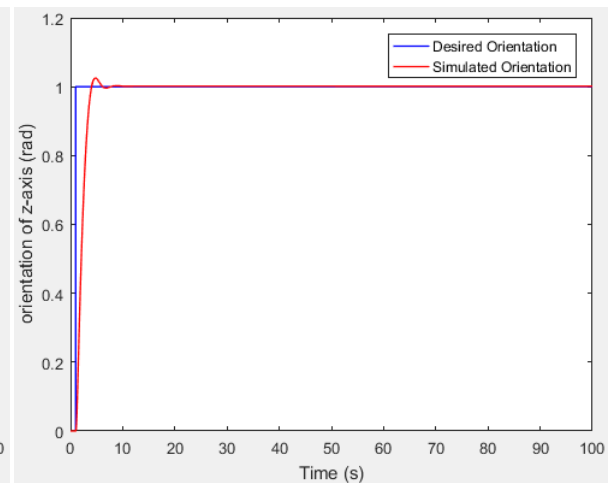
(c) Sway motion



(d) Pitch motion

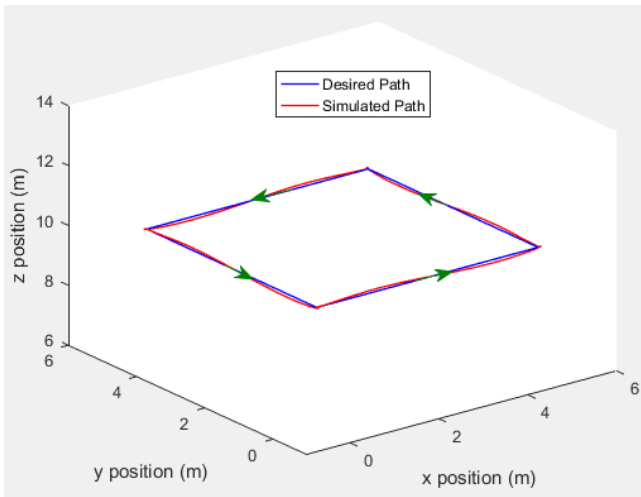


(e) Heave motion

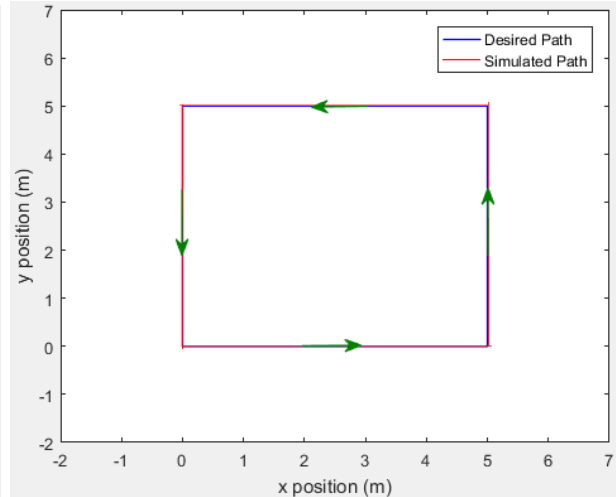


(f) Yaw motion

Figure 6.8 Step responses for the position in 6 DoFs using model-based PID

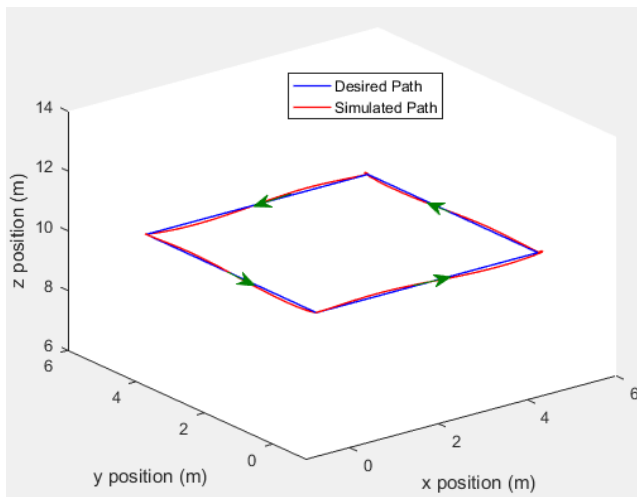


(a) 3D view

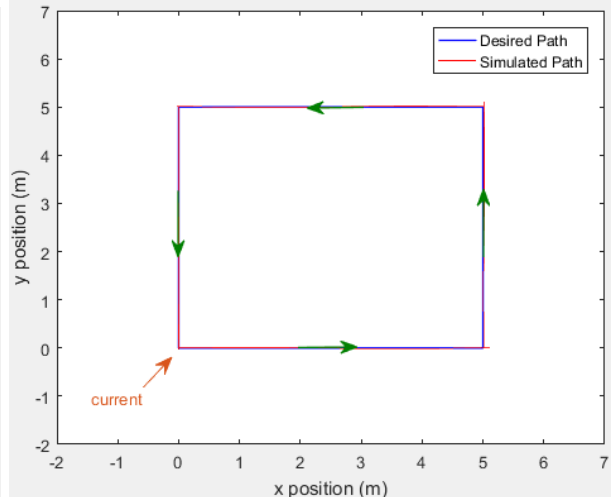


(b) 2D view

Figure 6.9 Path following simulation results with model-based PID without external disturbance



(a) 3D view



(b) 2D view

Figure 6.10 Path following simulation results with model-based PID applying current speed of 0.1 m/s on the x and y directions

6.2.3 Performance Comparison of Linear Model-less and Nonlinear Model-based PID Control Systems

A performance comparison of model-less and model-based PID control systems in terms of settling time and overshoot of step responses in 6 DoFs are listed in Table 6.3. Note that the settling time is defined as the time required for the response remains within 2% of the final value; and step responses of simulations in all DoFs have converged to the desired positions within 2% of steady-state error for both control systems. Table 6.3 demonstrates that the model-based PID control system has significant performance improvement compared with the linear PID control system although it requires longer time for computation. Note that the maximum updated rate for model-less and model-based control systems are 1.5 kHz and 640 Hz, respectively. As a control system generally does not require processing speed faster than 100 Hz, both designed control systems are fast enough for implementation. In summary, with 138% longer processing time, the model-based control has at least 42% of improvement in settling time and at least 62% of improvement in overshoot. Since the conventional PID control is linear and symmetric with constant gains, it is best suited to linear systems but suboptimal for nonlinear systems whereas the nonlinear model-based PID control system makes use of the dynamic model of the plant that results in responding dynamic effects on the system efficiently.

Table 6.3 Performance comparison of model-less and model-based control systems

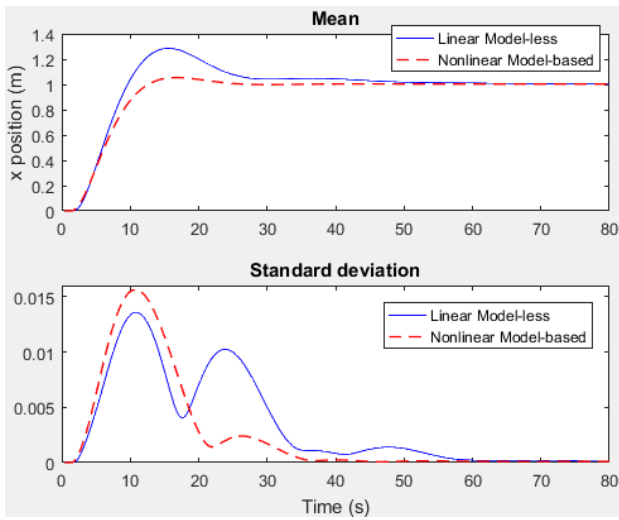
	Settling Time			Overshoot			Computation Time		
	Model-less	Model-based	Diff(%)	Model-less	Model-based	Diff(%)	Model-less	Model-based	Diff(%)
Surge	36 s	21 s	-42%	28.69%	5.49%	-81%	0.656 ms per iteration (1.5kHz)	1.563 ms per iteration (640Hz)	138%
Sway	41 s	22 s	-46%	30.68%	5.33%	-83%			
Heave	49 s	23 s	-53%	--	6.68%	--			
Roll	52 s	5.2 s	-90%	--	1.32%	--			
Pitch	52 s	5.2 s	-90%	--	1.32%	--			
Yaw	16 s	5.2 s	-67%	6.6%	2.51%	-62%			

6.3 Robustness Analysis of Control Systems

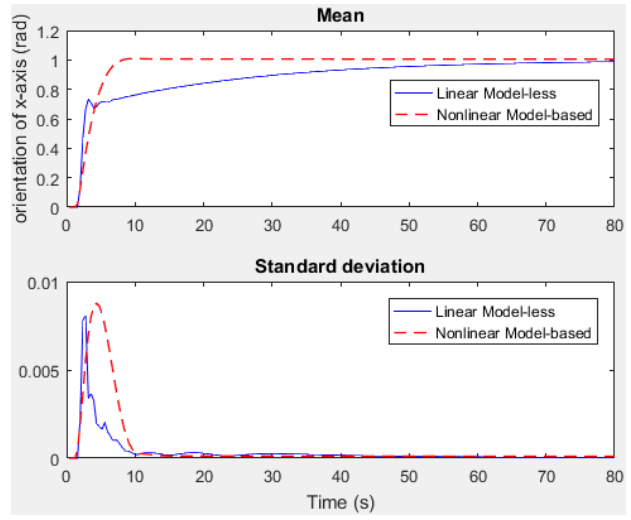
In this section, a set of representative Monte Carlo simulations are performed to examine the robustness of the linear model-less PID and the nonlinear model-based PID control systems with various scenarios. The first circumstance of simulations involve uncertainties of hydrodynamic parameters in the ROV's dynamic model to analyse how they affect the performance of both systems. In the second scenario, disturbance of water currents are taken into account in the simulation. Higher current speed introduces more current forces onto the vehicle, thus the two control systems' limitations on currents will be investigated. The third subset of simulations are performed while model uncertainties and water currents both occur. All Monte Carlo simulations are performed on a 100-trial basis and with an initial position of 10 m in depth as in Equation (6.12). The statistical analysis of both systems' robustness will be represented and compared.

6.3.1 Effect of Model Uncertainty

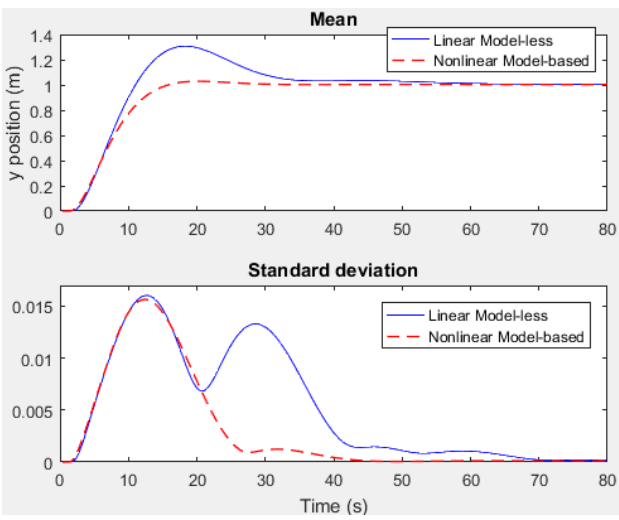
The first simulation subset considers model uncertainties within $\pm 10\%$ variation in hydrodynamics while no external disturbance is applied. In the simulations, each hydrodynamic parameter is added with a uniformly distributed noise between 10% lower and 10% higher of its value. Figure 6.11 compares the simulation results of model-less and model-based control systems in terms of the mean and standard deviation of 100 trials of step responses for 6 DoFs. Overall, both systems are reasonably robust with respect to model uncertainties such that while $\pm 10\%$ variation in hydrodynamics is introduced, the maximum diversity of responses produced is only about 1.5%. It is noticeable that the two systems have similar sensitivity towards hydrodynamic uncertainties where the variations in translational motions (around 1.5%) are slightly less than that in rotational motions (around 1%). Interestingly, in most motions, the model-based control system marginally has higher diversity in response (maximum 0.5% higher) than the model-less control system. This is because the model-based control system makes the use of the dynamic model of the ROV, thus its performance relies on the accuracy of the model more than the model-less control system in general.



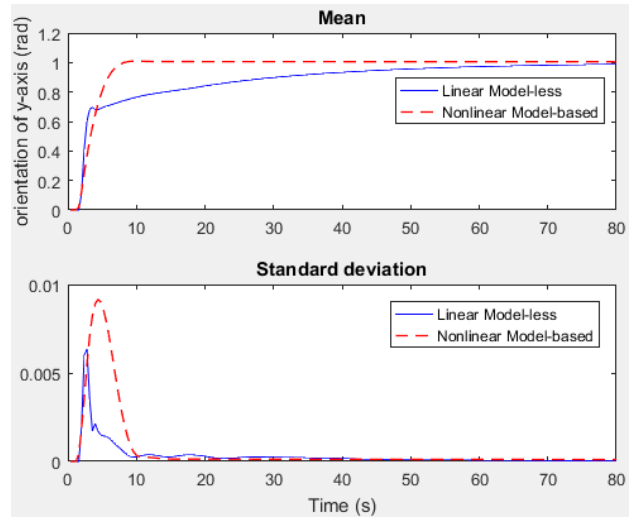
(a) Surge motion



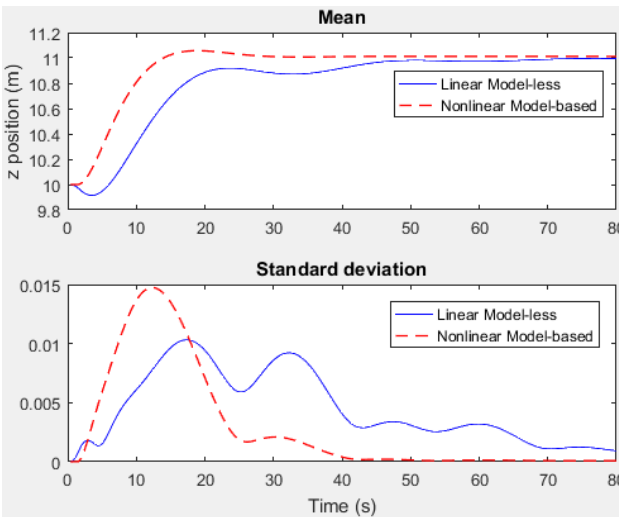
(b) Roll motion



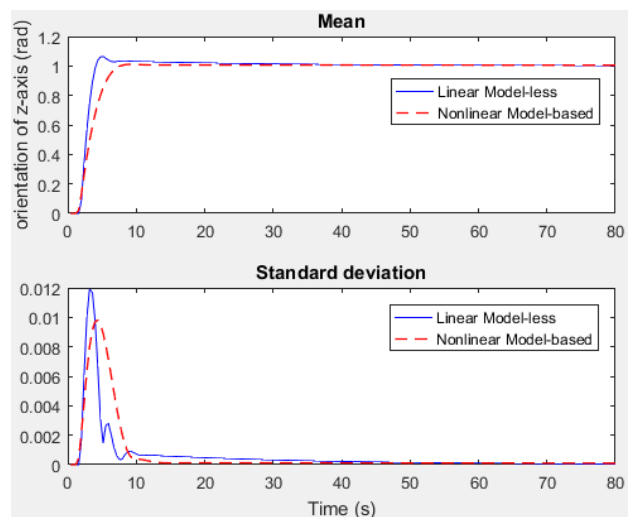
(c) Sway motion



(d) Pitch motion



(e) Heave motion



(f) Yaw motion

Figure 6.11 Comparison of step responses for 6 DoFs based on model-less and model-based control systems using Monte Carlo simulations with model uncertainties

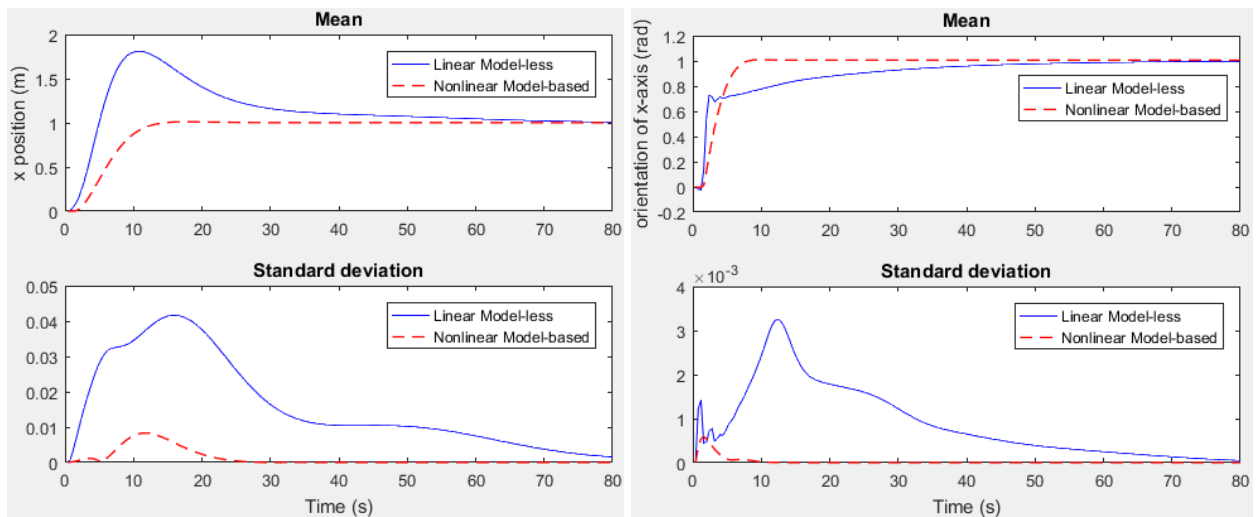
6.3.2 Effect of Current Disturbance

This second study investigates the effect of environmental disturbance of currents on the performance of the designed control systems while the model uncertainty is not considered. Since the ocean current is commonly assumed to be constant and irrotational in the inertial frame when describing its effects on marine vehicles (Fossen 2011), a water current is generated in the x, y and z directions in the simulations. The current velocity is set to 0.25 m/s with an added uniformly distributed noise ε between 10% lower and 10% higher of the current speed. Hence, the velocity of water current in 6-DoF is given by:

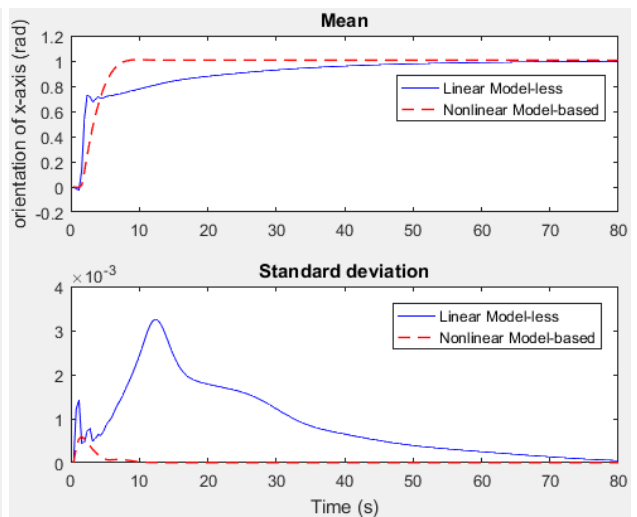
$$v_c = [0.25 + \varepsilon, 0.25 + \varepsilon, 0.25 + \varepsilon, 0, 0, 0]^T \quad (6.15)$$

Figure 6.12 compares the simulation results of using model-less and model-based control systems in presenting the mean and standard deviation of 100 trials of step responses in 6 DoFs. It can be seen that the water current affects the performance of the model-less control system considerably in terms of settling time and overshoot where it takes much longer (over 1.5 times) to converge in most DoFs (surge, sway, heave and yaw) after applying current, and the overshoot in translational motions have increased dramatically (to between 55% and 97%). On the other hand, the model-based control system shows its sufficient robustness in regard to current disturbance such that its performance remains with similar settling time in all DoFs and reduced overshoot in some DoFs (surge, sway and yaw) in the presence of water current. In addition, with $\pm 10\%$ variation of the current speed, the maximum diversity of responses produced by the model-based control system is only about 1% whereas that is about 7.5% by the model-less system.

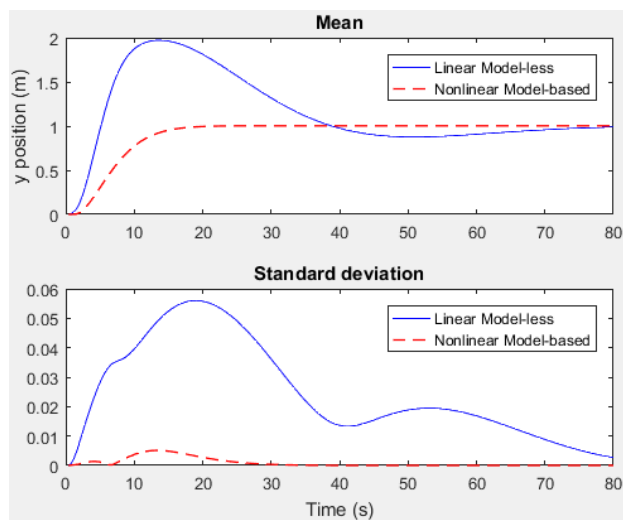
Since the model-based control system exploits the dynamic model and considers the nonlinearity of the current effect on the vehicle, the error for linearisation in the model-based PID controller is much smaller than that in the model-less PID controller. Hence, the model-based control system results in a much more accurate control behaviour and performance whereas the model-less control system is only effective for a relatively small range from the tuning point.



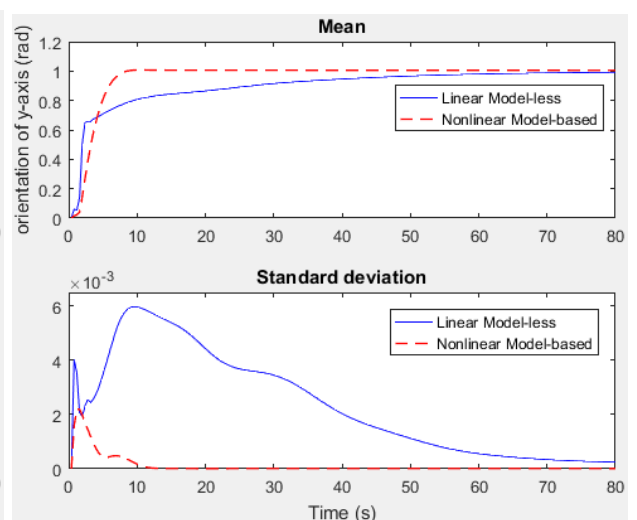
(a) Surge motion



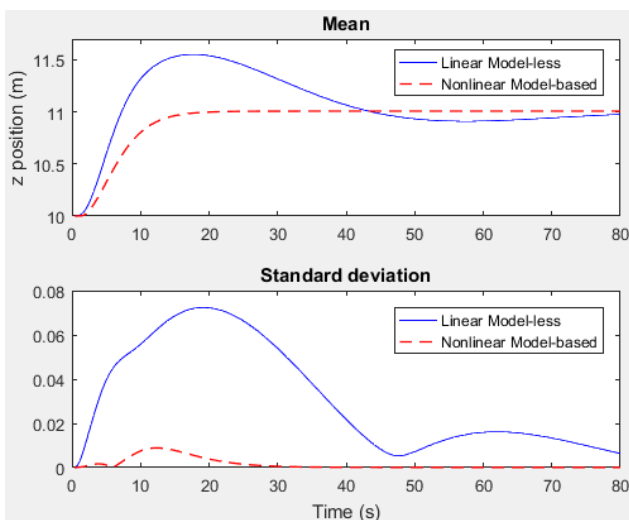
(b) Roll motion



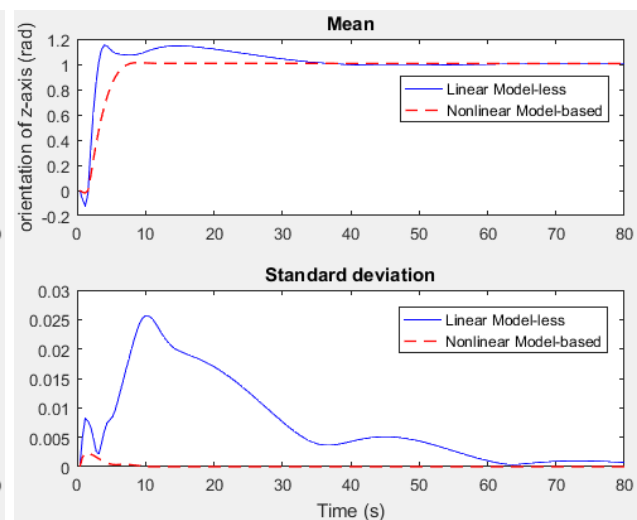
(c) Sway motion



(d) Pitch motion



(e) Heave motion



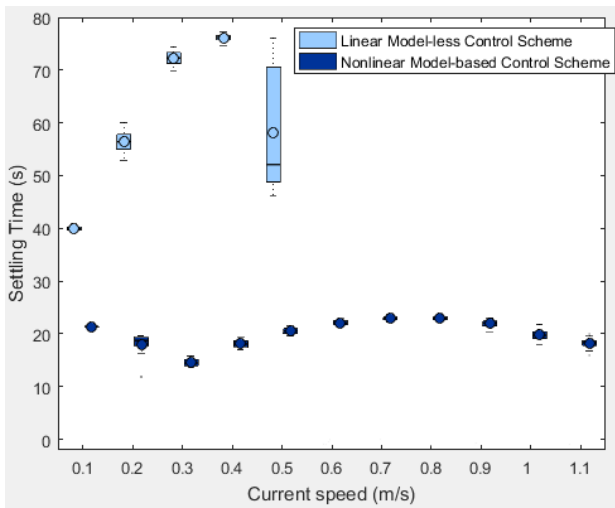
(f) Yaw motion

Figure 6.12 Comparison of step responses for 6 DoFs based on model-less and model-based control systems using Monte Carlo simulations applying water current at 0.25 m/s (within $\pm 10\%$ variation) in the x, y and z directions

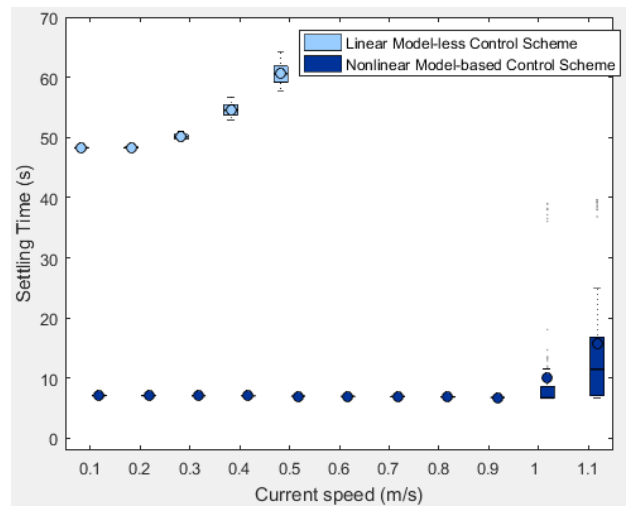
Next, a further study investigates the effect of various current speeds on the two control systems and explores the limitations of the current levels these two control systems can manage respectively in terms of adequate settling time and steady-state errors in all DoFs. The simulations were performed while applying each level of current velocities individually ranging from 0.1 m/s in step of 0.1 m/s until the controller is unable to converge to the desired state. An added uniformly distributed noise between 10% lower and 10% higher of the current speed is also applied. Figure 6.13 and Figure 6.14 represents statistical analysis comparison of the settling time and steady-state errors respectively in 6 DoFs for both model-less and model-based control systems. Overall, increments in the current speed has a far more noticeable impact on the performance of model-less control system than that of model-based control system in a way that both settling time and steady-state errors by the model-less control system rise significantly in most DoFs whereas that with the model-based control system varies in a limited range with marginal increase over the increase of the current speed. Moreover, the limitations on currents of the model-less and model-based control systems are found to be 0.4 m/s and 1.1 m/s, respectively as it can be seen from the Figure 6.14 where systems start failing to converge to their goal positions in some motions. These results also indicate that the settling time based on the model-based system and the current speed of 1.1 m/s correspond to the physical limitation of the vehicle.

6.3.3 Effect of Model Uncertainty and Current Disturbance

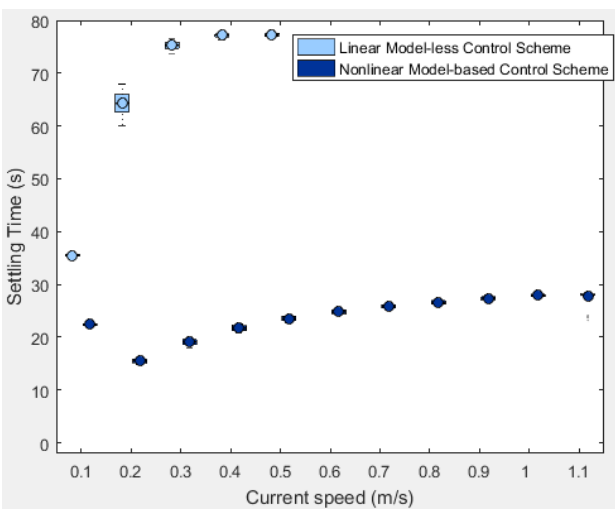
The final scenario includes the presence of both model uncertainties (hydrodynamics variation ranging within $\pm 10\%$) and environmental disturbance of constant irrotational current of 0.25 m/s in the x, y and z directions added within $\pm 10\%$ uniformly distributed noise. Figure 6.15 depicts the step responses in 6 DoFs with both model-less and model-based control systems in the form of the mean and standard deviation of 100-trial results. It is noticeable that while the model-based control system presents a much better overall performance on the mean than the model-less, the response variation produced with the model-based is greater than that by the model-less especially in rotational motions. This is because compared to model-less control, the model-based control system has greater resistance to current disturbance, while it has higher sensitivity to the accuracy of the dynamic model.



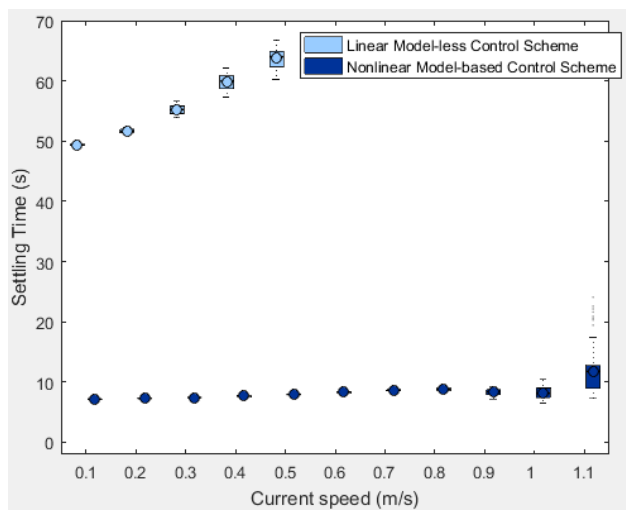
(a) Surge motion



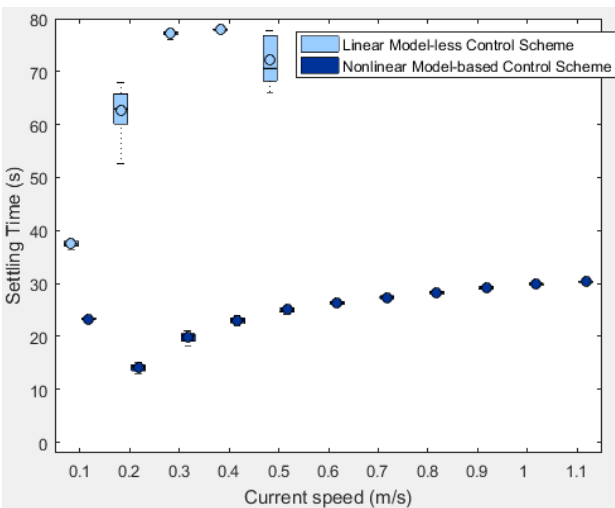
(b) Roll motion



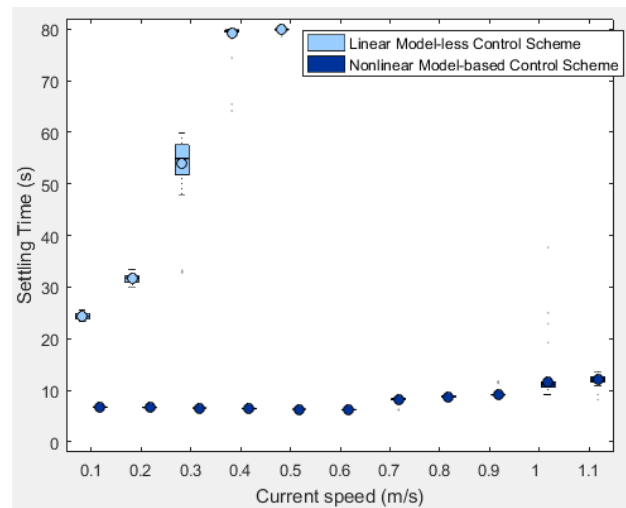
(c) Sway motion



(d) Pitch motion

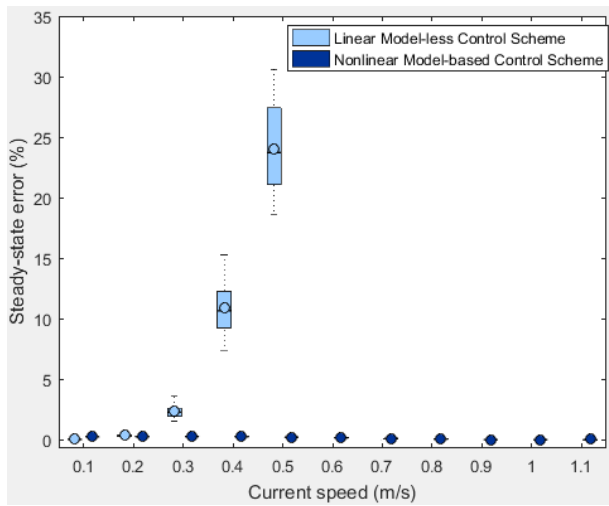


(e) Heave motion

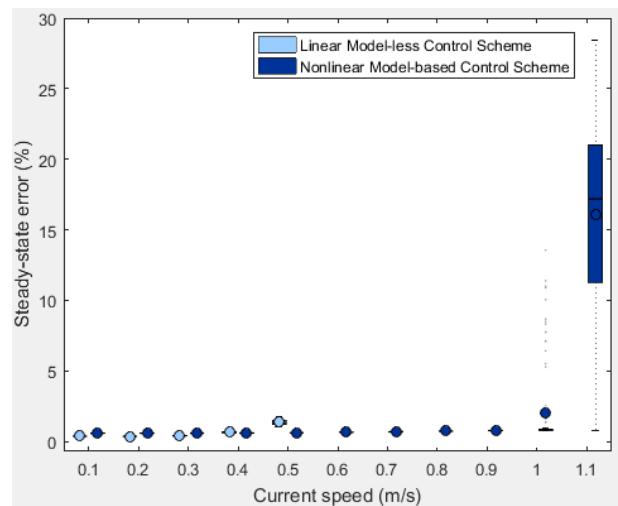


(f) Yaw motion

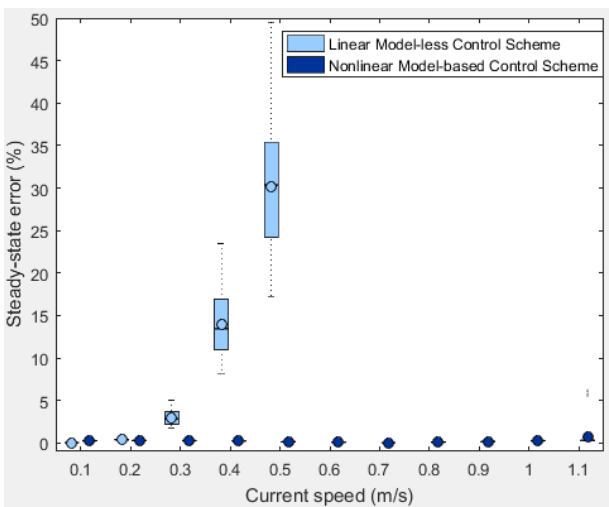
Figure 6.13 Settling time comparison of step responses for 6 DoFs based on model-less and model-based control systems using Monte Carlo simulations with increasing current speeds (within $\pm 10\%$ variation) in the x, y and z directions



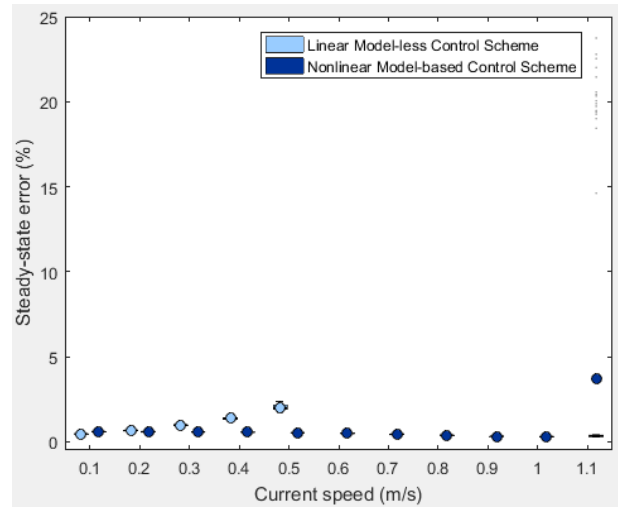
(a) Surge motion



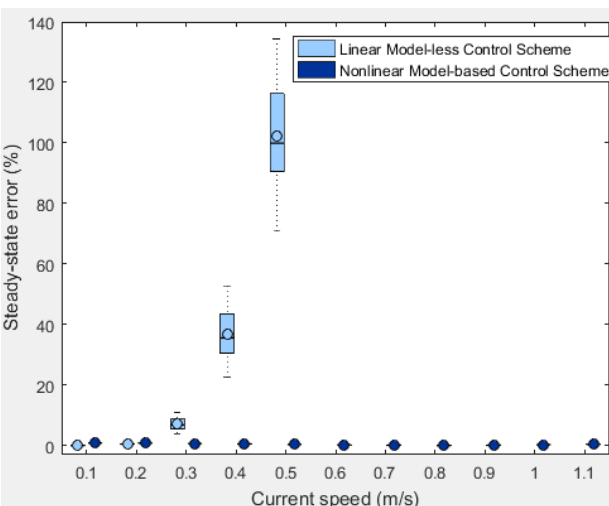
(b) Roll motion



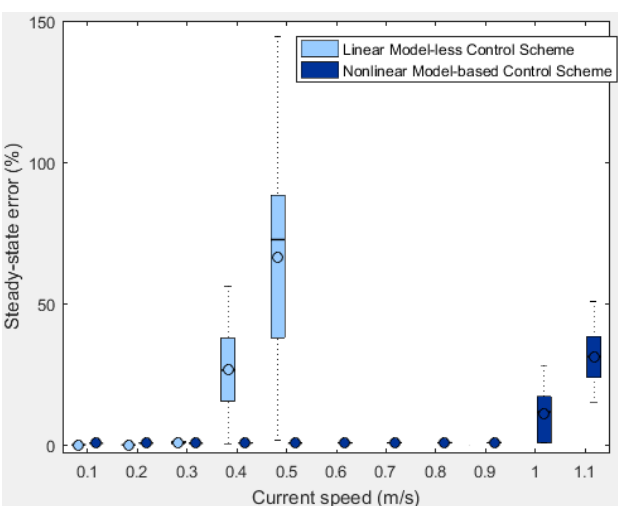
(c) Sway motion



(d) Pitch motion

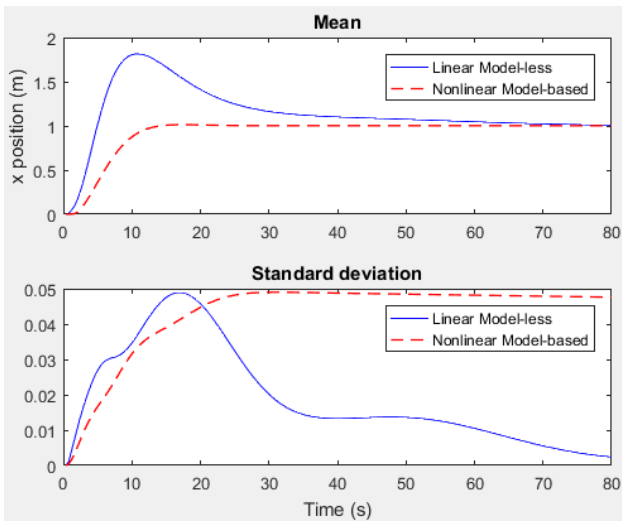


(e) Heave motion

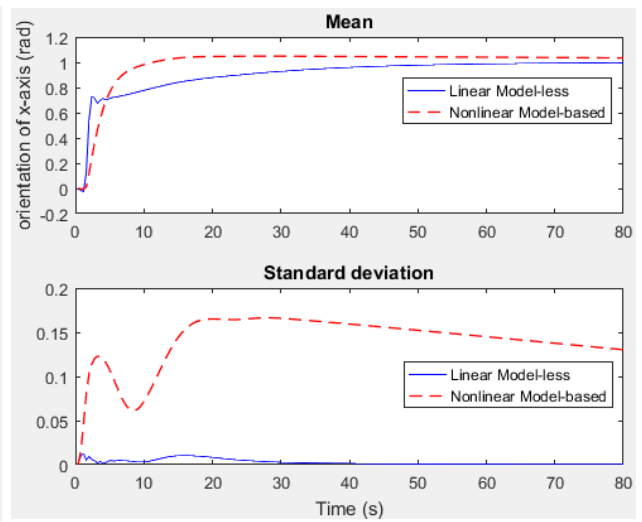


(f) Yaw motion

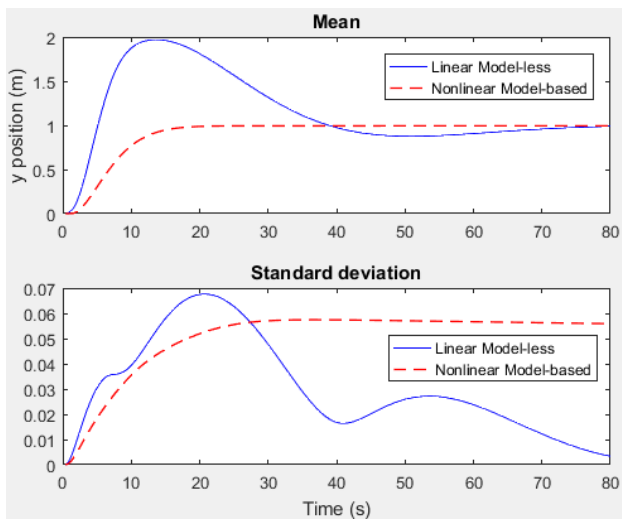
Figure 6.14 Steady-state error comparison of step responses for 6 DoFs based on model-less and model-based control systems using Monte Carlo simulations with increasing current speeds (within $\pm 10\%$ variation) in the x, y and z directions



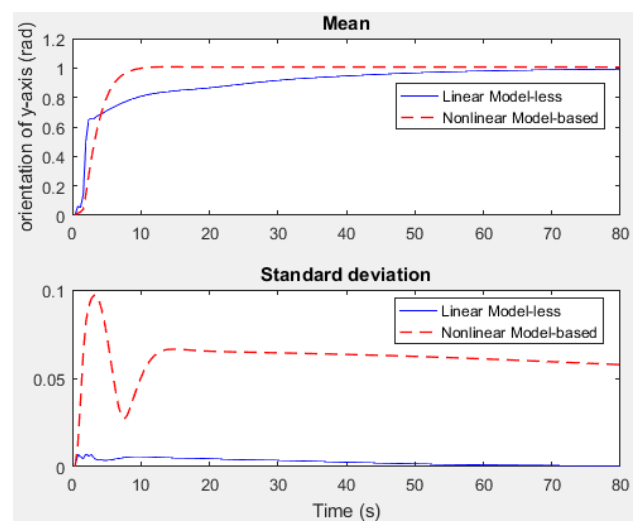
(a) Surge motion



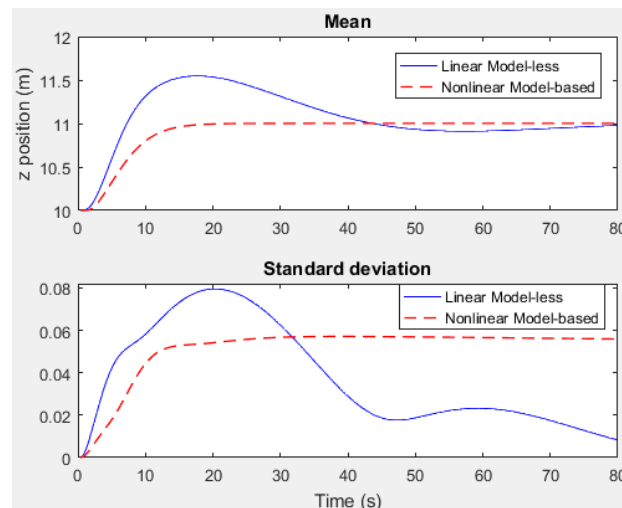
(b) Roll motion



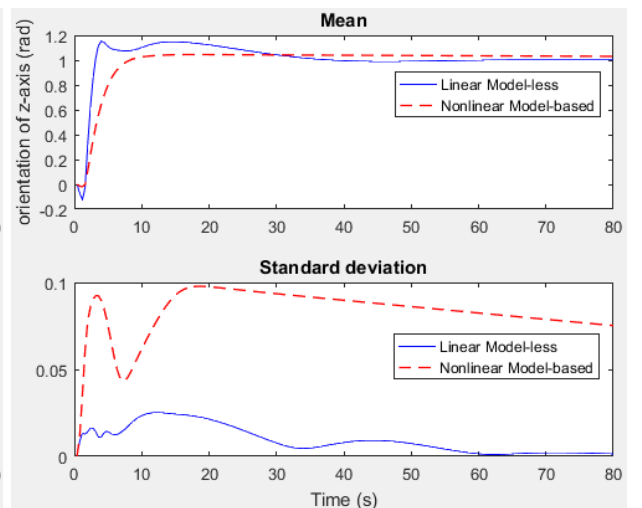
(c) Sway motion



(d) Pitch motion



(e) Heave motion



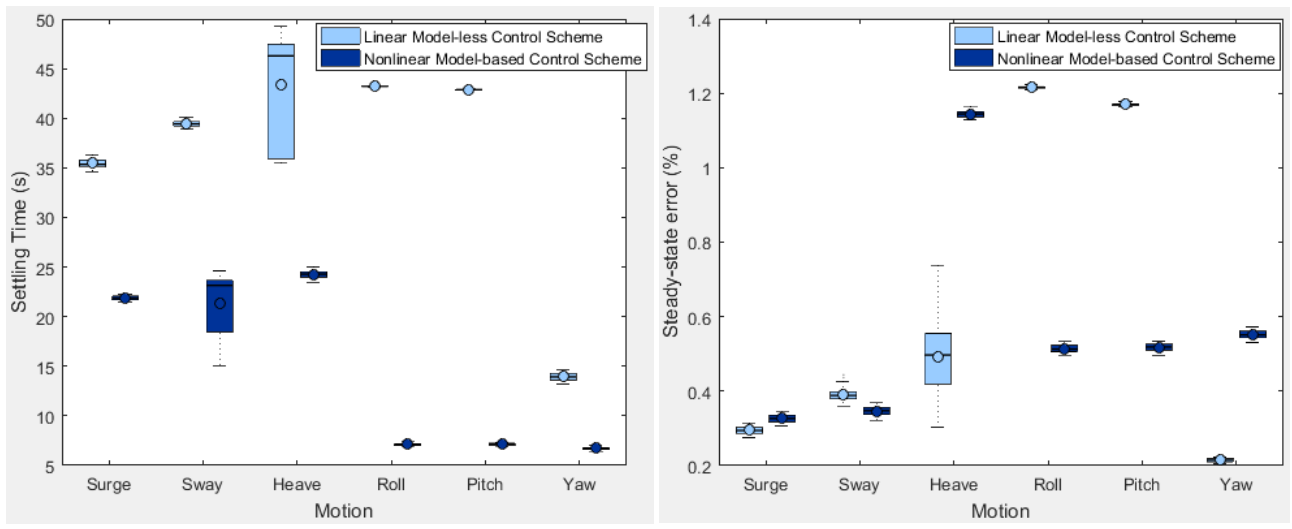
(f) Yaw motion

Figure 6.15 Comparison of step responses for 6 DoFs based on model-less and model-based control systems using Monte Carlo simulations in the presence of model uncertainties and current speed of 0.25 m/s with random noise in the x, y and z directions

6.3.4 Robustness Analysis of Model-less and Model-based Control Systems

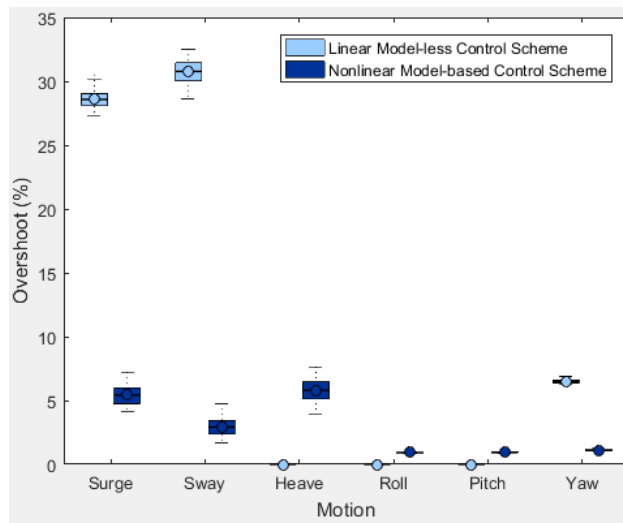
In this section, the robustness of the model-less PID and the model-based PID control systems are analysed based on previous three circumstances of Monte Carlo simulations and compared using statistical analysis techniques. The robustness analysis investigates system performance based on the settling time, steady-state errors and overshoot of step responses in 6 DoFs. Figure 6.16 compares analysis results for both designed control schemes with regards to model uncertainties simulated in Section 6.3.1. Overall, both systems' performance in rotational motions have high level of resistance to model uncertainties. On the other hand, the model uncertainty has greatest impact on settling time in heave motion with model-less control and in sway motion with model-based control as well as noticeable impact on the accuracy of heave motion control by model-less system whereas the overshoot by both control scheme are insignificantly sensitive to model uncertainties in general.

Figure 6.17 compares analysis results of both control systems in relation to current disturbances simulated in Section 6.3.2. In general, the model-based control scheme demonstrates a superior resistance to current disturbance and its variation in all DoFs if it is within the limitation of the system. In contrast, the water current has an significant impact on the performance of the model-less control scheme where the mean of settling time and overshoot have increased substantially in translational motions (note that currents are assumed to be irrotational in the simulations). Additionally, the current variation has noticeable impact on overshoot and control accuracy in translational motions with the model-less system.



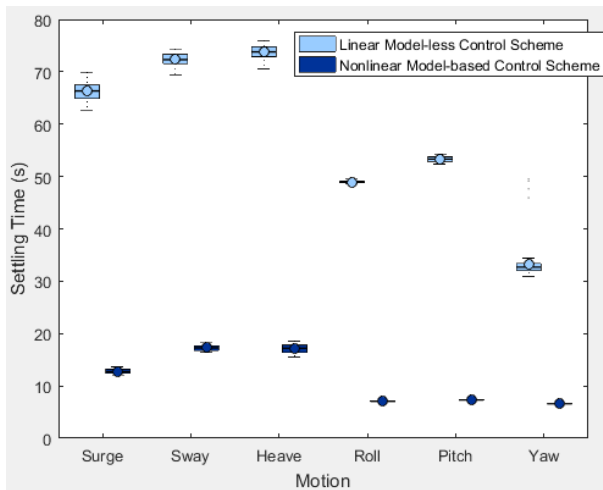
(a) Settling Time

(b) Steady-state error

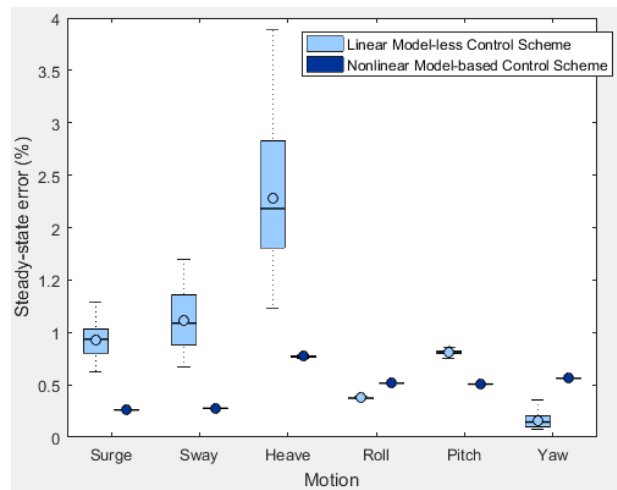


(c) Overshoot

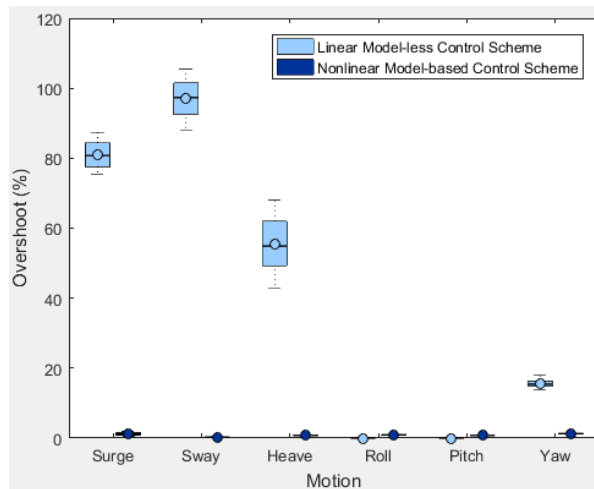
Figure 6.16 Robustness analysis comparison of two control schemes regarding model uncertainties



(a) Settling Time



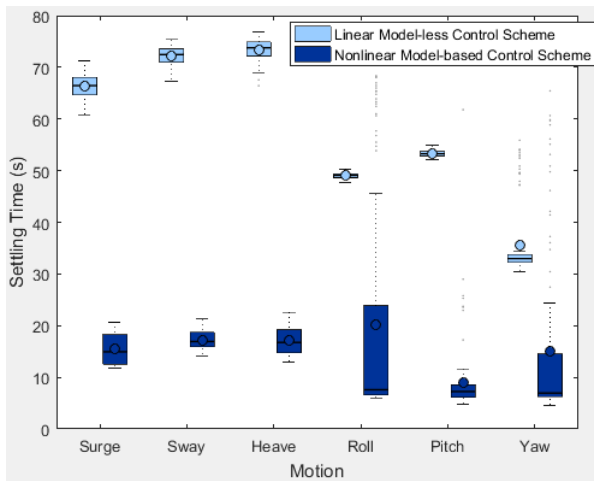
(b) Steady-state error



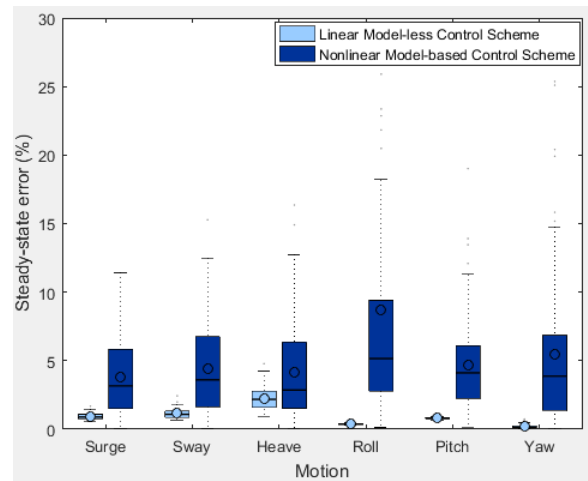
(c) Overshoot

Figure 6.17 Robustness analysis comparison of two control schemes regarding current disturbance

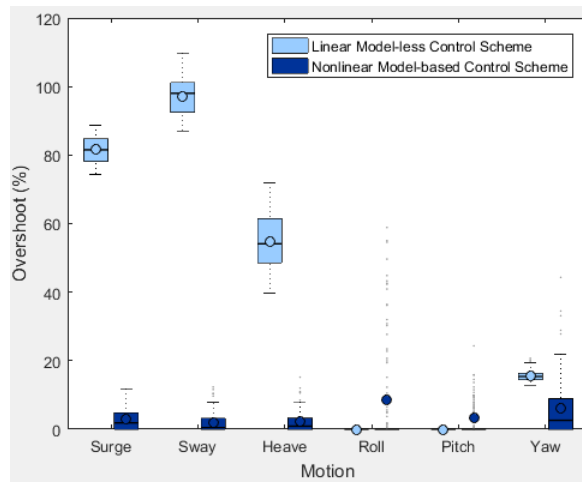
Figure 6.18 compares analysis results of two control systems for the circumstance of both model uncertainties and water currents simulated in Section 6.3.3. It can be seen that although the mean performance in settling time and overshoot of the model-based control is superior to that of the model-less control especially in translational motions, the accuracy and settling time based on the model-based control in most DoFs varies in a larger but acceptable range due to its sufficient resistance to current disturbance but reliance on the model accuracy. To sum up, according to the analysis based on these three circumstances of Monte Carlo simulations, the nonlinear model-based PID control system demonstrates an effective and robust performance in relation to moderate model uncertainties and environmental disturbance of currents whereas the linear model-less PID control scheme is resistant to model uncertainties yet not providing sufficient performance in the presence of current disturbance.



(a) Settling Time



(b) Steady-state error



(c) Overshoot

Figure 6.18 Robustness analysis comparison of two control schemes concerning both model uncertainties and current disturbance

6.4 Summary

In this chapter, a linear conventional PID controller and a nonlinear model-based PID controller have been developed respectively for the control system design of the BlueROV2 Heavy. Both designed control systems were simulated using Matlab Simulink to examine and compare their performance. Additionally, the robustness of the two systems have been analysed using Monte Carlo trials. The simulation results and statistical analysis demonstrate the effectiveness and robustness of the nonlinear model-based PID control system that is feasible to be implemented on the BlueROV2 Heavy for controlling its position while the linear model-less PID control system requires much longer time to achieve the desired position and is sensitive to the dynamic effect of environmental disturbance on the vehicle.

CHAPTER 7

CONCLUSION

7.1 Summary

This chapter will summarise the main components of the work achieved in this thesis and present conclusions highlighting relevant findings and observations from simulation results. Following this, recommendations of possible directions for future work will be presented.

The development of system modelling, identification and control systems for an ROV named BlueROV2 Heavy have been presented in this thesis. In the first phase of this thesis, a complete 6-DoF ROV's system modelling was conducted using a vectorial representation presented in Chapter 4. This includes the thruster model and the dynamic model of kinematics and kinetics where various matrices that form the mathematical model were derived on the basis of Fossen's work (Fossen 1994, Fossen 2002, Fossen 2011). In order to simplify the complex dynamic model and reduce the extensive unknown parameters, several assumptions made for the BlueROV2 Heavy based on its characteristics and relatively low speed operations were discussed in Section 3.3.

Inspired by the work of Indiveri (Indiveri 1998) and Caccia (Caccia, Indiveri et al. 2000), a system identification approach in immersion tank with the use of on-board sensors was proposed in Section 5.1 for determining parameters in the dynamic model. This approach employs static experiments for identifying damping parameters where the velocity of the vehicle is constant and the acceleration is zero; and utilises dynamic experiments for identifying system inertia parameters where the acceleration of the vehicle is non-zero. This approach is highly repeatable and cost effective, which makes it suited for the BlueROV2 Heavy as the vehicle is easily configurable and fully customisable. The bollard pull test in immersion tank with the use of a 6-DoF load cell was proposed in Section 5.3 for identifying thruster coefficients in the thruster model. Using an estimation technique of the least squares algorithm to estimate parameters from the experimental data was demonstrated in Section 5.1.1. However, due to the unavailability of the BlueROV2 Heavy, system identification experiments were not carried out. Alternatively, parameters in the models were determined by analysing the BlueROV2 Heavy's technical specifications from BlueRobotics

(BlueRobotics 2018b) and published literature relating to BlueROV from Sandøy (Sandøy 2016) presented in Section 5.2 and 5.3.

In the second phase of this thesis, a simulation study of the control system design was presented, with the use of the system model and parameters determined for the BlueROV2 Heavy, in Chapter 6. Various controller algorithms applicable to an underwater vehicle were discussed in detail, as presented in Section 2.2. Two 6-DoF control systems of linear model-less and nonlinear model-based were developed for the vehicle based upon the PID control algorithm presented in Section 6.1 due to its simplicity, practicability and ease of implementation. Step response of each DoF and path following simulations using these two control systems as well as result analysis and their performance comparison were presented in Section 6.2. Section 6.3 presented the results and analysis of a set of representative Monte Carlo simulations under various operating conditions in order to investigate the robustness of these two control systems. Three scenarios were set as in the presence of the model uncertainty, the current disturbance and the combination of the two. These simulation results were analysed based on the mean and standard deviation of the step responses for all DoFs based on 100 trials. Using statistical analysis and representation of boxplots, the robustness of two systems were examined and compared for control performance and accuracy.

7.2 Conclusions

Based on the work presented in this thesis, several conclusions can be drawn regarding the findings from the simulation studies. These conclusions are concerned with the performance of the two developed control systems in relation to settling time, steady-state error, overshoot and robustness to environmental disturbances and model uncertainties.

In the first simulation study of step response and path following simulations, it was seen that both the 6-DoF linear model-less PID and the 6-DoF nonlinear model-based PID control systems were able to track a simple trajectory (i.e. a single DoF is excited at a time) in all 6 DoFs without external disturbances. Although the technique of the linear conventional PID controller is relatively simple to implement, it produces long settling time for certain DoFs (about 50 secs in heave, roll and pitch) and noticeable overshoot in surge and sway motions

(about 30%). Furthermore, due to the highly nonlinear properties of the ROV's model, linear control schemes are incapable of producing sufficient manoeuvring performance in the presence of current disturbance from the external environment. The nonlinear model-based PID control system was formed by extending the PID controller with the concept of model-based control. In this design, the vehicle's dynamic model is taken advantage of to produce a predictive force and the PID controller is utilised to provide a corrective force for the residual error. As a result, the model-based control system has at least 42% of improvement in settling time and at least 62% of improvement in overshoot with 138% longer processing time whereas both systems are fast enough for implementation (i.e. the maximum updated rate for model-less and model-based control systems are 1.5 kHz and 640 Hz while a control system generally require processing speed of 100 Hz).

In the second simulation study of robustness analysis using Monte Carlo simulations, it was found that both model-less and model-based control systems are relatively insensitive (with 1.5% change) to the model uncertainty (with a $\pm 10\%$ variation in hydrodynamic parameters) in most DoFs (especially in rotational motions). The noticeable impacts of the model uncertainty were found to be on settling time in heave motion (greatest) and on steady-state error on heave motion with the model-less control; and on settling time in sway motion with the model-based control. In the presence of current disturbance, the model-based control demonstrates a superior robustness whereas the average settling time and overshoot have increased substantially in translational motions (currents were assumed to be irrotational) with the model-less control. The operational limits regarding current disturbance for model-less and model-based control were found to be current speed of 0.4 m/s and 1.1 m/s, respectively. For the scenario of both model uncertainties and water currents, the overall performance in settling time and overshoot of the model-based control is superior to that of the model-less control due to its sufficient resistance to current disturbance. However, since the model-based control relies on the accuracy of the model to a certain degree, the performance of settling time and steady-state error varies in a larger range compared with the model-less control. According to the statistical analysis of simulation results based on these three scenarios, the nonlinear model-based PID control system was validated to be robust with regards to moderate model uncertainties ($\pm 10\%$ variation in hydrodynamic parameters) and current disturbance up to 1.1 m/s current speed whereas the linear model-

less PID control system less insensitive to model uncertainties yet not capable of handling disturbances and only effective for a relatively small range from the tuning point.

7.3 Recommendations for Future Work

This section presents a summary of intended and possible work that could be undertaken to increase the accuracy of system identification and expand the functionality of the control system.

7.3.1 Improvement of System Identification

In this thesis, the unknown parameters in the derived models of BlueROV2 Heavy were currently determined by analysing technical specifications and published literature relating to BlueROV that could potentially have significant inaccuracy due to the effects of hydrodynamic, thruster-hull and thruster-thruster interactions, and different configuration of BlueROV. Therefore, once the BlueROV2 Heavy is available, it is essential to perform the system identification experiments for higher accuracy in identifying parameters.

The proposed system identification approach exploits the characteristics of the ROV and assumes decoupling between DoFs in hydrodynamics. As a consequence, hydrodynamic parameters for each DoF can be estimated independently with the use of the vehicle's state measurements obtained by on-board sensors. Under the consideration of measurement noise from on-board sensors, a state observer algorithm is then necessary to process the available measurements to attain an estimate of the position and velocity of the vehicle with minimal noise corrupting the solution. This estimated information from the observer can be also utilised in the state feedback control. This can be achieved by employing a recursive Bayesian filtering technique, which comprises the Kalman filter family and the particle filter family. Due to the highly nonlinear dynamic properties of the ROV, a nonlinear observer such as an Extended Kalman Filter (EKF) or non-Gaussian filtering of the particle filter can be chosen for their ease of implementation. The implementation examples for the EKF and the particle filter for ROV's observer can be found in literature of Dukan et al. (Dukan, Ludvigsen et al. 2011) and Zhao et al. (Zhao, Skjetne et al. 2014), respectively.

While various assumptions were placed on the vehicle to simplify its 6-DoF model and reduce the number of unknown parameters in the model, the accuracy of the obtained model might be decreased due to accumulated approximations. Therefore, relaxation of assumptions improves the accuracy of the ROV's model and ultimately leads to a more robust control system. In the kinetic equation of motion, the system inertia and hydrostatic terms can be attained by measuring, which are relatively accurate. However, the damping terms of hydrodynamics are depending on motion of fluid surrounding the vehicle and sensitive to the velocity that are challenging to obtain accurately. Hence, it is recommended to incorporate significant off-diagonal parameters of damping matrices to minimise assumptions and increase accuracy. Note that determining which off-diagonal terms are significant needs to be investigated in the future by utilising data from experiments.

7.3.2 Improvement of Controller

In the control system design, the gains of the PID controllers for both designed systems will need to be refined when model parameters for the BlueROV2 Heavy are updated and obtained from experimental system identification to attain optimal values. The developed control systems in this thesis concern position control of the vehicle for ROV's inspection and intervention purposes. The next stage is to include speed control to expand system capacity for surveying and mapping by integrating a desired velocity and the estimated state of velocity into the control system. This can be realised by applying a common technique used in robotics named computed torque control (Sciavicco and Siciliano 1996). This approach conducts state feedback linearisation that utilises a nonlinear mapping to transform the nonlinear system dynamics into a linear system. The examples of implementation of this approach for underwater vehicles can be found in literature (Silpa-Anan, Abdallah et al. 2000, Smallwood and Whitcomb 2004).

As existing control solutions reported in the literature review presented in Chapter 2, the PID controller is one of the control algorithms for underwater vehicles. The modern control technique of sliding mode control is becoming increasingly used due to its relatively simple implementation (Marco and Healey 2001) and insensitivity to model uncertainties and external disturbances and has been demonstrated to achieve robust control (Gomes, Sousa et al. 2003, Soyulu, Buckham et al. 2008, Haugen 2012). However, a particular limitation of

the conventional sliding mode control is the phenomenon of chattering, which is a high frequency oscillation introduced by the discontinuity in the control law. This oscillation can lead to unmodelled dynamics, excessive power consumption and system instability. Nevertheless, the chattering effect of sliding model control can be reduced by introducing a boundary layer around the sliding surface by applying saturation function (Slotine and Li 1991) or the sigmoid function (Edwards and Spurgeon 1998) under a continuous control law. Alternatively, another chattering elimination method is using higher order sliding modes to hide control discontinuity in its higher derivatives (Fridman and Levant 1996, Bartolini, Ferrara et al. 1998). This approach has been realised in literature presenting enhanced accuracy and robustness to external disturbances. Since sliding mode control can produce more accurate solution and has an equivalent computation load to model-based PID control, it is recommended for future development.

7.4 Epilogue

In summarising this thesis, it can be seen, through representative and quantitative simulations, that a 6-DoF control system utilising model-based control framework provides accurate and robust control performance compared with the linear conventional controller. While both developed control systems have satisfactory computation time for implementation, simulation results demonstrate significant performance improvement (i.e. at least 42% settling time reduction and at least 62% overshoot reduction) by the nonlinear model-based control (with the cost of 138% more processing time). Furthermore, it was seen that the nonlinear model-based control responds to dynamic effects of disturbances on the system efficiently and has a much larger operational range (up to 1.1 m/s current speed compared with up to 0.4 m/s current speed for model-less control). To conclude, from this thesis it is evident that the developed 6-DoF nonlinear model-based PID control system is feasible to be implemented in controlling the position of the BlueROV2 Heavy in all 6 DoFs.

Bibliography

Abkowitz, M. A. (1964). Lectures on ship hydrodynamics--Steering and manoeuvrability.

Abkowitz, M. A. (1980). Measurement of hydrodynamic characteristics from ship maneuvering trials by system identification.

Aili, A. and E. Ekelund (2016). Model-Based Design, Development and Control of an Underwater Vehicle.

Alessandri, A., et al. (1998). Application of LS and EKF techniques to the identification of underwater vehicles. Control Applications, 1998. Proceedings of the 1998 IEEE International Conference on, IEEE.

Alvarez, A., et al. (2009). "Folaga: A low-cost autonomous underwater vehicle combining glider and AUV capabilities." Ocean Engineering **36**(1): 24-38.

Amado-Filho, G. M., et al. (2012). "Occurrence and distribution of rhodolith beds on the Fernando de Noronha Archipelago of Brazil." Aquatic botany **101**: 41-45.

Antonelli, G., et al. (2001). "Adaptive control of an autonomous underwater vehicle: experimental results on ODIN." IEEE Transactions on Control Systems Technology **9**(5): 756-765.

Arnesen, B. O. (2016). Motion Control Systems for ROVs-Underwater Path-Following for a Videoray Pro 4 ROV, NTNU.

Åström, K. J. and T. Hägglund (1995). PID controllers: theory, design, and tuning, Instrument society of America Research Triangle Park, NC.

Åström, K. J. and T. Hägglund (2006). Advanced PID control. The Instrumentation, Systems, and Automation Society, Citeseer.

Bachmayer, R. and L. L. Whitcomb (2003). "Adaptive parameter identification of an accurate nonlinear dynamical model for marine thrusters." TRANSACTIONS-AMERICAN SOCIETY OF MECHANICAL ENGINEERS JOURNAL OF DYNAMIC SYSTEMS MEASUREMENT AND CONTROL **125**(3): 491-493.

Bartolini, G., et al. (1998). "Chattering avoidance by second-order sliding mode control." IEEE Transactions on Automatic control **43**(2): 241-246.

Berge, S. and T. Fossen (2000). "On the properties of the nonlinear ship equations of motion." Mathematical and Computer Modelling of Dynamical Systems **6**(4): 365-381.

Bessa, W. M., et al. (2010). "An adaptive fuzzy sliding mode controller for remotely operated underwater vehicles." Robotics and Autonomous Systems **58**(1): 16-26.

Blanke, M., et al. (2000). "Dynamic model for thrust generation of marine propellers." IFAC Proceedings Volumes **33**(21): 353-358.

BlueRobotics (2017). from <https://www.bluerobotics.com/store/rov/bluerov2/>.

BlueRobotics (2018a). "BlueROV2 Heavy Configuration Retrofit Kit." from <https://www.bluerobotics.com/store/rov/brov2-heavy-retrofit-r1-rp/>.

BlueRobotics (2018b). "BlueROV2 Heavy Retrofit Documentation." from <http://docs.bluerobotics.com/brov2-heavy/>.

BlueRobotics (2018c). "T200 Thruster." from <https://www.bluerobotics.com/store/thrusters/t200-thruster/>.

Caccia, M., et al. (2000). "Modeling and identification of open-frame variable configuration unmanned underwater vehicles." IEEE Journal of Oceanic Engineering **25**(2): 227-240.

Caccia, M. and G. Veruggio (2000). "Guidance and control of a reconfigurable unmanned underwater vehicle." Control engineering practice **8**(1): 21-37.

Capocci, R., et al. (2017). "Inspection-Class Remotely Operated Vehicles—A Review." Journal of Marine Science and Engineering **5**(1): 13.

Chalkiadakis, V., et al. (2017). Designing a small-sized autonomous underwater vehicle architecture for regular periodic fish-cage net inspection. Imaging Systems and Techniques (IST), 2017 IEEE International Conference on, IEEE.

Chen, H.-H., et al. (2007). Identification of hydrodynamic parameters for a remotely operated vehicle using projective mapping method. Underwater Technology and Workshop on Scientific Use of Submarine Cables and Related Technologies, 2007. Symposium on, IEEE.

Chin, C., et al. (2017). "Experimental validation of open-frame ROV model for virtual reality simulation and control." Journal of Marine Science and Technology: 1-21.

Chou, J. C. (1992). "Quaternion kinematic and dynamic differential equations." IEEE transactions on robotics and automation **8**(1): 53-64.

Christ, D. and L. Wernli (2007). "TheROV Manual: A User Guide for Observation Class Remotely Operated Vehicles."

- Chu, Z., et al. (2017). "Observer-based adaptive neural network trajectory tracking control for remotely operated vehicle." IEEE transactions on neural networks and learning systems **28**(7): 1633-1645.
- Cristi, R., et al. (1990). "Adaptive sliding mode control of autonomous underwater vehicles in the dive plane." IEEE Journal of Oceanic Engineering **15**(3): 152-160.
- de Barros, E. A., et al. (2008). "Investigation of normal force and moment coefficients for an AUV at nonlinear angle of attack and sideslip range." IEEE Journal of Oceanic Engineering **33**(4): 538-549.
- Do, K. D., et al. (2004). "Robust and adaptive path following for underactuated autonomous underwater vehicles." Ocean Engineering **31**(16): 1967-1997.
- Dukan, F. (2014). "Rov motion control systems."
- Dukan, F., et al. (2011). Dynamic positioning system for a small size ROV with experimental results. OCEANS, 2011 IEEE-Spain, IEEE.
- Edwards, C. and S. Spurgeon (1998). Sliding mode control: theory and applications, Crc Press.
- Egeland, O. and J. T. Gravdahl (2002). Modeling and simulation for automatic control, Marine Cybernetics Trondheim, Norway.
- Eidsvik, O. A. (2015). Identification of hydrodynamic parameters for remotely operated vehicles, NTNU.
- Eng, Y.-H., et al. (2014). "Added mass computation for control of an open-frame remotely-operated vehicle: Application using WAMIT and MATLAB." Journal of Marine Science and Technology **22**(4): 405-416.
- Eng, Y., et al. (2008). Identification of the hydrodynamics coefficients of an underwater vehicle using free decay pendulum motion. International MultiConference of Engineers and Computer Scientists.
- Erikson, U., et al. (2016). "Crowding of Atlantic salmon in net-pen before slaughter." Aquaculture **465**: 395-400.
- Faltinsen, O. (1990). "Sea loads on ships and ocean structures." Cambridge University, Cambridge, UK.
- Fernandes, D. d. A., et al. (2013). "Trajectory tracking motion control system for observation class ROVs." IFAC Proceedings Volumes **46**(33): 251-256.

- Fernandes, D. d. A., et al. (2015). "Output feedback motion control system for observation class ROVs based on a high-gain state observer: Theoretical and experimental results." Control engineering practice **39**: 90-102.
- Fossen, T. I. (1991). Nonlinear modelling and control of underwater vehicles, Fakultet for informasjonsteknologi, matematikk og elektroteknikk.
- Fossen, T. I. (1994). Guidance and control of ocean vehicles, John Wiley & Sons Inc.
- Fossen, T. I. (2002). Marine control systems: guidance, navigation and control of ships, rigs and underwater vehicles, Marine Cybernetics.
- Fossen, T. I. (2011). Handbook of marine craft hydrodynamics and motion control, John Wiley & Sons.
- Fossen, T. I. and T. A. Johansen (2006). A survey of control allocation methods for ships and underwater vehicles. Control and Automation, 2006. MED'06. 14th Mediterranean Conference on, IEEE.
- Franklin, G. F., et al. (1994). Feedback control of dynamic systems, Addison-Wesley Reading, MA.
- Fridman, L. and A. Levant (1996). Higher order sliding modes as a natural phenomenon in control theory. Robust Control via variable structure and Lyapunov techniques, Springer: 107-133.
- Goheen, K. and E. Jefferys (1990). The application of alternative modelling techniques to ROV dynamics. Robotics and Automation, 1990. Proceedings., 1990 IEEE International Conference on, IEEE.
- Goheen, K. R. (1986). The modelling and control of remotely operated underwater vehicles, University of London.
- Goheen, K. R. and E. R. Jefferys (1990). "Multivariable self-tuning autopilots for autonomous and remotely operated underwater vehicles." IEEE Journal of Oceanic Engineering **15**(3): 144-151.
- Goldstein, H. (1980). Classical mechanics, Pearson Education India.
- Gomes, R. M., et al. (2003). Modeling and control of the IES project ROV. European Control Conference (ECC), 2003, IEEE.
- Gonzalez, L. A. (2004). "Design, modelling and control of an autonomous underwater vehicle." Bachelor of Engineering Honours Thesis. The University of Western Australia.
- Goodman, A. (1960). Experimental techniques and methods of analysis used in submerged body research. Proceedings of the Third Symposium on Naval Hydrodynamics, National Academy Press.

Haugen, M. (2012). Modeling and Control of ROV Manipulator, Institutt for marin teknikk.

Healey, A. J. and D. Lienard (1993). "Multivariable sliding mode control for autonomous diving and steering of unmanned underwater vehicles." IEEE Journal of Oceanic Engineering **18**(3): 327-339.

Healey, A. J., et al. (1994). Toward an improved understanding of thruster dynamics for underwater vehicles. Autonomous Underwater Vehicle Technology, 1994. AUV'94., Proceedings of the 1994 Symposium on, IEEE.

Hoang, N. Q. and E. Kreuzer (2007). "Adaptive PD-controller for positioning of a remotely operated vehicle close to an underwater structure: Theory and experiments." Control engineering practice **15**(4): 411-419.

Hsu, L., et al. (2000). "Dynamic positioning of remotely operated underwater vehicles." IEEE Robotics & Automation Magazine **7**(3): 21-31.

Huang, H.-M. (2004). "Autonomy levels for unmanned systems (ALFUS) framework volume I: Terminology version 2.0." Special Publication (NIST SP)-1011.

Hughes, P. C. (1986). "Spacecraft Attitude Dynamics John Wiley and Sons." New York.

Humphreys, D. and K. Watkinson (1982). "Hydrodynamic stability and control analyses of the UNH-EAVE autonomous underwater vehicle." Marine Systems Lab. Rep., Univ. of New Hamp., Durham.

Indiveri, G. (1998). "Modelling and identification of underwater robotic systems." Computer Science.

Jakobsen, R. A. H. (2011). Automatic Inspection of Cage Integrity with Underwater Vehicle, Institutt for teknisk kybernetikk.

Javadi-Moghaddam, J. and A. Bagheri (2010). "An adaptive neuro-fuzzy sliding mode based genetic algorithm control system for under water remotely operated vehicle." Expert Systems with Applications **37**(1): 647-660.

Juul, D. L., et al. (1994). Submersible control using the linear quadratic gaussian with loop transfer recovery method. Autonomous Underwater Vehicle Technology, 1994. AUV'94., Proceedings of the 1994 Symposium on, IEEE.

Kalske, S. (1989). Motion dynamics of subsea vehicles, Espoo.

Kane, T. R., et al. (1983). "Spacecraft dynamics." New York, McGraw-Hill Book Co, 1983, 445 p.

Kim, J. and W. K. Chung (2006). "Accurate and practical thruster modeling for underwater vehicles." Ocean Engineering **33**(5-6): 566-586.

Kodogiannis, V., et al. (1996). "Neural network modelling and control for underwater vehicles." Artificial intelligence in Engineering **10**(3): 203-212.

Lapierre, L., et al. (2003). Nonlinear path following with applications to the control of autonomous underwater vehicles. Decision and Control, 2003. Proceedings. 42nd IEEE Conference on, IEEE.

Lewis, D., et al. (1984). "The simulation of remotely operated underwater vehicles." Proceedings, ROV'84: 245-252.

Li, Z., et al. (2012). "Robust adaptive motion control for underwater remotely operated vehicles with velocity constraints." International Journal of Control, Automation and Systems **10**(2): 421-429.

Liu, G. (1993). "Application of EKF technique to ship resistance measurement." Automatica **29**(2): 275-283.

Mai, C., et al. (2017). "Modeling and Control of Industrial ROV's for Semi-Autonomous Subsea Maintenance Services." IFAC-PapersOnLine **50**(1): 13686-13691.

Marco, D. B. and A. Healey (1998). "Surge motion parameter identification for the NPS Phoenix AUV."

Marco, D. B. and A. J. Healey (2001). "Command, control, and navigation experimental results with the NPS ARIES AUV." IEEE Journal of Oceanic Engineering **26**(4): 466-476.

Marsh, L., et al. (2013). "Getting the bigger picture: using precision Remotely Operated Vehicle (ROV) videography to acquire high-definition mosaic images of newly discovered hydrothermal vents in the Southern Ocean." Deep Sea Research Part II: Topical Studies in Oceanography **92**: 124-135.

Meirovitch, L. (1990). Dynamics and control of structures, John Wiley & Sons.

Mills, D. and C. Harris (1995). "Neurofuzzy modelling and control of a six degree of freedom AUV." Research Journal Image, Speech and Intelligent Systems.

Minorsky, N. (1922). "Directional stability of automatically steered bodies." Journal of ASNE **42**(2): 280-309.

Morrison, A. and D. R. Yoerger (1993). Determination of the hydrodynamic parameters of an underwater vehicle during small scale, nonuniform, 1-dimensional translation. OCEANS'93. Engineering in Harmony with Ocean. Proceedings, IEEE.

Naeem, W., et al. (2003). "LQG/LTR control of an autonomous underwater vehicle using a hybrid guidance law." IFAC Proceedings Volumes **36**(4): 31-36.

NationalOceanographyCentre (2018). "Isis Deep ROV Platform." from <http://www.noc.ac.uk/facilities/marine-autonomous-robotic-systems/deep-platforms>.

Newman, J. "Marine hydrodynamics, 1977." Massachusetts Institute of Technology, Cambridge, Massachusetts. Google Scholar: 19.

Nomoto, M. and M. Hattori (1986). "A deep ROV" DOLPHIN 3K": design and performance analysis." IEEE Journal of Oceanic Engineering **11**(3): 373-391.

NTNU (2018). "ROV Minerva." from <https://www.ntnu.edu/oceans/minerva>.

OceanExplorationTrust (2003). "ROV Hercules." from <http://www.oceanexplorationtrust.org/remotely-operated-vehicles>.

Perrier, M. and C. Canudas-De-Wit (1996). Experimental comparison of PID vs. PID plus nonlinear controller for subsea robots. Underwater Robots, Springer: 121-138.

Quigley, M., et al. (2009). ROS: an open-source Robot Operating System. ICRA workshop on open source software, Kobe, Japan.

Raimondi, F. M. and M. Melluso (2010). "Fuzzy/Kalman hierarchical horizontal motion control of underactuated ROVs." International Journal of Advanced Robotic Systems **7**(2): 12.

Raptis, I. A. (2010). Linear and nonlinear control of unmanned rotorcraft, University of South Florida.

Ridao, P., et al. (2004). "On the identification of non-linear models of unmanned underwater vehicles." Control engineering practice **12**(12): 1483-1499.

Rist-Christensen, I. (2016). Autonomous robotic intervention using ROV, NTNU.

Roman, C., et al. (2010). Application of structured light imaging for high resolution mapping of underwater archaeological sites. OCEANS 2010 IEEE-Sydney, IEEE.

Ross, A., et al. (2004). "Identification of underwater vehicle hydrodynamic coefficients using free decay tests." IFAC Proceedings Volumes **37**(10): 363-368.

SAAB (2002). "Seaeye Falcon & Seaeye Falcon DR." from <http://www.seaeye.com/falcon.html>.

Sandøy, S. S. (2016). System Identification and State Estimation for ROV uDrone, NTNU.

Sargent, J. S. and P. N. Cowgill (1976). Design considerations for dynamically positioned utility vessels. Offshore Technology Conference, Offshore Technology Conference.

Sarkar, T., et al. (1997). "A study of autonomous underwater vehicle hull forms using computational fluid dynamics." International Journal for Numerical Methods in Fluids **25**(11): 1301-1313.

Sarpkaya, T. and M. Isaacson (1981). "Mechanics of wave forces on offshore structures."

Sayyaadi, H. and T. Ura (1999). Multi input-multi output system identification of AUV systems by neural network. OCEANS'99 MTS/IEEE. Riding the Crest into the 21st Century, IEEE.

Sciavicco, L. and B. Siciliano (1996). Modeling and control of robot manipulators, The McGraw-Hill Companies, New York.

Sebastián, E. and M. A. Sotelo (2007). "Adaptive fuzzy sliding mode controller for the kinematic variables of an underwater vehicle." Journal of Intelligent and Robotic Systems **49**(2): 189-215.

Sedlazeck, A., et al. (2009). 3d reconstruction based on underwater video from roV kiel 6000 considering underwater imaging conditions. OCEANS 2009-EUROPE, IEEE.

Silpa-Anan, C., et al. (2000). Development of autonomous underwater vehicle towards visual servo control. Proceedings of the Australian Conference on Robotics and Automation. Melbourne, Australia.

Singh, H., et al. (2007). "Towards high-resolution imaging from underwater vehicles." The International journal of robotics research **26**(1): 55-74.

Slotine, J.-J. and S. S. Sastry (1983). "Tracking control of non-linear systems using sliding surfaces, with application to robot manipulators." International journal of control **38**(2): 465-492.

Slotine, J.-J. E. and W. Li (1991). Applied nonlinear control, Prentice hall Englewood Cliffs, NJ.

Smallwood, D. A. and L. L. Whitcomb (2003). "Adaptive identification of dynamically positioned underwater robotic vehicles." IEEE Transactions on Control Systems Technology **11**(4): 505-515.

Smallwood, D. A. and L. L. Whitcomb (2004). "Model-based dynamic positioning of underwater robotic vehicles: theory and experiment." IEEE Journal of Oceanic Engineering **29**(1): 169-186.

SNAME (1950). "Nomenclature for treating the motion of a submerged body through a fluid JR." New York: Technical and Research Bulletin: 1-5.

- Song, F. and S. M. Smith (2000). Design of sliding mode fuzzy controllers for an autonomous underwater vehicle without system model. Oceans 2000 MTS/IEEE Conference and Exhibition, IEEE.
- Sørensen, A. J. (2012). "Marine control systems propulsion and motion control of ships and ocean structures lecture notes."
- Soylu, S., et al. (2008). "A chattering-free sliding-mode controller for underwater vehicles with fault-tolerant infinity-norm thrust allocation." Ocean Engineering **35**(16): 1647-1659.
- SPERRE (2012). "SUB-FIGHTER 30K." from <http://sperre-as.com/portfolio/sub-fighter-30k/>.
- Strand, J. P. (1999). "Nonlinear Position Control Systems Design for Marine Yessels."
- Sun, Y. and C. Cheah (2003). Adaptive setpoint control for autonomous underwater vehicles. Decision and Control, 2003. Proceedings. 42nd IEEE Conference on, IEEE.
- Svendby, E. (2007). Robust control of ROV/AUVs, Institutt for teknisk kybernetikk.
- Triantafyllou, M. S. and F. S. Hover (2003). Maneuvering and control of marine vehicles, Massachusetts of Institute of Technology.
- Utkin, V. (1977). "Variable structure systems with sliding modes." IEEE Transactions on Automatic control **22**(2): 212-222.
- VideoRay (2018a). "Pro 3 ROV Image Gallery." from http://www.videoray.com/pro-3-rov-photo-gallery.html#!RigWorkerGTO_sm.
- VideoRay (2018b). "VideoRay Explorer ROV Images." from http://www.videoray.com/explorer-rov-photo-gallery.html#!Explorer_Display_sm.
- VideoRay (2018c). "VideoRay Pro 4 ROV Images." from http://www.videoray.com/videoray-pro-4-photo-gallery.html#!_SRC1370_sm.
- Wahl, A. and E. Gilles (1999). Model predictive versus linear quadratic control for the tracking problem of automatic river navigation. Control Conference (ECC), 1999 European, IEEE.
- Walther, D., et al. (2004). Detection and tracking of objects in underwater video. Computer Vision and Pattern Recognition, 2004. CVPR 2004. Proceedings of the 2004 IEEE Computer Society Conference on, IEEE.
- Wang, J.-S. and C. G. Lee (2003). "Self-adaptive recurrent neuro-fuzzy control of an autonomous underwater vehicle." IEEE transactions on robotics and automation **19**(2): 283-295.

Whitcomb, L. L. and D. R. Yoerger (1999). "Development, comparison, and preliminary experimental validation of nonlinear dynamic thruster models." IEEE Journal of Oceanic Engineering **24**(4): 481-494.

Yahya, M. and M. Arshad (2016). Position-based visual servoing for underwater docking of an autonomous underwater vehicle. Underwater System Technology: Theory and Applications (USYS), IEEE International Conference on, IEEE.

Yi, D. and H. Al-Qrimli (2017). "Identification of Hydrodynamics Coefficient of Underwater Vehicle Using Free Decay Pendulum Method." J Powder Metall Min **6**(161): 2.

Yoerger, D. and J. Slotine (1985). "Robust trajectory control of underwater vehicles." IEEE Journal of Oceanic Engineering **10**(4): 462-470.

Yoerger, D. R., et al. (1990). "The influence of thruster dynamics on underwater vehicle behavior and their incorporation into control system design." IEEE Journal of Oceanic Engineering **15**(3): 167-178.

Yuh, J. (1990). "Modeling and control of underwater robotic vehicles." IEEE Transactions on Systems, man, and Cybernetics **20**(6): 1475-1483.

Zhang, H., et al. (2010). "Using CFD software to calculate hydrodynamic coefficients." Journal of Marine Science and Application **9**(2): 149-155.

Zhao, B., et al. (2014). "Particle filter for fault diagnosis and robust navigation of underwater robot." IEEE Transactions on Control Systems Technology **22**(6): 2399-2407.

Ziegler, J. G. and N. B. Nichols (1942). "Optimum settings for automatic controllers." trans. ASME **64**(11).